Characterization of the performance of mineral oil based quenchants using CHTE Quench Probe System

By

Shuhui Ma

A Thesis

Submitted to the Faculty

Of the

WORCESTER POLYTECHNIC INSTITUTE

In partial fulfillment of the requirements for the

Degree of Master

In

Materials Science and Engineering

By

_____

June 27, 2002

APPROVED:

_____

Richard D. Sisson Jr. Advisor, Professor of Mechanical Engineering
Materials Science and Engineering Program Head

ABSTRACT

The performance of a series of mineral oil based quenchants has been investigated using the CHTE Quench Probe System and probe tips of 4140 steel to determine the cooling rate, heat transfer coefficient, Hardening Power (HP) and Tamura's V indices in terms of the physical properties of quenchants; e.g. viscosity and oil start temperature. The Quench Factor, Q, was also calculated in terms of the hardness of the quenched parts. The lumped parameter approximation was used to calculate the heat transfer coefficient as a function of temperature during quenching. The results revealed that the maximum cooling rate increases with decrease in quenchant viscosity. As viscosity increases, Tamura's V is nearly constant, while the HP decreases. For the selected oils, cooling ability of quenching oil increases with the increase in oil operating temperature, reaches a maximum and then decreases. The heat transfer coefficient increases with the increase in hardening power and maximum cooling rate. As the viscosity increases, the quench factor increases, which indicates the cooling ability of the oil decreases since the higher quench factor means the lower cooling ability of the oil. The hardness decreases with the increase in quench factor.

Also the effect of surface oxides during quenching in commercial oils is studied. It was found that for 4140 steel probes the formation of oxide in air increases the cooling rate and heat transfer coefficient, the cooling rate curve of 4140 steel probe heated in argon shows clear Leidenfrost temperature, the oxide layer may require a significant thickness to cause the decrease in heat transfer coefficient. For 304 stainless steel probes the cooling rate and heat transfer coefficient are quite similar in air and in argon.

Acknowledgements

First I would like to thank Prof. Richard D. Sisson, Jr. for his support and assistance as well as the Center for Heat Treating Excellence of the Metal Processing Institute at Worcester Polytechnic Institute. Also, I want to give my thanks to Dr. Maniruzzaman Mohammed for his help and creative ideas and to Juan Chaves for helping me start my research. My sincere thanks go to Torbjorn Bergstrom for his help, encouragement and assistance in measuring the roughness of the samples in my test.

I want to thank Rita Shilansky for the constant assistance that made this work possible. My thanks go to Celine McGee, who helped me to carry out some experiments, Olivier Prevot for helping me out with some excel problems and Marco Fontecchio for his ideas.

Furthermore, I must also acknowledge the patience and assistance of Jim Johnston, Todd Billings and Stephen Derosier for making the samples.

My sincere gratitude is given to my parents, my sisters and brother for their continuous encouragement, care and infinite love.

Table of Contents

ABSTRACT i
Acknowledgements ii
Table of Contents iii
List of Figures v
List of Tables viii
1. Introduction 2
2. Literature Review 4
2.1 Quenching and Its Stages 4
2.1.1 Film boiling phase 6
2.1.2 Nucleate boiling phase 6
2.1.3 Convection stage 7
2.2 Quenchant Chemistry 8
2.2.1 Mineral oils 8
2.2.2 Vegetable oils 12
2.3 Quenchant Characterization 14
2.4 Quenching probes 19
2.4.1 General Motors (GM) quenchometer 19
2.4.2 Grossmann Probe 21
2.4.3 IVF probe 21
2.4.4 The Drayton Probe 23
2.4.5 Nanigian-Liscic Probe 24
2.4.6 Tamura's Probes 25
2.5 Cooling curve analysis 26
2.5.1 Data Acquisition and Cooling Curve Analysis 26
2.5.2 Interpretation of cooling curves 28
2.6 Metallurgy of 4140 Steel and 304 Stainless Steel 30
2.6.1 Characteristics and TTT diagram of 4140 steel 30
2.6.2 Characteristics of 304 stainless steel 33

2.6.3 Theoretical understanding of heat transfer 34
2.6.4 Calculation of heat transfer coefficient 40
2.6.5 Thermoconductivity of 4140 steel and 304 stainless steel 43
2.6.6 Specific Heat of 4140 steel and 304 stainless steel 45
2.7 Quenching Performance Indices 47
2.7.1 Tamura V value 48
2.7.2 Hardening Power (HP) by IVF 48
2.7.3 Quench Factor Analysis 51
3. Characterization of the performance of mineral oil based quenchants using CHTE Quench Probe System 56
I Introduction 57
II Experimental Procedure 59
III Experimental Results and Discussion 61
IV Summary 75
4. The Effects of surface oxides on the quenching performance of 4140 steel in commercial mineral oils 77
I Introduction 78
II Experimental Procedure 80
III Experimental Results and Discussion 83
(A) Repeatability tests 83
(B) Comparison of cooling rate curves 90
(C) Comparison of heat transfer coefficients 96
(D) Theoretical calculation 100
IV Summary 104
References 105

List of Figures

Fig 2.1 Cooling mechanism [5]

Fig 2.2 The three cooling stages in quenching [3].

Fig 2.3 Gas chromatogram of the wolfson reference quench oil [5]

Fig 2.4 Expected hydrocarbons in a typical crude oil fraction [5]

Fig 2. 5 Cooling rate curves of various quench oils at 60oC [5]

Fig 2.6 Vegetable oil triglyceride structure [13]

Fig 2.7 Transformation diagram of low- alloy steel with cooling curves for various quenching media [5]

Fig 2. 8 GM quenchometer and principle of operation [5]

Fig 2.9 SAE 5145 Steel Probe used by Grossmann [27]

Fig 2.10 IVF test probe and handle [28]

Fig 2.11 Drayton probe and the portable quenching system

Fig 2.12 Schematic of Liscic-NANMAC probe--TGQAS Temperature Gradient Quenching Analysis System by Prof. Bozidar Liscic [1]

Fig 2. 13 JIS silver probe [5]

Fig 2.14 various representations of cooling curve data [5]

Fig 2.15 CCT diagram for a spring steel (50M7) with superimposed cooling curves [5]

Fig 2. 16 TTT diagrams of AISI 4140

Fig 2. 17 Cross sections of Fe-Cr-Ni ternary diagram [39]

Fig 2. 18 Thermal conductivity of 4140 steels and 304 stainless steels [39] [41] [32]

Fig 2. 19 Specific Heat of 4140 steels and 304 stainless steels [36] [1, 39, 42, 43]

Fig 2. 20 Specific heat of austenitic iron and 4140 as a function of temperature [36, 42]

Fig 2. 21 Key parameters for IVF hardening power equation [1]

Fig 2. 22 Oils ranked by hardening power. Calculated values of hardening power HP, matched to a

straight line for the quenching oils [53]

Fig 2. 23 Schematic illustrations on plot of CT function to calculate the Quench Factor

Fig 3- 1CHTE Quench Probe System

Fig 3- 2CHTE probe-coupling-connecting rod assembly

Fig 3- 3 typical cooling rate curves of CHTE 4140 steel probe in different mineral oils

Fig 3- 4 Cooling rates of CHTE 4140 steel probe at 800,700,600,550,500 and 400oC as a function of viscosity

Fig 3- 5 the maximum cooling rate as a function of viscosity

Fig 3-6 Cooling curves of CHTE probe in Houghton Martemp355 used quenching oil show excellent repeatability of the cooling rate

Fig 3-7 Cooling rate curves of CHTE probe in Houghton T7A mineral oil

Fig 3-8 Cooling rate of CHTE probe in Houghton Mar-temp 355

Fig 3-9 Cooling rate of CHTE probe in Burgdorf HR88A mineral oil

Fig 3-10 Cooing rate of CHTE probe in Burgdorf W72 mineral oil

Fig 3-11 Cooing rate of CHTE probe in Burgdorf Durixol V35 mineral oil

Fig 3-12 Cooing rate of CHTE probe in Burgdorf Durixol W25 mineral oil

Fig 3-14 Cooling rate curves of CHTE 4140 quenched in Burgdorf HR88A at different temperatures

Fig 3-15 Cooling curves of CHTE 4140 probes with different diameters quenched in Burgdorf W72

Fig 3-16 Typical heat transfer coefficient curves of CHTE 4140 steel probe as a function of temperature quenched in different mineral oils.

Fig 3-17 Heat transfer coefficient as a function of HP and CRmax for CHTE 4140 steel probe in different mineral oils

Fig 3-18 Quench Factor as a function of viscosity for CHTE 4140 steel probe in different mineral oils

Fig 3-19 Hardness as a function of quench factor for CHTE 4140 steel probe quenched in Houghton G, T7A and Durixol HR88A

Fig 4. 1Cooling rate curves of CHTE 4140 probe in T7A heated in air

Fig 4. 2 Cooling rate curves of CHTE 4140 probe in Houghton G heated in air

Fig 4. 3 Cooling rate curves of CHTE 4140 probe in DHR88A heated in air

Fig 4.4 Cooling rate curves of CHTE 304 probe in T7A heated in air

Fig 4.5 Cooling rate curves of CHTE 304 probe in Houghton G heated in air

Fig 4.6 Cooling rate curves of CHTE 304 probe in DHR88A heated in air

Fig 4.7 Cooling rate curves of CHTE 304 probe in T7A heated in argon

Fig 4.8 Cooling rate curves of CHTE 304 probe in Houghton G heated in argon

Fig 4.9 Cooling rate curves of CHTE 304 probe in DHR88A heated in argon

Fig 4. 10 Cooling rate curves of CHTE 4140 probe in DHR88A heated in argon

Fig 4. 11 The comparison of mean cooling rate for 4140 heated in air and argon and quenched in Houghton G as a function of temperature

Fig 4. 12 Cooling rate curves of CHTE 4140 probes heated in air and argon and quenched in T7A

Fig 4.13 Cooling rate curves of CHTE 4140 probes heated in air and argon and quenched in DHR88A

Fig 4.14 Cooling rate curves of CHTE 304 probes heated in air/argon and quenched in T7A

Fig 4.15 Cooling rate curves of CHTE 304 probes heated in air/argon and quenched in Houghton G

Fig 4.16 Cooling rate curves of CHTE 304 probes heated in air and argon and quenched in DHR88A

Fig 4.17 Cooling rate curves of CHTE 4140 steel and 304 stainless steel probe inT7A in air

Fig 4.18 Cooling rate curves of CHTE 4140 steel and 304 stainless steel probe inDHR88A in air

Fig 4.19 Cooling rate curves of CHTE 4140 and 304 stainless steel probe inT7A in argon

Fig 4. 20 Cooling rate curves of CHTE 4140 and 304 stainless steel probe in DHR88A in argon

Fig 4. 21 Heat transfer coefficients of CHTE 4140 steel probe quenched in T7A

Fig 4. 22 Heat transfer coefficients of CHTE 304 stainless steel probe quenched in T7A

Fig 4.23 Heat transfer coefficients of CHTE 4140 steel and 304 stainless probe quenched in T7A in air

Fig 4.24 Heat transfer coefficient of CHTE 4140 steel and 304 stainless probe quenched in T7A in Ar

Fig 4.25 The variation of thermal resistance of 4140 steels with the oxide thickness

List of Tables

Table 2. 1 IVF Probe Characteristics [28]

Table 2. 2 Drayton Probe Characteristics [29]

Table 2. 3 Mechanical properties of normalized and annealed 4140 [1]

Table 2. 4 Mechanical Properties of quenched and tempered 4140 steels [1]

Table 2. 5 Nomenclatures

Table 3- 1 Test matrix of CHTE 4140 steel probe quenched in commercial oils

Table 4. 1 Test matrix of 4140 and 304 steel probes in Houghton G, T7A and Durixol HR88A

Table 4. 2 R&R Study of 4140 steel probes in Houghton G

Table 4. 3 The variation of thermal resistance of 4140 steels with the oxide thickness

1. Introduction

The heat treatment of steel has a 3500-year history [1]; the main goal of heat treatment of steel is to achieve the desired combination of mechanical properties when subjected to controlled heat treatment.

Quenching, as one of the most important processes of heat treatment, can improve the performance of steel greatly, but an important side effect of quenching is the formation of thermal and transformational stresses that cause changes in size and shape that may result in cracks [2]. Therefore, the technical challenge of quenching is to select the quenchant medium and process that will minimize the various stresses that develop within the part to reduce cracking and distortion while at the same time providing heat transfer rates sufficient to yield the desired as-quenched properties such as hardness [1].

There are a wide variety of quenchants in use in industry including water, brine solutions, mineral and vegetable oils, aqueous polymers, salt baths and fluidized beds. Water and oil are the quenchants most commonly used to harden steel because they are readily quenchable. Water quenching is apparently much faster than oil quenching, so it is more possible to cause the crack during quenching, which makes oil quenching more common. The cooling abilities vary from oil to oil; therefore, it is critical to characterize how the physical and chemical properties of oils might affect their quenching performance as well as the fluid flow within the quench tank.

This thesis addresses the quenching behavior of different mineral oils according to their physical properties (viscosity, oil bath temperature). The cooling rates are experimental determined and used to calculate the heat transfer coefficients from experimental time-temperature data. These heat transfer coefficients can be used to

compare the heat transfer characteristics of different quenching oils as a function of temperature.

It is the goal of this thesis to determine the cooling rate, heat transfer coefficient, Hardening Power (HP) and Tamura's V indices in terms of the physical properties of quenchants; e.g. viscosity and oil start temperature. The Quench Factor, Q, in terms of the hardness of the quenched parts was also calculated. The effects of oxidation on the quenching performance of CHTE probes are also investigated using CHTE Quench Probe System and probe tips of 4140 and 304 stainless steels.

2. Literature Review

2.1 Quenching and Its Stages

"Heat Treatment can be defined as an operation or combination of operations involving the controlled heating and cooling of a metal in the solid state for the purpose of obtaining specific properties" [3].

As one of the most important heat treatment processes, quenching of steel refers to the cooling from the solution treating temperature, typically 845-870˚C (1550-1600˚F), into the hard structure-martensite [4]. Quenching is typically performed to prevent ferrite or pearlite formation and to facilitate bainite or martensite formation [4]. After quenching, the martensitic steel is tempered to produce the optimum combination of strength, toughness and hardness. For a specific steel composition and heat treatment condition, there is a critical cooling rate for full hardening at which most of the high temperature austenite is transformed into martensite without the formation of either pearlite or bainite [3].

As the steel is heated it absorbs energy that is later dissipated by the quenchant in the quenching process. It is important to understand the mechanisms of quenching and the factors that affect the process since these factors can have a significant influence on quenchant selection and the desired performance obtained from the quenching process. The shape of a cooling curve is indicative of the various cooling mechanisms that occur during the quenching process. For the liquid quenchants like water and oil, cooling generally occurs in three distinct stages, film boiling, nucleate boiling and convection stages, each of which has different characteristics. Figure 2.1 shows the cooling and cooling rate curves during the quenching process[5]. Figure 2.2 shows the phenomena

that occur during these three stages. The vapor phase corresponds to the film boiling stage and the boiling phase corresponds to the nucleate boiling stage.

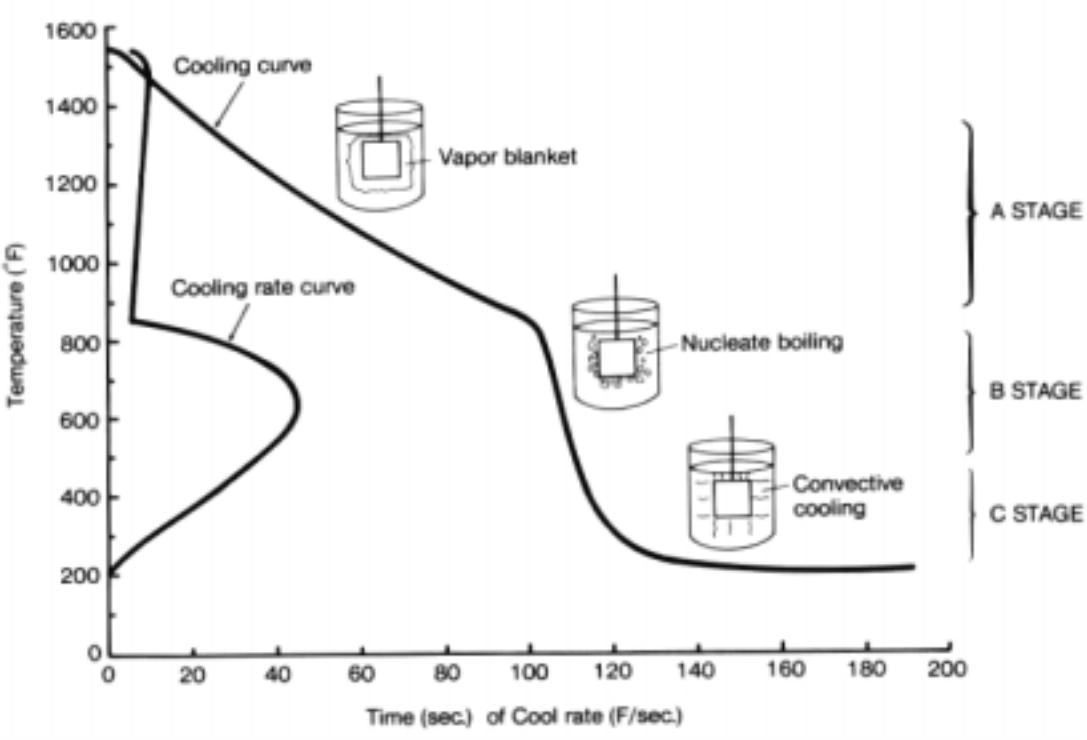

Fig 2.1 Cooling mechanism [5]

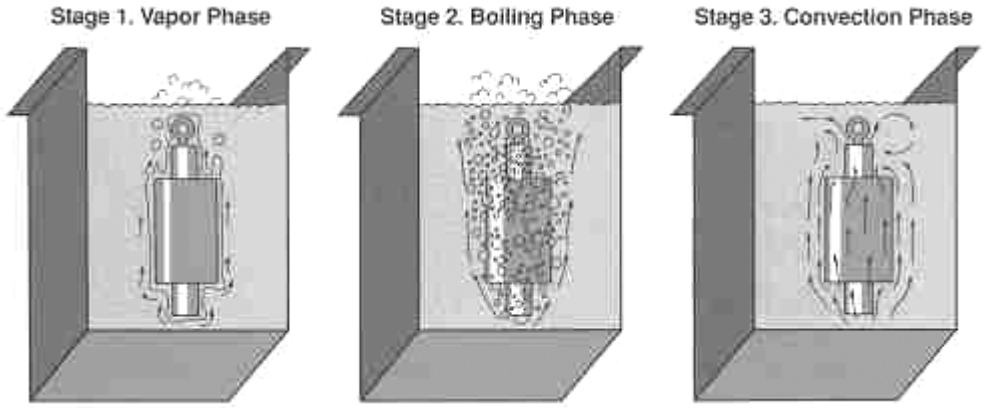

Fig 2.2 The three cooling stages in quenching [3].

2.1.1 Film boiling phase

The fist stage of cooling, which is denoted as A stage in figure 2.1, is characterized by the formation of a vapor film around the component [3]. This vapor blanket develops and is maintained while the supply of heat from the interior of the part to the surface exceeds the amount of heat needed to evaporate the quenchant and maintain the vapor phase. This film acts as an insulator and starts to disappear when the Leidenfrost temperature, the temperature above which a total vapor blanket is maintained, is reached. This is a period of relatively slow cooling during which heat transfer occurs by radiation and conduction through the vapor blanket. This stage is non-existent in parts quenched in aqueous solutions with more than 5% by weight of an ionic material as potassium chloride sodium hydroxide or sulfuric acid. In these cases quenching starts with nucleate boiling [3].

The wetting process occurs during the transition from film boiling to nucleate boiling. It occurs in repetitive waves that "rewet" the surface. The transition temperature from A- to B-stage cooling is classically known as the Leidenfrost temperature and is independent of the initial temperature the metal being quenched [5].

2.1.2 Nucleate boiling phase

Upon further cooling, stage B, or the nucleate boiling stage begins. This cooling mechanism is characterized by violent boiling at the metal surface. The stable vapor film eventually collapses and cool quenchant comes into contact with the hot metal surface resulting in nucleate boiling and high extraction rates. In the nucleate boiling stage correlations have been used for smooth surfaces, although no consideration is given for

other surfaces. Additionally, no definition of a smooth surface was given [1]. The objective regardless of the stage is to be able to calculate an effective heat transfer coefficient for the process. The lumped analysis model is one of models that are used to calculate heat transfer coefficient and obtain results in order to establish performance comparisons. This model enables an expedient means to obtain preliminary results for the study of the effect of surface roughness and high temperature oxidation on quenching performance.

2.1.3 Convection stage

Stage C, or the convective cooling stage, in figure 2.1 begins when the metal cools just below the boiling point of the quenching fluid [5]. As cooling continues, the surface temperature is below the boiling point of the quenching fluid and the metal surface is completely wetted by the fluid. At this point, the cooling rate is low and determined by the rate of convection and the viscosity of the quenching fluid. The B- to C-stage transition temperature is primarily a function of the boiling point of the quenchant, and the rate of heat removal in stage C is much slower than in stage B. When the cooling is in convection stage, boiling ceases and heat is removed by convection into the liquid. Heat is removed very slowly during this stage. Heat transfer rates in this region are affected by various process variables, such as agitation, quenchant viscosity and bath temperature, and by the viscosity of the quenchant medium.

During quenching the duration of the vapor phase and the temperature at which the maximum cooling rate occurs have a critical influence on the ability of the steel to harden fully. The rate of cooling in the convection phase is also important since it is

generally within this temperature range that martensitic transformation occurs and it can, therefore, influence residual stress, distortion and cracking.

2.2 Quenchant Chemistry

Oils used for quenching applications include various petroleum distillates (mineral oil) and animal fats (vegetable oil)-generally mixtures of chemical structures with a range of molecular weights and thus vary widely in composition, properties, and heat-removal characteristics, depending on the source and extent of refinement [5]. These oils may also be blended with various additives. Some data show that quenching oils, whether mineral or fat derived, can be formulated to produce similar quenching properties [5]. The quenching with vegetable oils is beneficial to the environment, but availability, price, stability and quenching performance currently favor the selection of mineral oils [5].

2.2.1 Mineral oils

Mineral oils have been used as quenchant for a long time since a wide range of quenching characteristics can be obtained through careful formulation and blending of the oils and additives. Mineral oils can be any petroleum oil, as contrasted to animal or vegetable oils. Also a highly refined petroleum distillate, or white oil, used medicinally as a laxative. Mineral oils used in quenching are analogous to other petroleum products, including engine oils, spindle oils, and industrial lubricating oils such as gear lubricants. [6] Although petroleum oils are usually refined for specific applications, they remain complex mixture with a variety of possible compositions, which may vary even when produced by a single refinery [5].

The complexity of a quench oil can be shown by gas chromatography, an analytical technique that separates mixtures based on differences in component volatility and adsorptivity. The complexity of the mixture, or the number of individual components, can be determined by counting the number of peaks in the chromatogram, which provides a characteristic "fingerprint" of the oil [5]. The chromatographic complexities of the Wolfson reference quench oil that has been proposed as a standard for the International Organization for Standardization draft on quench oil [7]are illustrated in figure 2.3 [8].

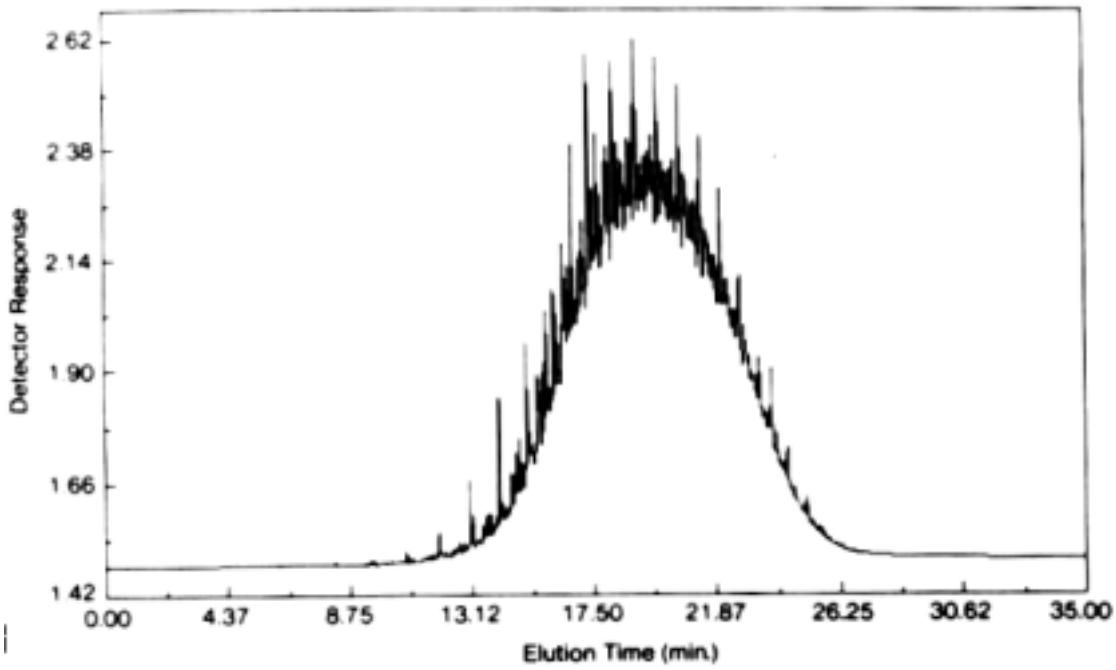

Fig 2.3 Gas chromatogram of the wolfson reference quench oil [5]

The components of a petroleum oil are many, including paraffinic, naphthenic, and various oxygen-, nitrogen-, and sulfur-derived open-chain and cyclic derivatives. The specific composition of a petroleum oil varies with the source of the crude oil. Generally the mineral oils are distilled from the C_{26} to C_{38} fraction of petroleum and composed of branched paraffins (C_nH_{2n+2}) and cycloparaffins (C_nH_{2n}) together with a small amount of

aromatics (Benzene ring and its derivatives). Within individual molecule, there are some cycloparaffin rings, aromatic rings and the necessary paraffin and olefin side or connecting groups. The difference in the cooling performance from oil to oil has much to do with how much unsaturated components with the oil.

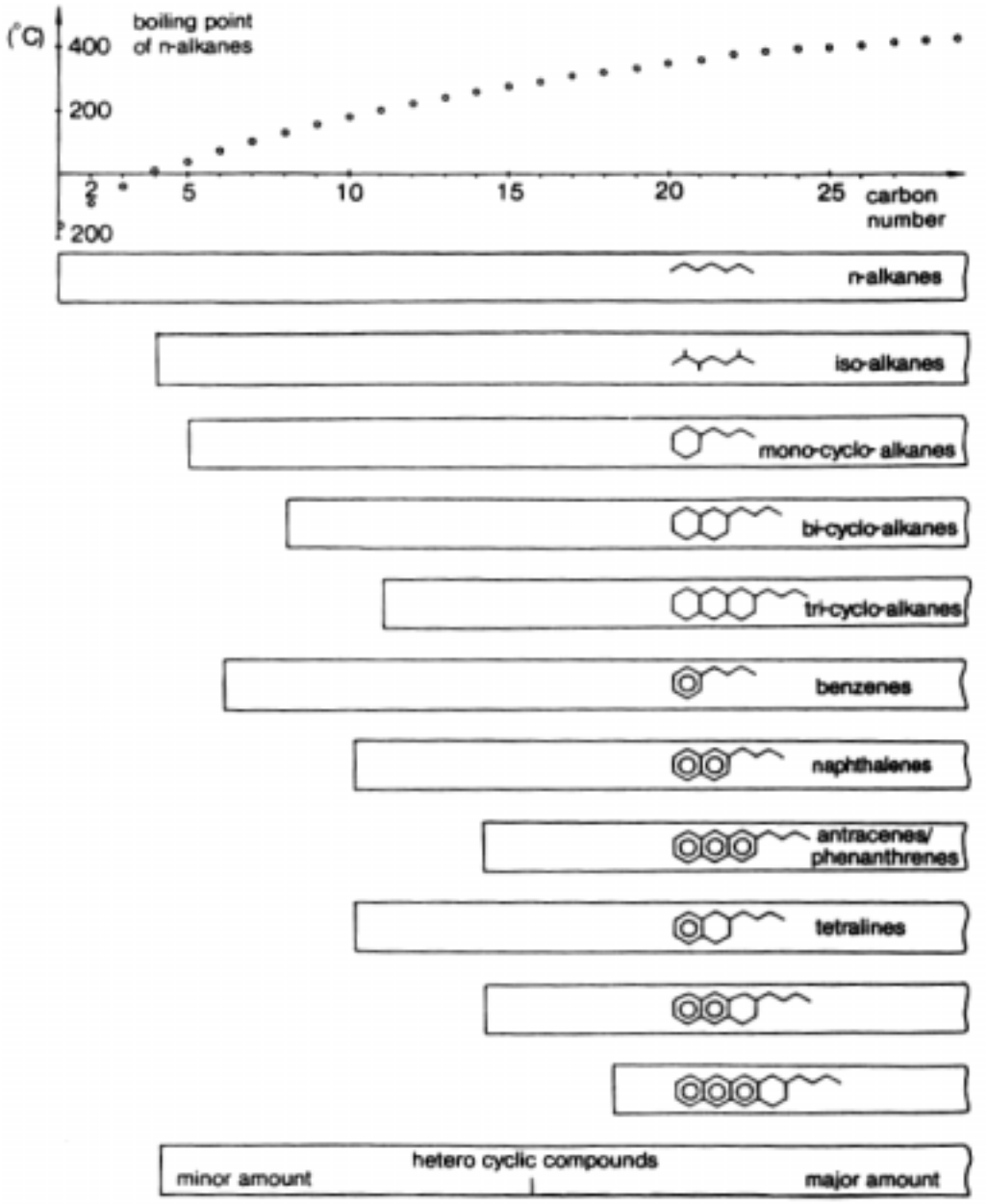

Fig 2.4 Expected hydrocarbons in a typical crude oil fraction [5]

The volatility of components in an oil, which is usually inversely proportional to its flash point, decreases as the average molecular size or carbon number of the components increases [5]. Figure 2.4 lists several petroleum oil components and their relative volatilities. The more volatile a component, the lower its flash point.

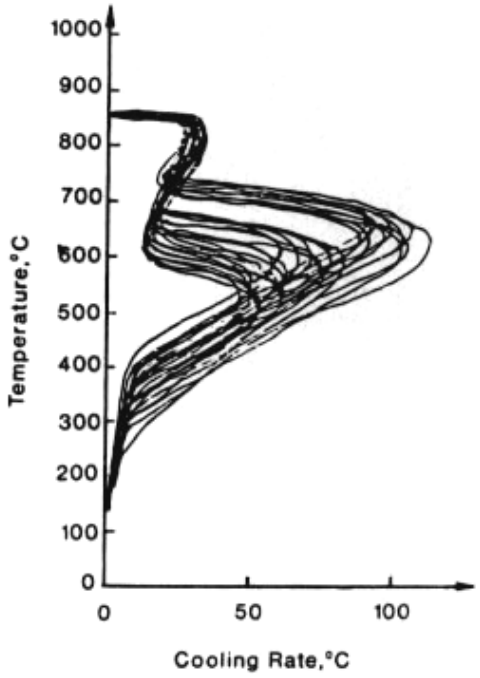

Fig 2. 5 Cooling rate curves of various quench oils at 60°C [5]

The compositional complexity of quench oils affects their quenching performance. Segerberg [9] compared a series of mineral-oil-base quenchants under standard conditions and obtained a wide variety of cooling rates as shown in figure 2.5. It is clear that even straight mineral oils vary in quenching performance. Formulated oils can produce an even wider range of cooling rates.

Windergassen [10] reported that quenching oils that contain substantial quantities of naphthenic derivatives usually exhibit inferior cooling characteristics, a greater deposit-forming tendency, and lower flash points than paraffinic oils. The lower flash

points are particularly deleterious in heat-treating applications. Protsidim et al [11]also showed that small changes in the compositions of the quench oils resulted in significant changes in quenching properties. Tensi [12] has shown that the quench severity of a particular oil is directly related to its ability to wet a metal surface. Usually the particular additive or combined additive is added into the oil to accentuate the wettability of an oil, thus having a dramatic effect on oil properties including sludging, staining and so forth. The wettability of an oil can be quantified by measuring "rewetting" time or measuring the contact angle of the oil on that surface.

2.2.2 Vegetable oils

Although mineral oils have traditionally been one of the most commonly used quenching media, unlike water, they are being subjected to ever-increasing controls due to increasingly stringent governmental regulations regarding their use [13]. Routine disposal and inadvertent release into the environment, especially into the soil where they may leach into drinking water aquifers, is being increasingly regulated by governmental agencies. Thus far, the most commonly cited basestocks for the formulation of environmentally friendly quenchants are vegetable oils including canola oil and soybean oil derivatives and so on [14].

Vegetable oils are compounds of carbon, hydrogen, and oxygen, which are found naturally in all plants. Vegetable Oils are defined as liquid glycerides, which is also called 'salts of organic acids' and generally consist of three kinds of substances: Saturated fat, polyunsaturated fat, and Monounsaturated fat.

Vegetable oils are typical natural occurring triglycerides with the generic structure shown in figure 2.6. Each vegetable oil is characterized by the particular type and concentration [13]. Oil is removed from the vegetable beans (or seed) in an "expelling" process [13]. Expelling can be performed by either pressing the bean (or seed) or, more commonly, by a solvent extraction process. Expulsion by solvent extraction is a three-step process: bean preparation, oil extraction and solvent stripping, and reclamation.

Fig 2.6 Vegetable oil triglyceride structure [13]

The triglyceride structure of vegetable oils in figure 2.6 can be generated by the following chemical reaction of the radicals of $(CH_3)_3$-$(CH_2)_{3n}$-C_3H_5 with such organic acids as $\mathbf{C_nH_{2n-1}COOH}$, e.g. Oleic acid ($C_{17}H_{33}COOH$))[15]. "n" is the integer equal to or greater than 1.

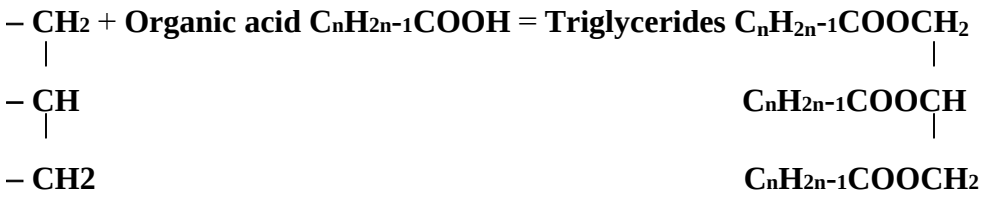

The different kinds of oils found in nature are due to the number of fatty acids. One kind of oil generally has some kind of predominant acid in it, and along with this predominant acid it will have besides a number of the other acids in smaller amounts

[15]. The different acids each have different properties, and impart these differences to the oils in which they occur.

No oil has any fixed combination of the different fatty acids present in it, but the proportions of these will vary with locality, soil, season, and other factors. This accounts for differences between the same species of oil from different places, or harvested at different times [15].

The following is the list of common fatty acids and their source [15].

- Lauric acid- cocoanut, palm nut
- Oleic acid-most vegetables: $\mathbf{C_{17}H_{33}COOH}$
- Linolenic acid- linseed and drying oils: $\mathbf{C_{17}H_{31}COOH}$
- Stearic acid: $\mathbf{C_{17}H_{35}COOH}$
- Palmitic acid- palm and vege and animal. : $\mathbf{C_{15}H_{31}COOH}$
- Arachidic acid- peanut.

'Drying' is defined as readiness with which they absorb oxygen.

- Drying oils: Linseed prilla, Tung, Chinese wood, Soya.
- Semi-drying: Cottonseed, Corn, Sesame, Rape.
- Non-drying: Peanut, Olive, Castor, and Almonds.

Iodine number is defined as the number of milligrams of iodine absorbed by 1 gram of oil. The iodine value and the absorbing power of oxygen run parallel. Iodine number can be used to identify the oil [15].

2.3 Quenchant Characterization

Quenching is a critical step in the production of heat treatable steel alloys. In most cases the most rapid quench from the solution heat treatment temperature is required to

develop the best properties, but quite often lower quench rates are used to minimize residual stress from the quenching operation. In 1968 Vruggink reviewed methods of evaluating the effects of quench rate on mechanical properties, and concluded that the simplest and most effective method was to quench in different media.

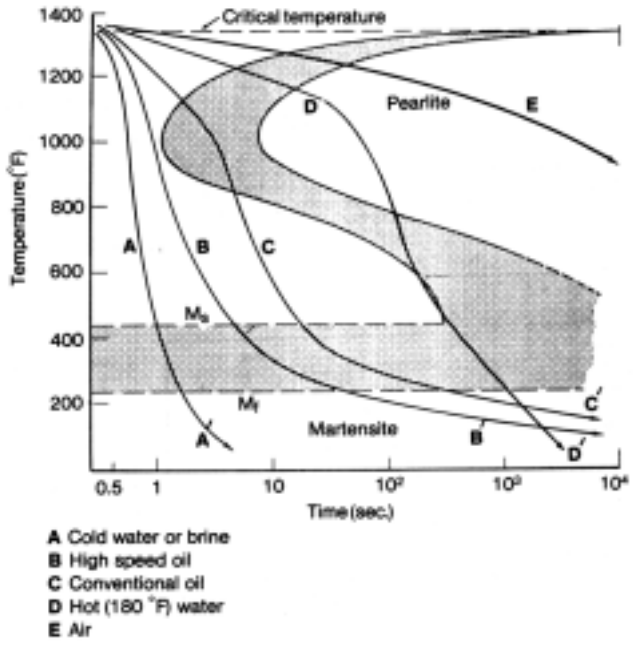

Fig 2.7 Transformation diagram of low- alloy steel with cooling curves for various quenching media [5]

Figure 2.7 shows a sample transformation diagram of low alloy steel with cooling curves for various quenching media.

In figure 2.7, curve A shows water or brine used as a quenchant. It is fast enough to avoid the nose and full transformation to Martensite is attained. The fast oil shown in curve B, although slower than the water, also attains full Martensite transformation. Both A and B reach the Martensite start and Martensite finish temperature without touching the nose. Conventional oil, hot water, and air do not accomplish this and thus do not form a pure Martensitic structure. The product will have a mixture of phases.

The three cooling stages were observed by Scott in his studies. The studies showed three distinctive mechanisms of heat dissipation. In general the fundamental properties of liquids determining quenching power are thermal conductivity, viscosity, specific heat, and heat of vaporization [1].

French found that cooling at the surface of steel bodies in liquids at low velocities is seldom uniform. The effects described suggest the need for cooling rates above the critical cooling rates for steel to be hardened. This can be accomplished by changing coolant composition, and to providing adequate circulation and volume of coolant [1].

French was also one of the first to record information on properties of quenchants in order to properly characterize them. Up to that time, there had been less concern for gathering of data of the quenching fluids. French provides a list of properties as specific heat, flash point, fire point, initial boiling point, final boiling point, final vapor temperature and parts per million of solids. These properties had not been readily available in the literature at that time.

Prof. Tamura identified four stages of cooling and correlated these four cooling stages with the specific physical properties of quenchant. [16-19]. The first stage was difficult to observe due to the initial heating up of the small probe. Time in this stage depends on specific heat, viscosity, thermal conductivity, and difference in temperature between solution temperature and the boiling point of the liquid. No specific name was given to this stage except that it is the first one.

The second stage (this is the first stage that is detected most of the time) is the vapor blanket stage. There is a temperature in excess of the critical overheat temperature (COHT) this stage ends at the Leidenfrost Point (Characteristic Temperature). This

temperature is dependent on the vapor pressure, latent heat, boiling point, viscosity, and activity of the liquid towards the probe surface.

Third Stage (Nucleate Boiling) has the highest cooling rate. Cooling in this stage depends on the boiling point of the liquid.

Fourth Stage (Convection Cooling), which exhibits the lowest cooling rate, is affected by the difference of the viscosity and temperature difference of the boiling point and the temperature of the liquid. Cooling rate increases if: critical temperature, latent heat, and wettability increase, and if vapor pressure and viscosity are decreased.

He also conducted a simultaneous investigation of the cooling process and generation of surface and center cooling curves by movie recording of the interfacial cooling process at the quenched hot metal surface. These results were correlated with chemical and physical properties of the liquid quenching media.

Tamura created the concept of Master Cooling Curves. The cooling curves obtained from a probe depend on the cooling characteristics of the quenchant, thermal constants, and size and shape of the probe. Tamura developed the Master Cooling Curve concept that is only dependent on the quenching oil. This methodology was developed from the results of experiments done with steel and silver probes. The methodology permits the evaluation of the oil performance without the effects of the size and the material of the probe. Prof. Tamura found that the Characteristic Temperature (Leidenfrost) and the convection start temperature of surface cooling curves are independent of probe size, and the cooling speed changes as a function of the size of the probe. Center cooling curves have a more complicated behavior not [20].

The use of the cooling curve analysis improved the quenchants and heat treatment technologies in Japan Prof. Tamura studied the cooling ability of various aqueous liquids, animal and vegetable oils, as well as mineral oils. He compared mineral and fatty oils, studied deterioration of quenching oils, thermal decomposition and polymerization, and use of oxidation inhibitors [20].

Tamura also studied ability of aqueous solutions in oils, aqueous solutions, and animal and vegetable solutions [21]. Tamura found that rich solutions of non-volatile solutes of $MnSo_4$ and Na_2CO_3 increase the cooling rate considerably, in the 700-500 °C range and reduce it at 300°C relative to distilled water.

He determined the cooling ability of animal and vegetable oils. Increasing molecular weights decreases vapor pressure, increases boiling point and critical temperature, and reduce the vapor blanket stage. In general, increasing molecular weight reduces the ability to differentiate the four stages of cooling. An increase in the aromatic hydrocarbon in mineral oils of similar molecular weight decreases vapor pressure, increases the critical start temperature and boiling point, as well as the wettability. Naphthenic cooling rates are greater than parafinic [22].

Prof. Tamura studied extensively the effects of distillation, hydrocarbon types, and refining on the cooling curve behavior of mineral oils. The addition of lighter oil will reduce the characteristic temperature (Leidenfrost Temperature). The cooling curves of unrefined oils exhibit slightly higher critical temperatures and higher cooling rate, probably caused by adsorption of impurities and the difference of viscosity at a higher temperature range [22].

Tamura also studied the deterioration of quenching oils. Oil deterioration is accompanied by a change in cooling rates, surface discoloration, formation of sludge, and decrease in flash point. He performed a detailed investigation of the degradation processes of the oil by modeling the oil oxidation and thermal decomposition.

Mr. Segerberg has devised a method to rate oils in terms of relative hardening power with the assistance of a portable quenchant tester [23]. The goal of his work is to select the quenchant best suited for a particular application. The later section describes the Relative Hardening Power (HP) by IVF. A formula has been developed using three characteristic points in the cooling rate curve. These points are: the transition temperature from film boiling to nucleate boiling, the cooling rate between 500^{o}C and 600^{o}C, and the transition temperature from nucleate boiling to convection. The quenching system generates the cooling and cooling rate curves and provides the necessary data to use the IVF hardening power equation. The IVF quenching system that complies with ISO 9950 is now widely used in industry [23].

2.4 Quenching probes

The quenching probes have been produced in a great variety of shapes, including cylinders, spheres, square bars, plates, rings and coils, round disks and production parts. Also the probes have been constructed of various materials, including alloy and stainless steels, silver, nickel, copper, gold and aluminum [5].

2.4.1 General Motors (GM) quenchometer

The cooling rates produced by quench oils are often classified on the basis of the GM quenchometer or nickel ball test [24, 25]. The GM quenchometer, which can

measure the heat removal properties of the quenchants, uses the Curie temperature of a metal as a means to obtain a characterization of a quenching fluid. The Curie temperature is the temperature at which a metal becomes magnetic.

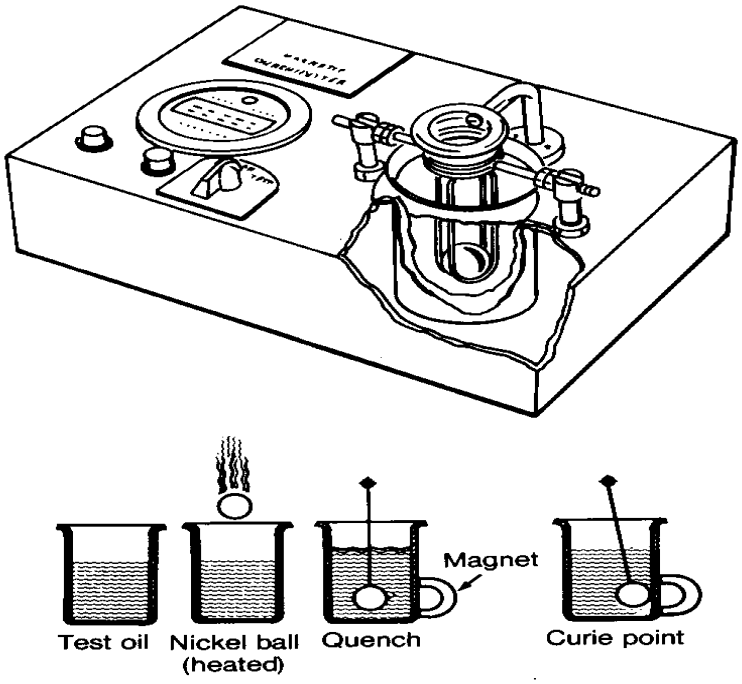

Fig 2. 8 GM quenchometer and principle of operation [5]

Details of this test are given in ASTM Standard D 3520. The test involves heating a 22mm diameter nickel ball to 885^{o}C and then dropping it into a wire basket suspended in a beaker containing a 200mL of the quenchant oil at 21 to 27^{o}C [26]. A timer is activated as the glowing nickel ball passes a photoelectric sensor [5]. A horseshoe magnet is located outside the beaker as close as possible to the nickel ball. As the ball cools, it passes through its Curie point (354^{o}C), the temperature at which it becomes magnetic [5]. When the ball becomes magnetic, it is attracted to the magnet, activating a sensor that stops the timer, as shown in figure 2.8.

The cooling time needed to reach Curie temperature is referred to as heat extraction rate or quenchometer time. The oils are then classified in slow, medium and fast [5]. The classification is slow oils 15-20 seconds, medium oils 11-14 seconds and fast oils 8-10 seconds [1].

2.4.2 Grossmann Probe

One of the earliest probes used is shown in figure 2.9 [27]. This probe was constructed from a 100x300mm (4x12in) SAE 5145 alloy by cutting it in half, yielding two 100x150mm sections. A chromel-alumel thermocouple was hydrogen brazed to the center of the bottom half. The thermocouple wires were passed through a 13mm hole drilled through the top half of the bar. A steel tube, used as a handle, was welded to the top section, and both sections were then welded together. The cooling time-temperature data were collected using Speedomax equipment manufactured by Leeds & Northrup Company.

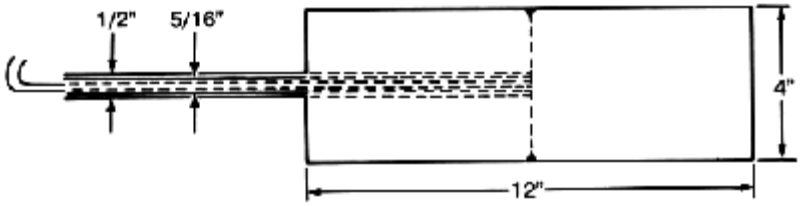

Fig 2.9 SAE 5145 Steel Probe used by Grossmann [27]

2.4.3 IVF probe

The IVF probe is based on the ISO9950 standard and is manufactured by the Swedish Institute of Production Engineering Research. The probe and system are described in the following paragraphs. The information in table 2.1 has been summarized from IVF Quench test, portable test equipment for quenching media [28].

Figure 2.10 shows IVF probe. The test probe is fastened to the handle using a standard thermocouple plug-and-socket connection. This allows measurement to be made, for example, with thermocouples embedded in components.

Table 2. 1 IVF Probe Characteristics [28]

IVF PROBE	
Probe size	Probe body: Φ12.5 mm x 60 mm Overall Length: 600 mm
Material	Inconel 600
Thermocouple Location	Center along long axis
Weight	Handle 0.45kg, test probe 0.35kg
Acc./Fixtures	Handle with start button
ISO 9950 Compliant	Yes

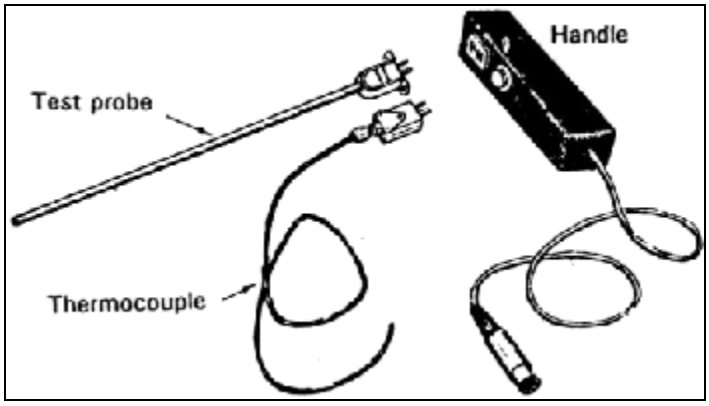

Fig 2.10 IVF test probe and handle [28]

IVF probe has many applications due to its portability; these applications can be listed as follows [28]:

- On-site measurement of the cooling characteristics of a quenchant, directly in the quench tank, so as to test the cooling performance at various positions in the

quench tank, check the effect of the rate of flow on cooling performance and follow changes in the cooling performance of a quenchant.

- ❖ Laboratory measurements
- ❖ Tests with different quenchants e.g. oils, polymers, water and salt
- ❖ Incoming inspection of quenchants

2.4.4 The Drayton Probe

The following tables and paragraphs describe the Drayton Probe System. The system is used for routine quality testing, diagnostic work, safety checks, process control, quenchant selection and development of new formulations. The data has been summarized from Drayton Probe Systems: Quenchalyzer [29]

Table 2. 2 Drayton Probe Characteristics [29]

	Drayton Probe
Probe Size	12.5 mm Diameter x 60 mm length
Overall Length	375 mm, 750 mm
Material	Inconel 600
T/C Location	Center along long axis
Acc./Fixtures	None
ISO 9950 Compliant	Yes

Drayton probe and the portable quenching system can be seen in figure 2.11. This system has the key features and benefits: in-plant or laboratory use; static or agitated testing; suitable for oils, aqueous polymers, salt or brine; high level of test reproducibility and consistency; extensive windows based software; provides instant graphic and numeric comparisons.

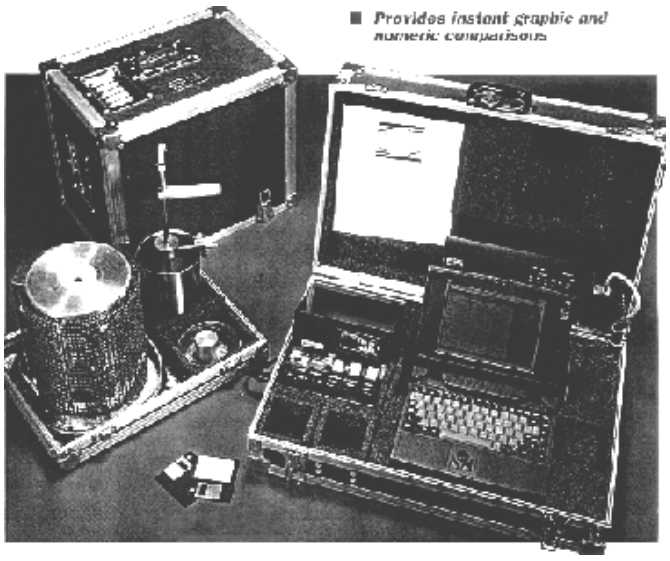

Fig 2.11 Drayton probe and the portable quenching system [29]

2.4.5 Nanigian-Liscic Probe

The LISCIC -NANMAC probe, as shown in figure 2.12, is a cylindrical probe 200 mm long and 50 mm in diameter. It is made of AISI304 steel and is instrumented with three thermocouples placed on the same cross-section plane in the middle of the probe's length. One thermocouple is placed at the surface. This thermocouple is a special type, which utilizes flat ribbon and is known as "self-renewing" thermocouple. The second thermocouple is placed at 1.5 mm below the surface and the third one at the center of the cross-section. This probe is reported to be particularly sensitive for measuring heat flux during quenching because it measures the temperature gradient from the surface to the center of the probe. The key feature of this probe is that it measures and records the temperature on the very surface of the probe, with a very response time of (10^{-5} sec.). The probe is capable of recording fast changing temperatures.

The software used with the probe (TGQAS) calculates heat transfer coefficients on the probe surface and cooling curves in any arbitrary point of the round bar cross-

section of different diameters. The software also predicts microstructure and hardness in any of those points after quenching, for every steel grade the CCT diagram of which are stored in the software.

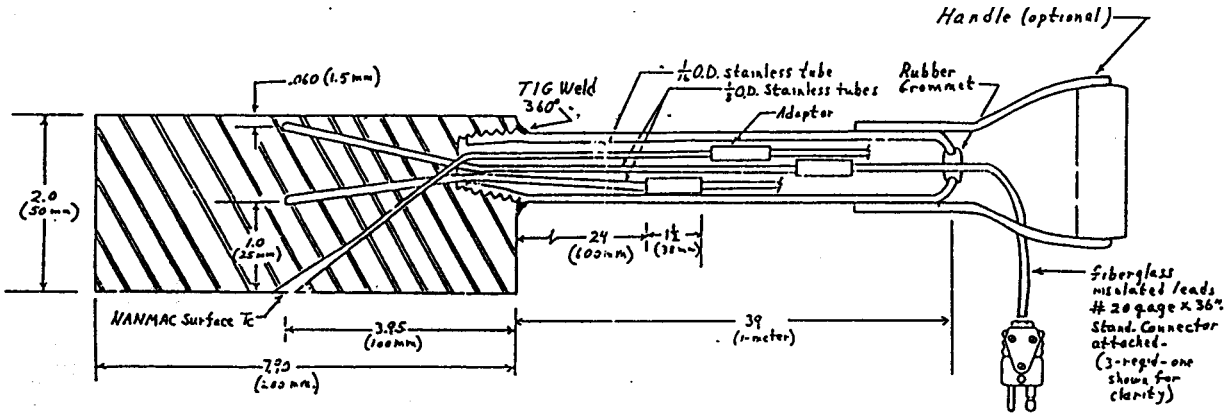

Fig 2.12 Schematic of Liscic-NANMAC probe--TGQAS Temperature Gradient Quenching Analysis System by Prof. Bozidar Liscic [1]

2.4.6 Tamura's Probes

In order to gain insight into the quenching process, it has been proposed that it is critically important to model the heat-transfer properties that occur at the metal surface during quenching. In such an analysis, the quenchant is considered to be a heat-transfer fluid that controls the rate of heat loss over the range of metal temperatures during the quenching cycle. Thus, the heat-transfer properties of the quenchant determine the metallurgical properties obtained [5].

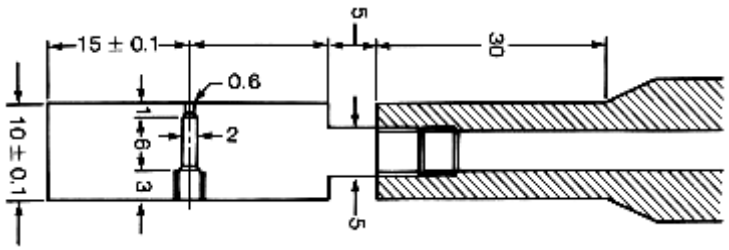

Fig 2. 13 JIS silver probe [5]

Tagaya and Tamura [30] developed a Japanese Industrial Standard (JIS) for cooling curve acquisition that utilizes a cylindrical silver probe with a thermocouple assembly specifically constructed to determine the surface temperature change with time during quenching. The JIS probe, as shown in figure 2.13, was used by Tamura in his classic work describing the development of master cooling curves [30] and quench oil characterization [31], but it has not gained wide acceptance in Western industry since the concern has been expressed regarding the cost of silver used in the probe construction, problems in maintaining a clean surface and the comparative difficulty of preparing delicate surface thermocouple assemblies.

2.5 Cooling curve analysis

Various methods have been developed to simplify the measurement of cooling power, including the General Motors (GM) quenchometer, the hot wire test, the 5-second interval test, and the cooling curve test. Of these procedures, the cooling curve test has been generally accepted as the most useful means of describing the mechanisms of quenching [32]. Cooling curves are particularly sensitive to factors that affect the ability of quenchants to extract the heat, including quenchant type and physical properties, bath temperature and bath agitation.

2.5.1 Data Acquisition and Cooling Curve Analysis

The need to acquire sufficient data to adequately define a cooling curve for subsequent analysis has long been recognized. Special data acquisition devices, including hardware such as oscillographs, were used for work reported by Jominy, French and

others [5]. However, this equipment is difficult to calibrate, which has inhibited widespread use of cooling curve analysis. Currently, sufficient data acquisition rates can be achieved with personal computers equipped with analog-to-digital (A/D) converter boards.

Although computer hardware is available, there are no published guidelines for selecting a data acquisition rate, which varies with probe alloy, size and quench severity. Probably the best method for selecting the required acquisition rate is to determine it experimentally [5]. This can be done by repeatedly quenching a probe in cold water, one of the more severe quenchants, and collecting data at various acquisition rates and comparing which data acquisition rate can give a smooth cooling rate curve in the maximum cooling rate region. Although higher data acquisition rates are preferred, they may lead to data storage problems.

After sufficient data are collected, cooling curve analysis can be started. Cooling curves are relatively easy to obtain experimentally by using an apparatus that typically consists of an instrumented probe and a system for data acquisition and display. Such system can be purchased or custom built. Either way, it is important that the user understand the basic system components [5]. One of the most important components is the quench probe used for cooling curve acquisition. There are a variety of quenching probes, as mentioned in section 2.4. To choose which kind of probe to use depends on the specific condition and requirement. Figure 2.14 shows two representations of the cooling curve data. The cooling data can be plotted as time-temperature, cooling rate-temperature or cooling rate-time curves.

Cooling curves analyses commonly use probes with spherical and cylindrical geometries. However, plate-shaped probes [33] are occasionally chosen when the primary focus is to model cooling and heat transfer from plate stock.

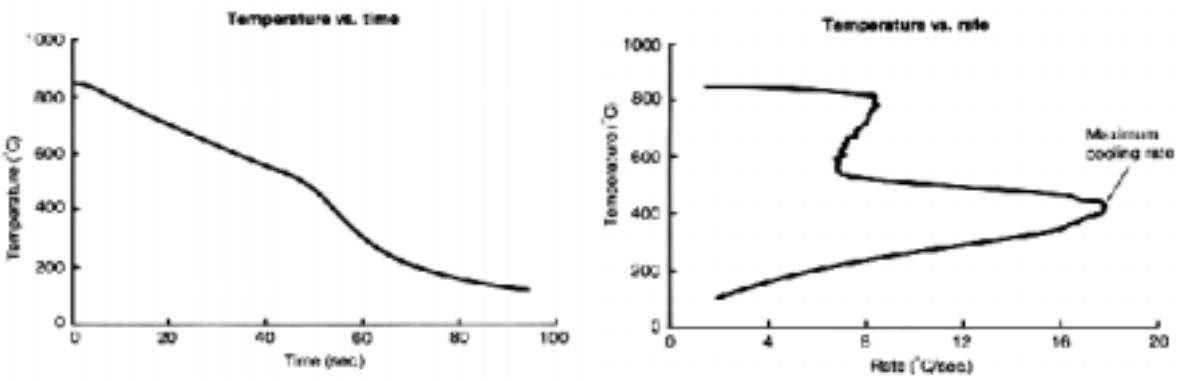

Fig 2.14 various representations of cooling curve data [5]

2.5.2 Interpretation of cooling curves

Once the cooling time-temperature data are in hand, they must be interpreted. Ideally, cooling curves should be correlated with metallurgical properties of interest.

One of the oldest methods of cooling curve interpretation involved taking the first derivative of the time-temperature curve obtained during the quenching of a probe with the desired cross section [5] to obtain the maximum cooling rate of the specific quenchant. The cooling curve can also be interpreted by comparison with CCT diagrams, as shown in figure 2.15. By comparing the maximum cooling rate and the critical cooling rate read from CCT diagram, which is considered to be the cooling rate at the nose of the austenite-to-pearlite transformation curve, the phase transformation during quenching can be determined. To obtain maximum hardness in a quenched part, it would be necessary to

select a quenchant that produces a maximum cooling rate equal to or greater than the critical cooling rate.

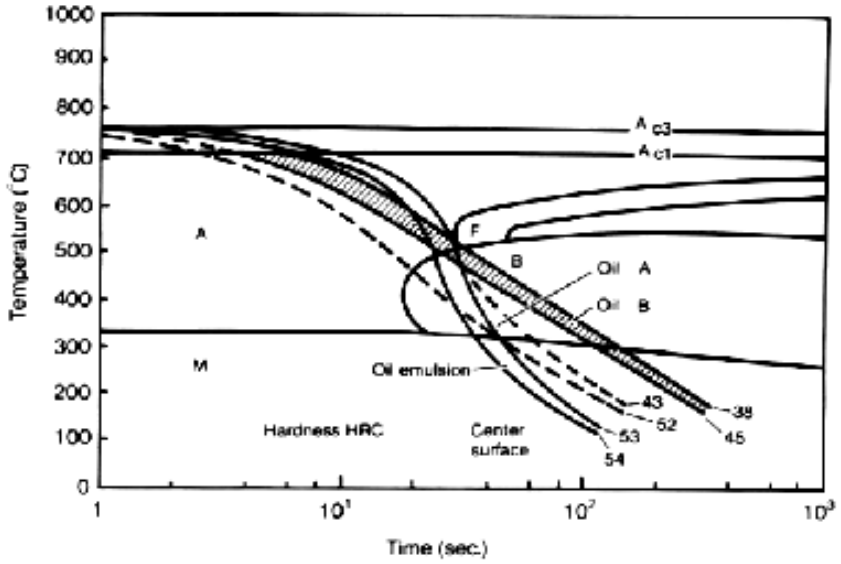

Fig 2.15 CCT diagram for a spring steel (50M7) with superimposed cooling curves [5]

Liscic [34] demonstrated that one method of obtaining a useful correlation between cooling rates during a quench and hardness was to integrate the area under cooling rate curves. A plot of accumulated area versus time can then be used to quantify the progression of the quench cycle. Thelning [35] reported a similar method involving the integration of the area under the cooling rate curve between two temperatures, e.g. 600 to 300^{o}C.

To simplify cooling curve interpretation, Tamura et al. developed a quantity called the "V-value", which is proportional to the ability of an oil quenchant to harden steel [31]. The cooling rate can also be related to Grossmann quench severity factor, which is an indication of the hardness of the as-quenched specimen, and such quenchant performance indices as hardening power, Castrol index and quench factor, which will be discussed in detail in section 2.7.

2.6 Metallurgy of 4140 Steel and 304 Stainless Steel

2.6.1 Characteristics and TTT diagram of 4140 steel

According to their carbon content, the plain carbon steel can be categorized as high-carbon steel (>0.60%), medium-carbon steel (0.30-0.60) and low-carbon steels (<0.30%). [36] 4140 can be classified as the medium-carbon steels with the chemical composition of 0.38-0.43 C by weight.

AISI 4140 steel is made with chromium and molybdenum alloy additives. Chromium from 0.5 to 0.95% is added with a small amount of molybdenum (from 0.13 to 0.20%). These small amounts of these two elements increase the strength, hardenability and wear resistance of the 41xx series of alloy steels [37].

The chemical composition and typical applications of 4140 steels are listed below: AISI-SAE 4140 steel has 0.40 % Carbon, 0.58% Manganese, 0.95% Chromium, and 0.20% Molybdenum. Low alloy steels with chromium and molybdenum, because of their increased hardenability, can be oil quenched to form martensite instead of being water quenched since the slower oil quench reduces temperature gradients and internal stresses due to volume contraction and expansion during quenching. Distortion and cracking tendencies can be minimized.

4140 is among the most widely used medium-carbon alloy steels. Relatively inexpensive considering the relatively high hardenability 4140 offers. Fully hardened 4140 ranges from about 54 to 59 HRC, depending upon the exact carbon content. Forgeability is very good, but machinability is only fair and weldability is poor, because of susceptibility to weld cracking [38].

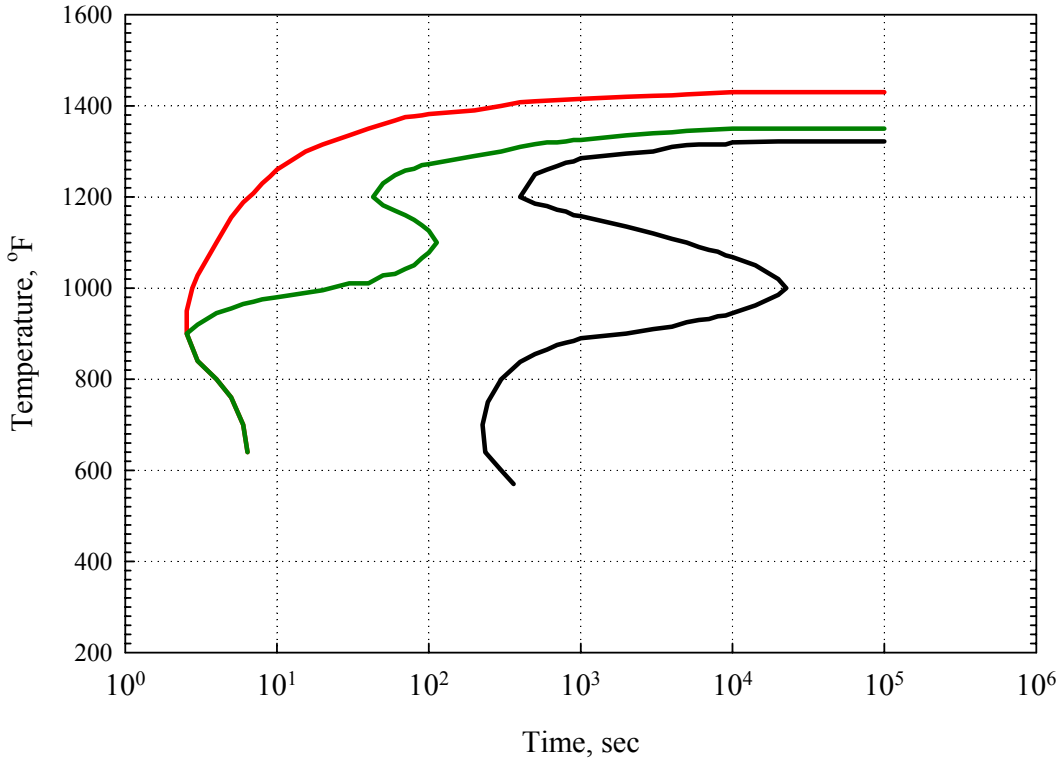

Fig 2. 16 TTT diagrams of AISI 4140

Figure 2.16 is TTT diagram of AISI 4140, which indicates the phase transformation from austenite to martensite or bainite or pearlite depending on the cooling rate that can be achieved from specific quenchant. Such diagram is valuable since the cooling curve can theoretically be superimposed upon it to predict heat-treatment response. The steel begins to transform at the Ms Temperature and is fully hardened at the Mf temperature.

The starting and ending temperature of martensitic transformation Ms and Mf, which is quite critical for understanding of quenching process of 4140 steels, can be read from the diagram. Ms = 640°F = 337.78°C and Mf = 425°F = 218.33 °C. Also in order to get the complete martensite and avoid the formation of pearlite or bainite, the quenchant

must be able to cool the component fast enough to miss the nose of the curve for pearlite formation.

The microstructure of alloy 4140 after being fully annealed at 691°C consists of a blocky ferrite and course pearlite. After austenitizing at 843°C and oil quenching a martensitic structure is produced and with subsequent tempering at 315°C, a fine tempered martensitic structure is the result. Martensite in low alloy steels consists of packets of fine units of martensite called laths that align themselves parallel to one another to form packets [37]. The orientation of the units or laths within a packet is limited, and frequently large volumes of laths within a packet have only one orientation. Therefore many of the boundaries within a packet are low-angle and as an approximation, the entire packet has essentially one orientation.

The mechanical properties of normalized and annealed low-alloy AISI 4140 steel are the following [1]:

Table 2. 3 Mechanical properties of normalized and annealed 4140 [1]

AISI No	Treatment	Yield Strength (psi)	Tensile Strength (psi)	Elongation %	Reduction in area %	Hardness .Bhn	Impact Strength (IZOD) ft-lb
4140	Normalized (1600 °F)	95000	148000	17.7	46.8	302	16.7
	Annealed (1500 ° F)	60500	95000	25.7	56.9	197	40.2

Table 2. 4 Mechanical Properties of quenched and tempered 4140 steels [1]

AISI No	Tempering Temp. °F	Tensile strength (psi)	Yield Strength (psi)	Elongation %	Reduction in area %	Hardness Bhn
4140	400	257000	238880	8	38	510
	600	225000	208000	9	43	445
	800	181000	165000	13	49	370
	1000	138000	121000	18	58	285
	1200	110000	95000	22	63	230

2.6.2 Characteristics of 304 stainless steel

The stainless steels can be categorized by a structure nomenclature: Austenitic, Ferritic and Martensitic stainless steels [39]. The austenitic stainless steels represent the largest group of stainless steels in use, making up 65 to 70% of the total for the past several years. The austenitic alloys used most often are those of the AISI 300 series. Collectively, these enjoy their dominant position because of a general high level of fabricability and corrosion resistance and because of the varied specific combinations of properties that can be obtained by different compositions within the group, providing useful material choices for a vast number of applications. Types 302 and 304 have somewhat greater stability and improved corrosion resistance [39]. Type 304, one of the alloys of AISI 300 series based on the Fe-Cr-Ni ternary system, is the most widely produced stainless steel and is used considerably at elevated temperatures.

According to the ternary diagram for Fe-Cr-Ni system, generally compositions approximating the leaner AISI 300-series stainless steels would be predicted to fall either within the $\alpha+\gamma$ field or just outside of it, depending on the specific composition. Figure 2.17 is the cross sections of Fe-Cr-Ni ternary, which reveals how the shape of the austenite (γ) field changes with increasing total nickel plus chromium contents. At 70,80 and 90% iron, the $\gamma/(\alpha+\gamma)$ boundary slants backward such that a fully austenitic alloy close to boundary at 1000^{o}C can contain some ferrite when heated. For type 304, according to its composition 18-20% Cr, 8-12%Ni, it is within $\alpha+\gamma$ region below 1300^{o}C, as shown by the arrow in the figure, which means if 304 type of probe is quenched at 850^{o}C, then quenching process will start with $\alpha+\gamma$.

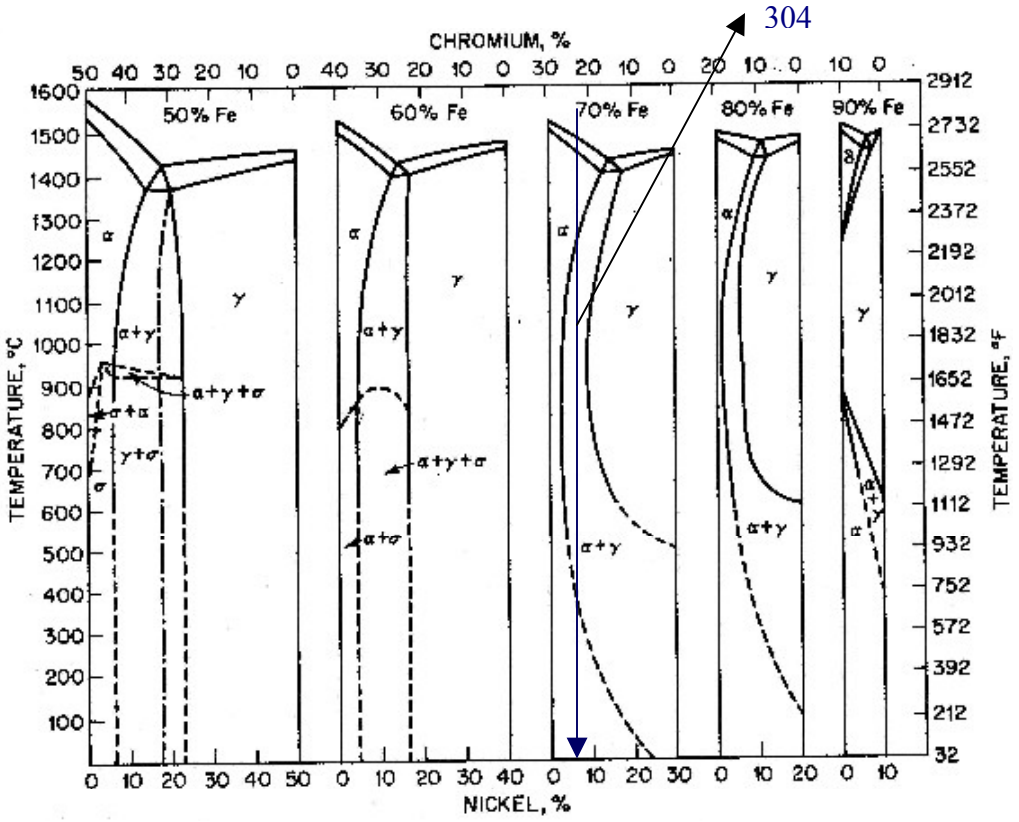

Fig 2. 17 Cross sections of Fe-Cr-Ni ternary diagram [39]

2.6.3 Theoretical understanding of heat transfer

Heat transfer during quenching of hot metal parts is controlled by different cooling mechanisms at three different quenching stages: film boiling, nucleate boiling and convection, as mentioned in the previous sections. The parameters that affect the heat transfer during quenching in liquid quenchant will be identified and discussed below phase by phase.

2.6.3.1 Film boiling heat transfer

Upon immersion into the quench fluid, the part will first be surrounded by vapor blanket; the quenching starts with the film boiling. In this range heat transfer rate is minimum and heat transfer occurs mainly through radiation. The part cools slowly in this

regime. As the part cools, film becomes unstable and the mechanism is then called partial film boiling or transition boiling.

The total heat transfer coefficient during film boiling is generally expressed as the sum of a convective coefficient, h_c, and an effective radiation coefficient (fh_r), where f is a constant. The heat transfer coefficient has different expressions depending on the geometry and orientation of the part being quenched. For *Film boiling on horizontal plates,* Sciance et al [45] model is found to be very good when compared with experimental results on four organic liquids. For minimum heat flux in the film boiling regime, the equation for convective heat transfer coefficient using this model is

$$h_c = 0.425\left\{\frac{(k_G)^3 H'_{fg}\rho_G g(\rho_L-\rho_G)}{\mu_G(T_w-T_{sat})[g_c\sigma/g(\rho_L\rho_G)]^{1/2}}\right\}$$

This equation can also be expressed in generalized form as

$$(Nu_B)_f = 0.425(Ra_B^*)_f^{1/4}\left[\frac{H'_{fg}}{c_{pG}(T_w-T_{sat})}\right]_f^{1/4} \qquad \text{Eqn. 2.6.3-1}$$

Where $(Nu_B) = \dfrac{h_c B}{k_G}$

$$(Ra_B^*) = Gr_B^* \Pr_G = \left[\frac{B^3\rho_G(\rho_L-\rho_G)g}{\mu_G^2}\right]\left(\frac{c_{pG}\mu_G}{k_G}\right)$$

B = Laplace reference length = $\left[\dfrac{g_c\sigma}{g(\rho_L-\rho_G)}\right]^{1/2}$

And f (subscript) means that the physical properties of the vapor are evaluated at pressure p_L and temperature T_f.

For *Film Boiling on horizontal cylinders,* Sciance et al [45] suggested the following correlation for horizontal cylinder

$$\left(Nu_B\right)_f = 0.369\left[\frac{Ra_B^*}{\left(T_r\right)^2}\right]_f^{0.267}\left[\frac{H'_{fg}}{c_{pG}\left(T_w - T_{sat}\right)}\right]_f^{0.267} \qquad \text{Eqn. 2.6.3-2}$$

Which is based on their study of methane, ethane, propane and n-butane on the surface of horizontal gold-plated cylinder 0.81 in. in diameter by 4 in. long.

For *Film Boiling on a Vertical Surface,* Bromley [46] recommended an equation very similar to Eqn. (2.6.3-2), with a change in the characteristic length *D* and *L* is the vertical distance from the bottom of the plate. Hsu and Westwater [47] modified the correlation considering boundary layer above the heated surface and its transition from laminar to turbulent flow. The correlation becomes

$$\left(Nu_L\right)_f = 0.943\left(Ra_L^*\right)_f^{1/2}\left\{\frac{H_{fg}\left[1 + 0.34c_{pG}\left(T_w - T_{sat}\right)/H_{fg}\right]^2}{c_{pG}\left(T_w - T_{sat}\right)}\right\}^{1/2} \qquad \text{Eqn. 2.6.3-3}$$

Equations 2.6.3-1, -2 and-3 can be combined together and simply represented with the following form:

$$\left(Nu_B\right) = M\left(Ra\right)_L^m\left[\frac{AH'_{fg}}{c_{pG}\left(T_w - T_{sat}\right)}\right]^n \qquad \text{Eqn. 2.6.3-4}$$

Where M, A, l and n are constants. From equation 2.6.3-4 and the definition of Ra number, it can be seen that heat transfer coefficient can be affected by such factors as the viscosity of vapor film and the liquid quenchant, surface tension, the density of vapor film and the liquid quenchant, the latent heat and the specific heat. If these properties are known, then the heat transfer coefficient in film boiling stage can be calculated. Among these the heat transfer coefficient is proportional to the reciprocal of the viscosity, which means the heat transfer coefficient will decrease with the increase in the viscosity of the quenchant, given other properties constant.

2.6.3.2 Nucleate boiling heat transfer

With further decrease in temperature, partial films are broken into numerous bubbles and the quench media contacts the part directly. The liquid near the hot surface becomes superheated and tends to evaporate, forming bubbles wherever there are nucleation sites such as tiny pit or scratches on the surface. The bubbles transport the latent heat of the phase changes and also increase the convective heat transfer by agitating the liquid near the surface. This corresponds to rapid heat transfer. The part is still very hot and the quench media boils vigorously. In this regime, heat transfer is very high for only a small temperature difference.

The heat removed from the heated surface by the boiling liquid is assumed to be by the following mechanisms:

(i) heat absorbed by the evaporating microlayer (q_{ME});

(ii) heat energy expended in re-formation of the thermal boundary layer (q_R) and

(iii) heat transferred by turbulent natural convection (q_{NC}).

The total boiling heat flux is obtained from the above three fluxes [48] as

$$q_{tot} = \frac{q_{ME} t_g + q_R t_w}{t_g + t_w} + q_{NC} \qquad \text{Eqn. 2.6.3-5}$$

The heat flux associated with the microlayer evaporation [49] is given by

$$q_{ME} = \frac{\gamma \phi \sqrt{\pi}}{10} B^2 Ar^{0.27} Ja(\alpha_l)^{3/2} \cdot \sqrt{t_g} \rho_l H_{fg} \left(\frac{N}{A} \right) \qquad \text{Eqn. 2.6.3-6}$$

Where N/A is the nucleation site density, $\gamma = \sqrt{\left(\frac{k_s \rho_s C_{ps}}{k_l \rho_l C_{pl}} \right)}$, $\phi = \left[1 - \left(\frac{D_d}{D} \right)^2 \right]$ and D_d is the diameter of the dry area under the bubble.

$$Ja = \frac{c_p \rho_L (T_w - T_b)}{H_{fg} \rho_G},\ Ar = \left(g/\nu_l^2\right) \cdot \left(\sigma/\rho_l g\right)^{3/2}.$$

The heat flux associated with the thermal boundary layer re-formation [49] is

$$q_R = 2\sqrt{\left(\frac{k_l \rho_l C_{pl}}{\pi t_w}\right)} \cdot \left(\frac{N}{A} \cdot a\right) \cdot \left(T_w - T_{sat}\right) \qquad \text{Eqn. 2.6.3-7}$$

Using the heat transfer coefficient McAdams [50] estimated in turbulent natural convection, the heat flux due to turbulent natural convection can be estimated from

$$q_{NC} = \frac{0.14 k_l}{L} (Gr \cdot \Pr)^{1/3} \left[1 - \left(\frac{N}{A}\right) \cdot a\right] \cdot \left(T_w - T_{sat}\right) \qquad \text{Eqn. 2.6.3-8}$$

From the expressions in equations 2.6.3-5,6,7 and 8, it can be said that the kinetic viscosity, density, specific heat, latent heat, the temperature between the heated part and the quenchant, surface tension and the thermal conductivity are playing important roles in the calculation of heat flux (heat transfer coefficient). Also the heat flux is proportional to $(1/\nu)^n$, which indicates the heat flux increases as the kinetic viscosity decreases.

2.6.3.3 Convection heat transfer

The last regime is the natural convection regime; the surface of the part has cooled to a temperature below the boiling point/range of the quench media. The heat is transferred by the natural convection of the liquid.

Churchill [51] suggested a general convection correlation that is applicable to a variety of natural convection flows for which the primary buoyant driving force is directed tangential to the surface. The correlation is given by

$$\overline{Nu}_L = \left(a + 0.331 b (Gr \Pr)_L^{1/6}\right)^2 \qquad \text{Eqn. 2.6.3-9}$$

Where, $b = \frac{1.17}{\left[1+\left(0.5/\mathrm{Pr}\right)^{9/16}\right]^{8/27}}$

$$\left(Gr_x = \frac{g\beta(T_w - T_\infty)x^3}{\nu^2}\right)$$

$$Pr_L = \frac{c_p \nu}{k_L}$$

The empirical constant *a* varies for various geometries [51].

In convection stage, equation 2.6.3-9 shows the heat transfer can be related to the kinetic viscosity, the specific heat, the thermal conductivity, the coefficient of thermal expansion, the temperature difference between the hot metal part and the liquid and also the distance from the leading edge of the boundary layer formed on the heated surface x.

In summary, many physical properties of the quenchant affect the calculation of heat transfer coefficient during the quenching process: the viscosity, the specific heat, the surface tension, the density, the latent heat and the thermal conductivity. From these values the heat transfer coefficients can be calculated for each quenching stage. However, some of these properties are very hard to measure. Among these physical properties, the viscosity of the quenchant is relatively easier to obtain and also plays an important role in the calculation of heat transfer coefficient since it is proportional to the reciprocal of heat transfer coefficient. Therefore, the quenching performance of the mineral oil based quenchant is correlated with their viscosities in this work to determine how heat transfer coefficient changes with the viscosity.

Table 2.5 gives the definition of all the variables shown in the above equations.

Table 2. 5 Nomenclatures

a	area of influence of the bubble on the heating surface	T_b	boiling temperature
A	area of the heating surface	V	velocity
Ar	Archimedes number	Δp	pressure drop
B	constant	α	thermal diffusivity
C_p	specific heat at constant pressure	γ	a parameter
D	instantaneous bubble diameter	δ	Boundary/thermal layer thickness
D_b	departure diameter of the bubble	μ	viscosity
D_d	diameter of dry area under the bubble	λ	latent heat of vaporization
G	Volumetric flow rate	ν	kinematic viscosity
g	Acceleration due to gravity	ρ	density
g_c	Conversion ratio	σ	surface tension
Gr	Grashof number	ϕ	parameter
h	heat transfer coefficient	*Subscripts*	
H_{fg}	Latent heat of evaporation	*	refers to critical value, or nondimensional parameter
Ja	Jacob number	*crit*	refers to critical value
K,k	thermal conductivity	*l*	liquid
N	Number of active nucleation sites	*sat*	saturation
P	external pressure	*tot*	total
Pr	Prandtl number	*v*	vapor
q,q''	heat flux	*w*	wall
R_a	roughness	*s*	solid
t_g	bubble growth time	*Superscripts*	
t_w	waiting time to grow new bubble	*f*	Refers to saturated liquid
T	temperature	*fg*	Refers to phase change from liquid to vapor
T_w	wall temperature	*g,G*	Refer to gas or vapor condition

2.6.4 Calculation of heat transfer coefficient

The calculation of heat transfer coefficient is very critical for understanding the quenching performance of different quenching media. Generally there are three important modes of heat transfer: heat conduction, thermal radiation and heat convection. But since

the thermal resistance to conduction in the solid is small compared to the external resistance and also the probe tip in our experiments is very tiny, so we may ignore small differences of temperature within the probe, assume that the spatial temperature within the system is uniform and only consider the convective heat transfer between probe tip and quenching fluid. This approximation is called the *lumped thermal capacity model* [52]. This model is valid when the Biot number (Bi) is much less than 0.1 and can be expressed by the following equations:

$$-h_c A (T-T_e) = \rho V C_p(T) dT/dt \qquad \text{Eqn. 2.6.4-1}$$

Where:

h_c=heat transfer coefficient averaged over the surface area, W/m^2-K

A=surface area, m^2

T=temperature of the wall, ^oC

T_e=temperature of the oil, ^oC

ρ=Density, kg/m^3

V=volume, m^3

$C_{p=}$specific heat, J/kg*^oC

dT/dt=derivative of the temperature with respect to time.

To use cooling rate data to calculate the average heat transfer coefficient the following must be considered. This solution must assume constant surface area, density, specific heat, and volume. The specific heat in a quenching application can vary. The density can also vary but to a lesser extent.

Rearranging equation 2.6.4-1,

$$h_c = \rho \frac{V}{A} C_p(T) \frac{dT}{dt} (T - T_e) \qquad \text{Eqn. 2.6.4-2}$$

For cylindrical probe tip,

$$\frac{V}{A} = \frac{\pi r^2 * H}{2\pi r * H} = \frac{r}{2} \qquad \text{Eqn. 2.6.4-3}$$

Where,

H- height of cylindrical probe tip

r- radius of probe tip

Also, the biot number can be calculated using the equation 2.6.4-4 as follows.

$$\text{Biot} = h L_c / k. \qquad \text{Eqn. 2.6.4-4}$$

Where:

h=mean heat transfer coefficient

L_c=Volume/Surface Area, (approximately =radius/2 for a cylinder)

k=thermal conductivity of the steel

For calculation of the heat transfer coefficient in equation 2.6.4-2, ρ, V/A, and T_e are constant, since they are physical properties of the steel or oil. T and dT/dt are experimental data. However, the specific heat of the steel varies with the temperature. Therefore, how to choose the specific heat of the steel is important in determining the heat transfer coefficient. Also in equation 2.6.4-4, the thermal conductivity of the steel is also critical to calculate the Biot number. The selection of the specific heat and the thermal conductivity for 4140 steel and 304 stainless steel will be discussed as follows.

2.6.5 Thermoconductivity of 4140 steel and 304 stainless steel

Thermal conduction is the phenomenon by which heat is transported from high to low-temperature regions of a substance. Thermoconductivity is a measure of the rate at which a material transmits heat. If a thermal gradient of one degree per unit length is established over a material of unit cross-sectional area, then the thermal conductivity is defined as the quantity of heat transmitted per unit time [40]. It is best defined in terms of Fick's First Law:

$$q = -k\frac{dT}{dx} \qquad \text{Eqn.2.6.5.1}$$

Where,

q - Heat flux or heat flow per unit time per unit area, W/m^2.

k – thermal conductivity, W/m*K.

dT/dx – Temperature gradient through the conducting medium, K/m

There are a variety of methods for the measurement of thermal conductivity due to the difficulty of obtaining a controlled heat flow in a prescribed direction such that the actual boundary conditions in the experiment agree with those assumed in the theory. Generally these methods fall into two categories: the steady-state and the nonsteady-state methods. In the steady-state methods of measurement, there are longitudinal heat flow method, the Forbes' bar method, the radial heat flow method, the direct electrical heating method and the thermal comparator method. In the category of nonsteady-state methods, there are the periodic and the transient heat flow methods [41].

The thermal conductivity, k, is a function of temperature. For 4140, it can be obtained from two different sources: I) ASM Metals Handbook (1977) [36]. Adding the polynomial trendline into the scattered data points generated the following polynomial

equation, which indicated the variation of thermal conductivity with temperature, $k = 10^{-7}T^3 - 0.0002T^2 + 0.0327T + 40.82$, W/m*K. II) Thermophysical Properties of Matter (TPRC) (1970) [41]. In the same way, one polynomial equation was generated from the original data. $k = 5*10^{-8}T^3 - 8*10^{-5}T^2 + 0.014T + 40.197$, W/m*K. The more recent data of the thermal conductivity from ASM Metals Handbook is used in calculating the Biot number for 4140 steels.

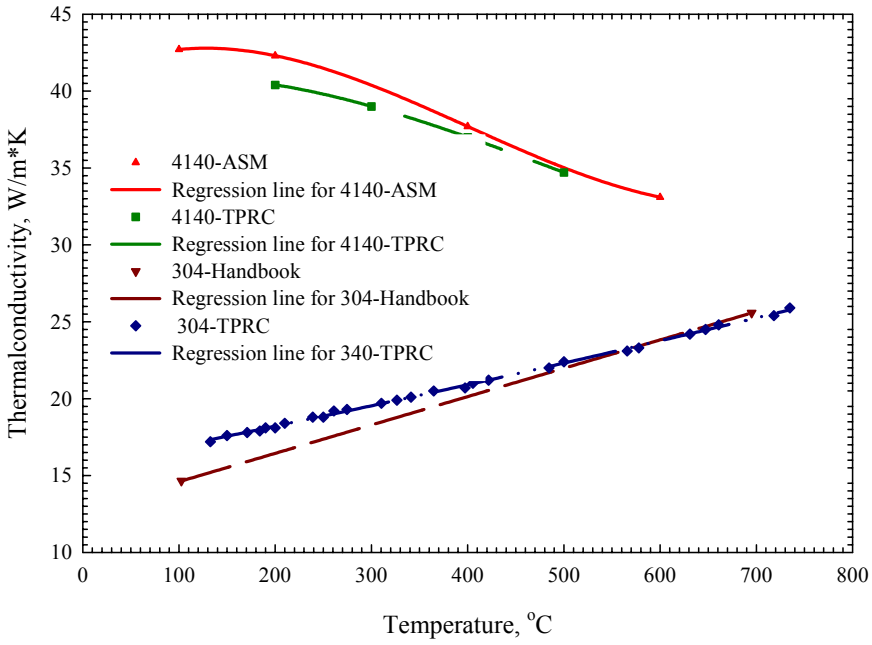

Fig 2. 18 Thermal conductivity of 4140 steels and 304 stainless steels [39] [41] [32]

For 304 stainless steel, the thermal conductivity data can be obtained from (1) Handbook of Stainless Steels [39], one equation can be generated as k = 0.0184T + 12.751, W/m*K; (2) Thermophysical Properties of Matter (TPRC) [41], the following equation can be obtained: $k = 2*10^{-6}T^2 + 0.0123T + 15.66$, W/m*K. The TPRC data was chosen since the original data have more data points. All the thermal conductivity curves for 4140 steel and 304 stainless steel are shown in Figure 2.18.

2.6.6 Specific Heat of 4140 steel and 304 stainless steel

A solid material, when heated, experiences an increase in temperature signifying that some energy has been absorbed. Heat Capacity C_p is a property that is indicative of an alloy's ability to absorb heat from the external surroundings; it represents the amount of energy required to produce a unit temperature rise [40]. In mathematical terms, the heat capacity C_p is expressed as follows:

$$C_p = \frac{dQ}{dT} \qquad \text{Eqn. 2.6.6.1}$$

Where dQ is the energy required to produce a dT temperature change. Specific heat represents the heat capacity per unit mass and has various units. According to the environmental conditions accompanying the transfer of heat, there are two ways in which this property may be measured: one is heat capacity at constant volume C_v and the other is heat capacity at constant pressure C_p.

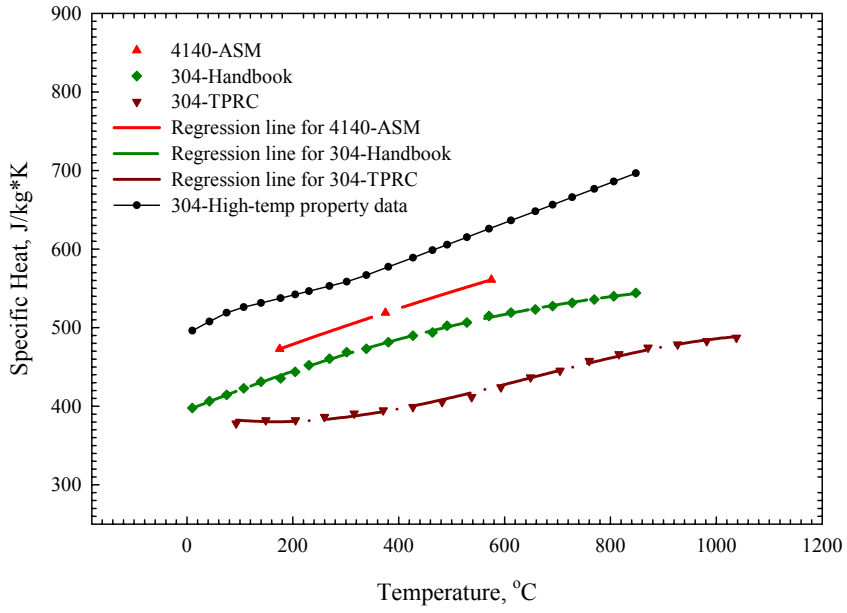

Fig 2. 19 Specific Heat of 4140 steels and 304 stainless steels [36] [1, 39, 42, 43]

The specific Heat data for 4140 whose phase transformation follows the Fe-Fe_3C phase diagram can be obtained from ASM (American Society of Metals) Metals Handbook [4], which can be fitted into one polynomial equation to cover the entire temperature range, $C_p = -5*10^{-5}T^2 + 02575T + 429.47$ J/Kg*K. Or two straight lines with slightly different slopes can be used to cover the entire range of temperature variation [1]. The equation used for temperatures under 375°C is C_p=0.23T+432.75 and the one for temperatures above 375°C is C_p=0.21T+440.25. The curves are shown in Figure 2.19. Both methods are compared; there is no much difference for calculation of heat transfer coefficient of 4140 steel probes.

However, for very fast cooling, 4140 steel probes transforms from austenite to martensite at 337.78°C, which makes the calculation of heat transfer coefficient more complex since it is hard to get specific heat for martensite structure. But we can assume the probe remains austenite during the quenching process and use the specific heat of austenite to do the calculation for the entire temperature range. Since it is not that easy to find the source for the specific heat of austenitic 4140, we can use the specific heat of pure austenitic iron to do some approximation. The red line in figure 2.20 is the specific heat for pure austenitic iron [44]. The dark red line is the specific heat for 4140 steel [36]. First at higher temperature, e.g. around 850°C, the difference between the specific heat of pure austenitic iron and that of 4140 steel is assumed to be ΔC_p, then by deducting ΔC_p from specific heat of pure iron the C_p of austenitic 4140 can be generated as shown in Figure 2.20, which can be used later to calculate the heat transfer coefficient of 4140 steel probe.

For 304 stainless steels, the specific heat data can be obtained from three sources: (1) Handbook of Stainless Steel (1977) [36], (2) Thermophysical Properties Research Center (1970) [42], (3) High-temperature Property Data: Ferrous alloys (1988) [43]. Since the third source gives the most recent data, so the C_p data from the third source was chosen for 304 stainless steel probe. Three linear segments are used in this case: at temperature below 83.2°C, C_p=0.3542T+492.58; 83.2<T<315.5°C, C_p=0.1665T+508.2; T>315.5°C, C_p=0.2551T+480.26. The curves of specific heat for 304 stainless steel are given in Figure 2.19.

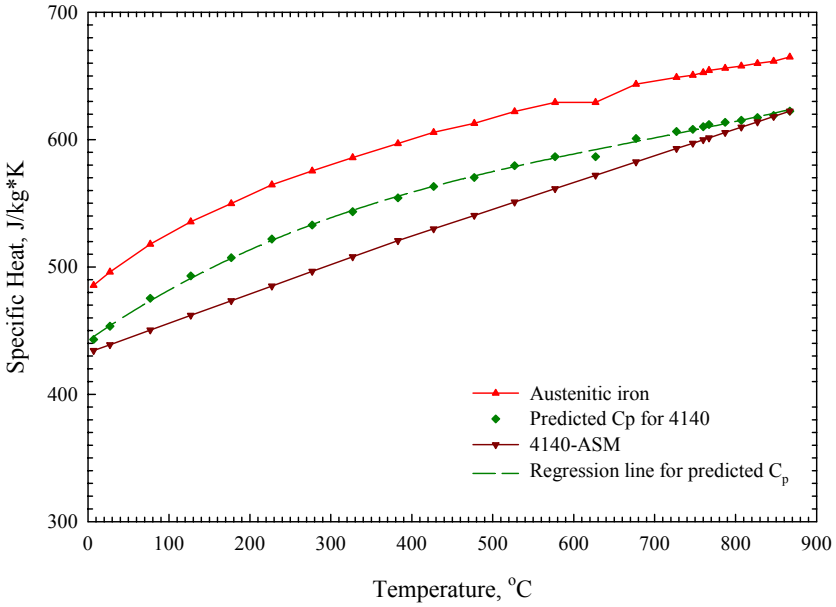

Fig 2. 20 Specific heat of austenitic iron and 4140 as a function of temperature [36, 42]

2.7 Quenching Performance Indices

The cooling characteristics of a quench oil depend on the base oil used, refinement processes, additives used to increase cooling capacity, and wettability.

Quench severity may be quantified the Tamura V Value, Relative Hardening Power (HP) by IVF, and Quench Factor Analysis.

2.7.1 Tamura V value

The V value was developed to characterize the ability of quenchant oil to harden steel [5]. The advantage of V values is that it includes steel transformation characteristics. V-values were calculated from cooling curves include steel transformation characteristics. The V-values are calculated from cooling curves and the Continuous Cooling Transformation Curve with the following relationship [5].

$$V=\left(Tc-Td/Ts-Tf\right) \qquad \text{Eqn. 2.7.1-1}$$

Where:

Tc=Temperature at the beginning of the second cooling stage, in ^{o}C

Td=Temperature at the beginning of the third cooling stage, ^{o}C

Ts=Temperature where martensitic transformation begins, ^{o}C

Tf=Temperature where martensitic transformation ends, ^{o}C

The use of the V-Value for quenchant classification was developed initially for oils that have cooling rates of similar Tc and Td. Synthetic quenchants exhibit significantly different cooling rates for those two temperatures and as a result this method should not be used for polymer quenchant characterization.

2.7.2 Hardening Power (HP) by IVF

The IVF, (Swedish Institute of Production Engineering Research) has tested oils available in Sweden. ISO9950 method has been used and hardening tests have been

carried out. In this way, the oils have been grouped according to their performance [1]. The criteria are, transition temperature between vapor phase and boiling phase, transition temperature between boiling phase and convection phase, and the critical cooling rate in the critical ferrite and pearlite nose temperature range. A simple formula for hardening power has been developed for comparison and classification of one oil relative to another.

Figure 2.21 shows the key parameters from the cooling curves and cooling rate curves that are considered in the hardening power equation of IVF.

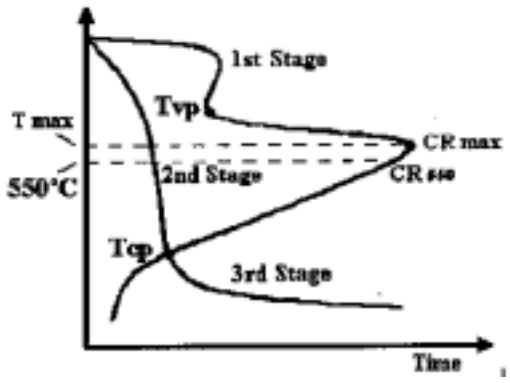

Fig 2. 21 Key parameters for IVF hardening power equation [1]

In order to enable the selection of adequate quenching oil IVF has derived a formula based on three characteristic points in the cooling rate curve for each of the oils. The International Federation of Heat Treaters (FHT) has approved this hardening power equation. Considering the temperature of transition from film boiling to nucleate boiling, the max cooling rate in the 500 ^{o}C to 600^{o}C range, and the transition temperature from nucleate boiling to convection regime, the hardening power is calculated from the regression equation that follows [1]:

$$HP = 91.5 + 1.34Tvp + 10.88CR - 3.85Tcp \qquad \text{Eqn. 2.7.2-1}$$

Where:

HP= Hardening power

Tvp=transition temperature between vapor phase and boiling phase

CR=cooling rate in °C/Sec. Over the temperature range (500-600) °C

Tcp=Transition temperature between the boiling phase and the convection phase, °C

The formula has been matched to a straight line by a method of least squares. The coefficients of the formula are chosen so that the range of HP values for oils considered is 10-1000. Some oils may have negative values (refer to figure 2-21). The formula is used for rating and comparison of oils and the hardening power (HP) is a dimensionless quantity.

Selecting characteristic points:

- Tvp must not be too low.
- The rate of cooling in the vapor phase also depends on the size.
- Small parts will be hardened even if cooling is carried out in quenching oil with a long vapor film phase.

Tamura and others have shown that different types of steels need different cooling characteristics to achieve maximum hardness. Tcp should be as low as possible in order to attained maximum hardness. If the temperature is above the Martensite start, bainite may form.

Cooling curve and hardening performance will vary depending on the degree of refining and additives. For lower alloy steels the ferrite and pearlite nose is displaced towards longer times, which means that the materials are more easily hardened.

Segerberg proposes different methods [53] for testing cooling power and for testing hardening oils that are ranked by hardening power (Figure 2.22).

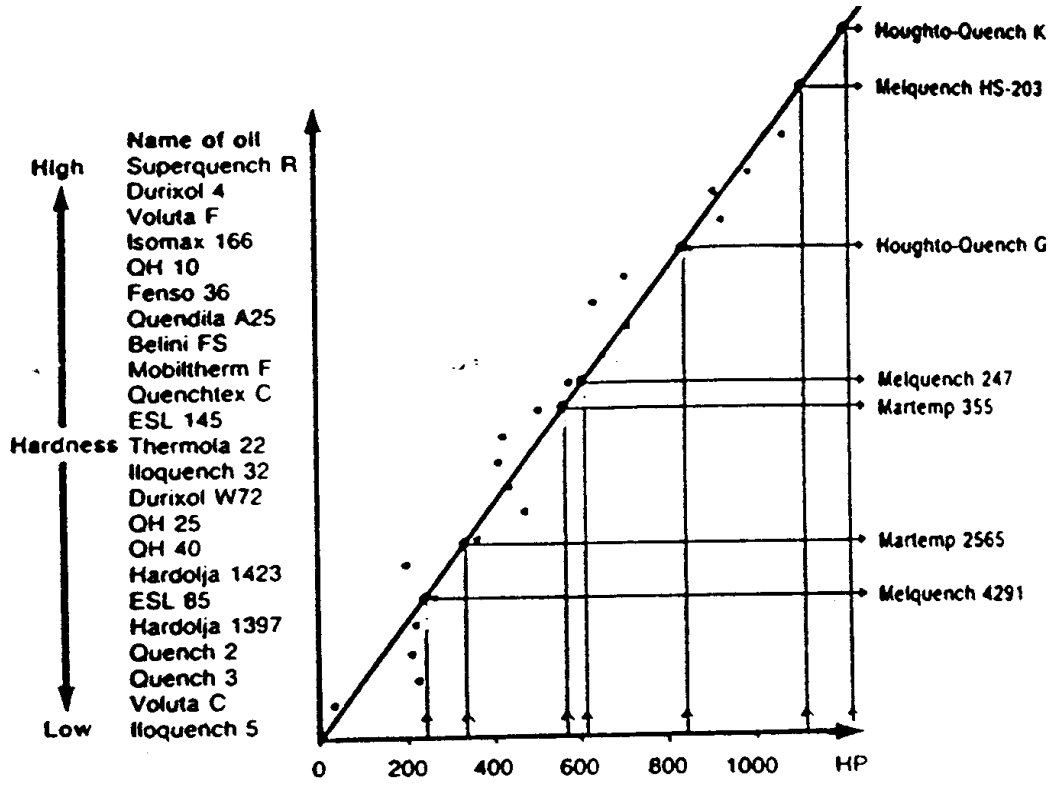

Fig 2. 22 Oils ranked by hardening power. Calculated values of hardening power HP, matched to a straight line for the quenching oils [53]

2.7.3 Quench Factor Analysis

To predict the metallurgical consequences of quenching, it is necessary to determine the heat transfer performance of the quenchant medium during the cooling process. Cooling curve analysis is considered an excellent method to obtain this information. Quench Factor analysis interrelates cooling curve shape with as quenched steel hardness [4]. This method provides a single number that interrelates the cooling rate produced by a quenchant and the transformation rate of the alloy as described by the time-temperature-property (TTP) curve [4]. This curve as shown in figure 2.23 is a

graphical representation of the start of a transformation curve that influences a property as hardness or strength.

The quench factor is typically calculated from the cooling curve and a C_T function, an equation that describes the transformation in the steel. The quench factor, Q, is calculated by determining the average temperature between the data points on the cooling curve. The C_T value is then calculated at that temperature using equation 2.7.3-1[4]:

$$C_T = -K_1 * K_2 * Exp\left[\frac{K_3 * K_4^{\,2}}{RT(K_4 - T)^2}\right] * Exp\left[\frac{K_5}{RT}\right] \qquad \text{Eqn. 2.7.3-1}$$

Where:[4]

C_T= critical time required to form a constant amount of a new phase or reduce the hardness be a specific amount

K_1= constant which equals the natural logarithm of the fraction untransformed during quenching (typically 99%: Ln (0.99)=-0.01005)

K_2= constant related to the reciprocal of the number of nucleation sites

K_3= constant related to the energy required to form a nucleus

K_4= constant related to the solvus temperature

K_5= constant related to the activation energy for diffusion

R= 8.3143 J/K*mole

T= absolute temperature (K)

Lower quench factor values are associated with higher hardness and strength [4]. The critical value is the maximum value that results in the desired hardness or strength and this value can be defined in terms of maximum amount of transformation during

cooling [4]. Quench factors can be calculated from time-temperature curves and the equation describing the transformation kinetics (C_T function).

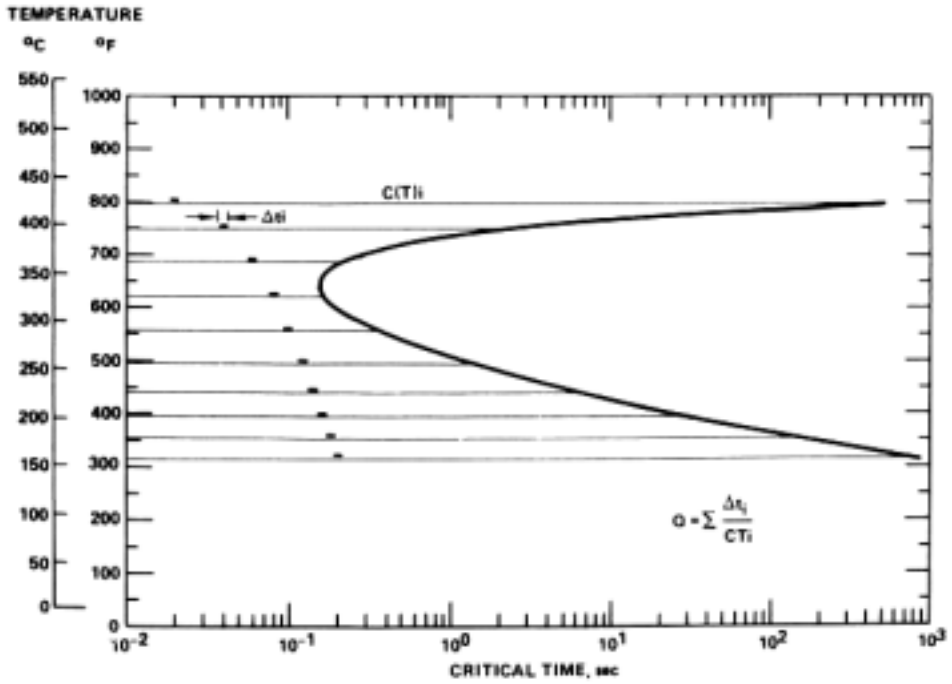

Fig 2. 23 Schematic illustrations on plot of C_T function to calculate the Quench Factor [54]

C_T is the time required to form 1% of new phase or to reduce the hardness by as specified amount (the locus of the critical time values as a function of temperature forms the TTP curve) [5]. The quench factor QF is calculated for each step of the cooling curve.

$$q_f = \frac{\Delta t_i}{C_{Ti}} \qquad \text{Eqn. 2.7.3-2}$$

Where:

Δt = Time step used in cooling curve data acquisition.

The incremental quench factor represents the ratio of the amount of time steel was at a particular temperature divided by the time required for a specific amount of transformation, typically 1% at a temperature [5].

The incremental quench values are summed up over the entire transformation range between Ar_3 (Austenitizing) and M_s (Martensite start) to produce the cumulative quench factor Q_f:

$$Q_f = \sum q_f = \sum_{T=M_s}^{T=Ar_3} \frac{\Delta t_i}{C_{Ti}} \qquad \text{Eqn.2.7.3-3}$$

Advantages of Quench Factor Analysis (QFA)

- The quench factor provides a single number describing quench severity
- The quench factor is related to the hardness in the quenched product
- Intermediate manual interpretations are not required.

Disadvantages of Quench Factor Analysis (QFA)

- Very few TTP curve coefficients have been published for steel alloys.

Paper I

Characterization of the performance of mineral oil based quenchants using CHTE Quench Probe System

by

Shuhui Ma, Mohammed Maniruzzaman

and Richard D. Sisson, Jr.

To be submitted to the 13th Congress of the International Federation for Heat Treatment and Surface Engineering(IFHTSE) and ASM Intl. Surface Engineering Congress, October 2002, Columbus, OH

3. Characterization of the performance of mineral oil based quenchants using CHTE Quench Probe System

Shuhui Ma, Mohammed Maniruzzaman and Richard D. Sisson, Jr.
Center for Heat Treating Excellence, Metal Processing Institute
Materials Science and Engineering Program, Mechanical Engineering Department
Worcester Polytechnic Institute, Worcester, MA 01609, USA

Abstract

The performance of a series of mineral oil based quenchants has been investigated using the CHTE Quench Probe System and probe tips of 4140 steel to determine the cooling rate, heat transfer coefficient, Hardening Power (HP) and Tamura's V indices in terms of the physical properties of quenchants; e.g. viscosity and oil start temperature. The Quench Factor, Q, in terms of the hardness of the quenched parts was also calculated. The lumped parameter approximation was used to calculate the heat transfer coefficient as a function of temperature during quenching. The results revealed that the maximum cooling rate increases with decrease in quenchant viscosity. As viscosity increases, Tamura's V is nearly constant, while the HP decreases. For the selected oils, cooling ability of quenching oil increases with the increase in oil operating temperature, reaches a maximum and then decreases. The heat transfer coefficient increases with the increase in hardening power and maximum cooling rate. As the viscosity increases, the quench factor increases, which indicates the cooling ability of the oil decreases since the higher quench factor means the lower cooling ability of the oil. The hardness decreases with the increase in quench factor.

I Introduction

Quenching is a traditional and old art. However, lack of understanding of the properties and selection of the quenchant can result in hardness inadequate, distortion, cracks or scrapping of costly-machined components, together with the environmental problems of smoke, fumes and fire hazards. There are a wide variety of quenchants available at this time, including water, salt solutions, aqueous polymers vegetable oils and mineral oils. Among them the mineral oils remain dominant since a wide range of quenching characteristics can be obtained through careful formulation and blending of the oils and additives.

Quenching oils can be divided into several categories, depending on the operational requirements, which include quenching speed, operating temperature and ease of removal [3]. Quenching speed is important because the speed influences the hardness and depth of hardening that can be obtained in part being quenched. According to the quenching speed, the oils can be classified as normal, medium and high speed quenching oils. The temperature of operation of quenching oil will have influences on the following factors: the lifetime of the oil, the quenching speed, the viscosity and the resulted distortion of components. Cold quenching oils are designed for general-purpose use at temperature of up to 80^{o}C for applications where distortion during quenching is not a problem. Hot quenching oils are designed for use at higher temperatures of up to 200^{o}C for controlling distortion during quenching and a process also known as marquenching.

In this work, a series of quenching experiments have been performed to study the performance of a variety of commercial mineral oil based quenchants as a function of the viscosities and the reusability of CHTE 4140 steel probes. The CHTE Quench Probe System [1] was used with 4140 steels probe tips. Lumped parameter analyses were used to calculate the heat transfer coefficient as a function of temperature during quenching. Hardening Power (HP), Tamura's V were also calculated to characterize the quenchants. The quenching performance of mineral oils was correlated with their viscosity and oil operating temperature. The results revealed that the maximum cooling rate increases with the decrease in viscosity of mineral oil. Quench Factor analysis is a very important way to characterize the different liquid quenchants. Quench factor was calculated for seven mineral oils and correlated with the hardness of the corresponding samples. The hardness decreases with the increase of quench factor.

II Experimental Procedure

CHTE Quench Probe System

The CHTE Quench Probe System is shown in Fig. 3-1. The system consists of notebook PC based data-acquisition system, pneumatic cylinder with air valve, a small box furnace, 1-L size beaker for quenchant and K-type thermocouple-connecting rod-coupling-interchangeable probe tip assembly. The pneumatic cylinder rod moves the probe down into the quench tank from the box furnace. The pneumatic cylinder is connected to the pneumatic valve by two white tubes as shown.

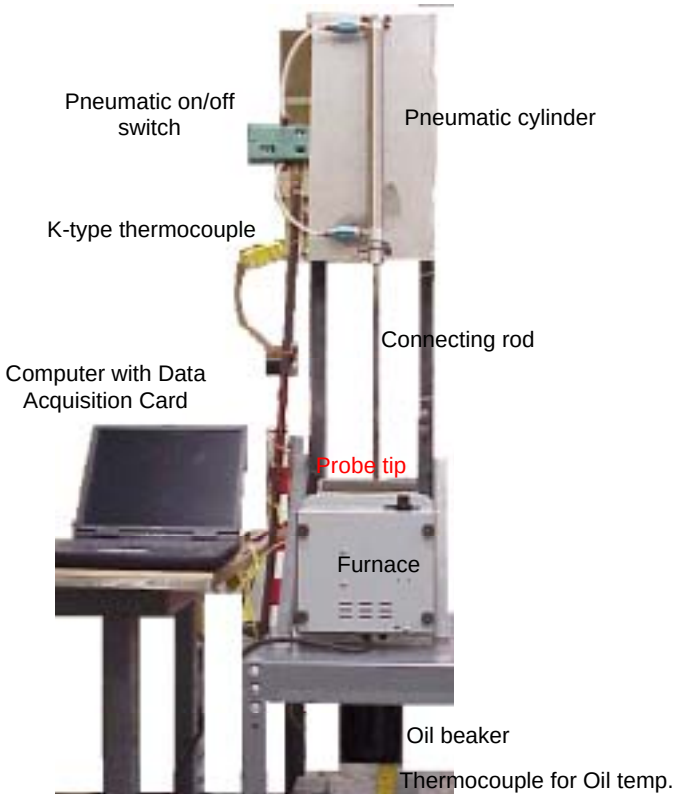

Fig 3- 1CHTE Quench Probe System [1]

The dimensions of the probe along with the coupling and the connecting rod are shown in Fig. 3-2. The main feature of this characterization system is the ability of changing the

probe tip. The probe tip can be fabricated from any metallic alloy of interest to be heat treated using quenching process. A detailed description of the operating procedure is given in Appendix A.

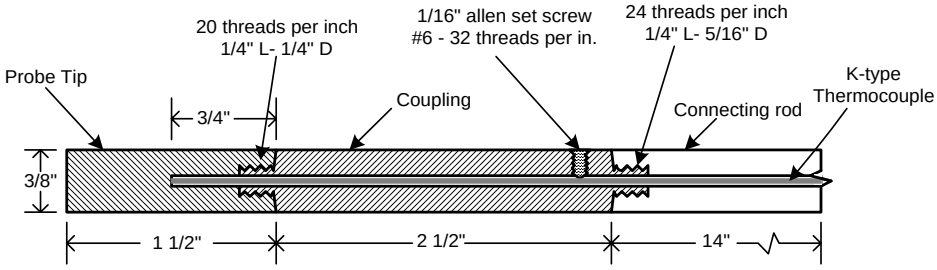

Fig 3- 2CHTE probe-coupling-connecting rod assembly [1]

Materials

In our experiments the probe tips are made of 4140 steels since it is one of the most widely used medium-carbon alloy steels and relatively inexpensive. It has cylindrical shape, 9.5 mm diameter by 38.1 mm length, to enable expedient calculation. Medium surface finish with R_a range of 1.0 to 2.0 μm is used for the test.

Table 3- 1 Test matrix of CHTE 4140 steel probe quenched in commercial oils

Name of the oils	Type of oils	Viscosity at 40°C	Operating Temperature	No of trials
Durixol V35	Very fast	10.4	50/80^{0}C	5
Durixol W72	Fast	21	50-80^{0}C	5
Durixol W25	Medium	46	50-150^{0}C	5
Durixol HR88A	Moderate	120	90-180^{0}C	5
T-7-A	Moderate	44.275	Room temperature	5 (reu.) 5(rep.)
Mar-temp 355	Moderate	68.2	50-150^{0}C	5
Houghton G	Medium	22.5	Room Temperature	5

According to the range of their viscosities, seven mineral oils have been selected from two different manufacturers: Houghton International and Burgdorf and have been tested on the reusability of probes. Some information of these oils and experimental plan are given in table 3-1.

Design of experiments

For each type of oil, as shown in table 3-1, five experiments have been performed using the same renewed probe to test the repeatability and reusability of probes. A new probe has been used for each oil and has been renewed after each quenching. The probe surface has been cleaned lightly using 180 grit abrasive papers to make the surface clean and free of prior oxide layer buildup, and then ultrasonically cleaned in acetone to remove the small pieces of oxide attached on the surface. Surface roughness was measured using Mahr-Federal Perthometer PRK before each trial to make sure the surface finish for the same set of experiments is comparable. Mass and diameter were also measured to determine their change after renewing each time. For the oils in table 3-1, two of these oils, T7A and Houghton G, can be used directly at room temperature, (i.e. 25^{o}C) but the other five oils (that is, Durixol V35, W25, W72, HR88A and Mar-temp 355) must be heated up to around 60^{o}C to achieve their optimum cooling abilities.

III Experimental Results and Discussion

Comparison of different oils

Figure 3-3 shows the typical cooling rate curves of CHTE 4140 probe quenched in all seven mineral oils. These seven mineral oils that have been tested are: Houghton – T7A, G and Mar-temp 355 and Burgdorf – Durixol W72, W25, HR88A and V35. The variation in maximum cooling rate from fastest oil to slowest oil is quite high, roughly 208 ^{o}C/sec to 120 ^{o}C/sec. The cooling ability of quenching oil depends on how fast the oil can extract the heat from the surface of the probe tips.

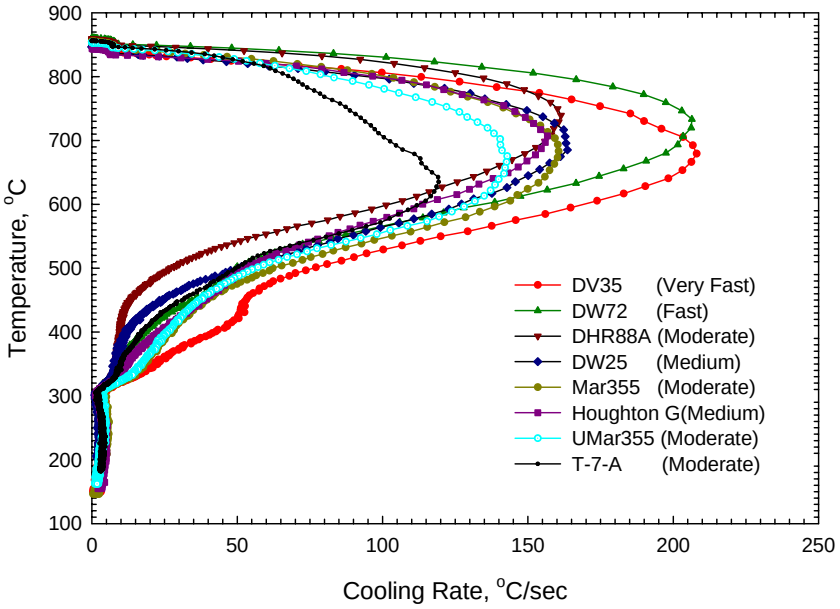

Fig 3- 3 typical cooling rate curves of CHTE 4140 steel probe in different mineral oils

Cooling Rate vs. Viscosity

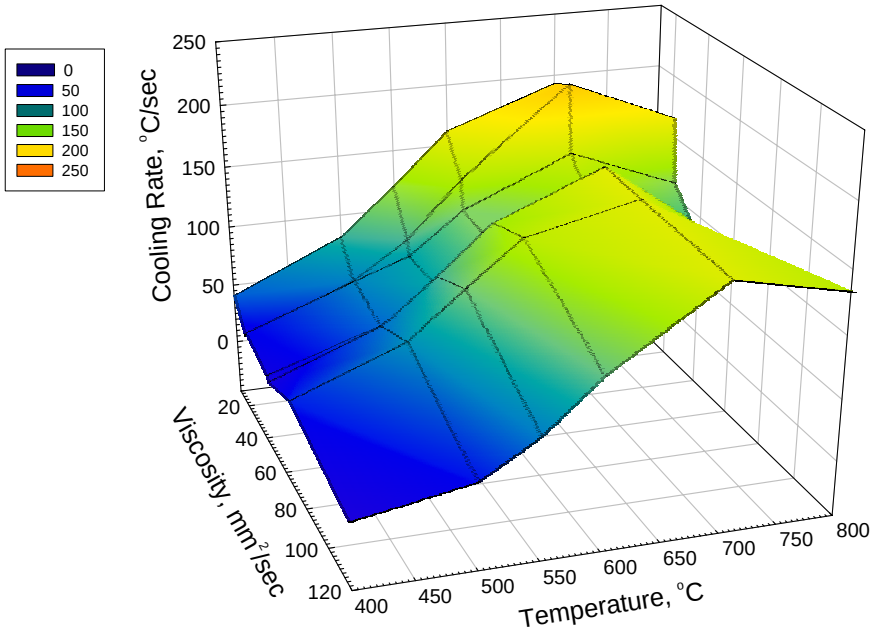

Fig 3- 4 Cooling rates of CHTE 4140 steel probe at 800,700,600,550,500 and 400°C as a function of viscosity

The cooling rates of 4140 steel probes at temperatures 800, 700, 600, 550, 500 and 400°C in seven mineral oils have been plotted against the viscosities of these oils in figure 3-4. The general trend is that the cooling rate increases as the viscosity decreases, because the quenchant with low viscosity can flow more easily and transport the heat from the surface of probes faster, given that other factors constant. Among these several temperatures, the cooling rate at 700°C is the highest, which indicates that the maximum cooling rate most probably happens around this temperature. Figure 3-5 shows the maximum cooling rate as a function of viscosity, from the regression line it can be seen the maximum cooling rate decreases with the increase of viscosity.

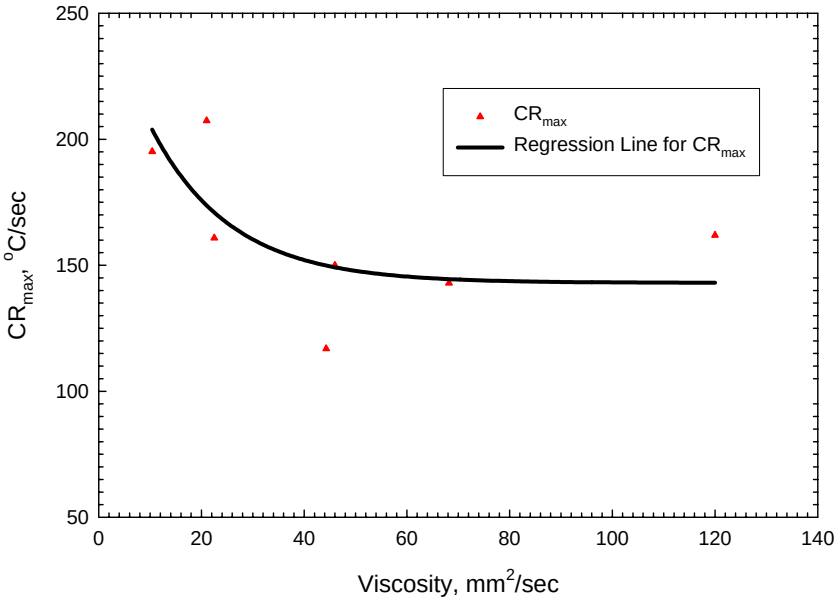

Fig 3- 5 the maximum cooling rate as a function of viscosity

Repeatability of 4140 steel probes

Figures 3.6-3.12 show the experimental investigation of 4140 steel probe tips in a variety of commercial quenching oils respectively. Five experiments have been done on each

type of oil. As can be seen, Houghton Mar-temp355, used Martemp355 and Burgdorf Durixol HR88A, W25 show excellent repeatability of cooling rate, the variation of maximum cooling rate for these oils is within 5%, while Houghton T-7-A and Burgdorf Durixol V35, W72 are not as repeatable, compared with the other four. The probe shows the obvious degradation in T-7-A from test to test. The change of maximum cooling rate for Durixol V35 is from 182.68 ^{o}C/sec to 208.08 ^{o}C/sec with a variation roughly 13%. For Durixol W72, only one curve is a bit out of range, but the other four curves are pretty consistent. Also there is no too much change in partial film boiling region (that is, transition between film boiling and nucleate boiling) and convective phase from curve to curve for each oil, but the variation does occur in nucleate boiling region, which indicates that it is very difficult to control this part to make it same from trial to trial.

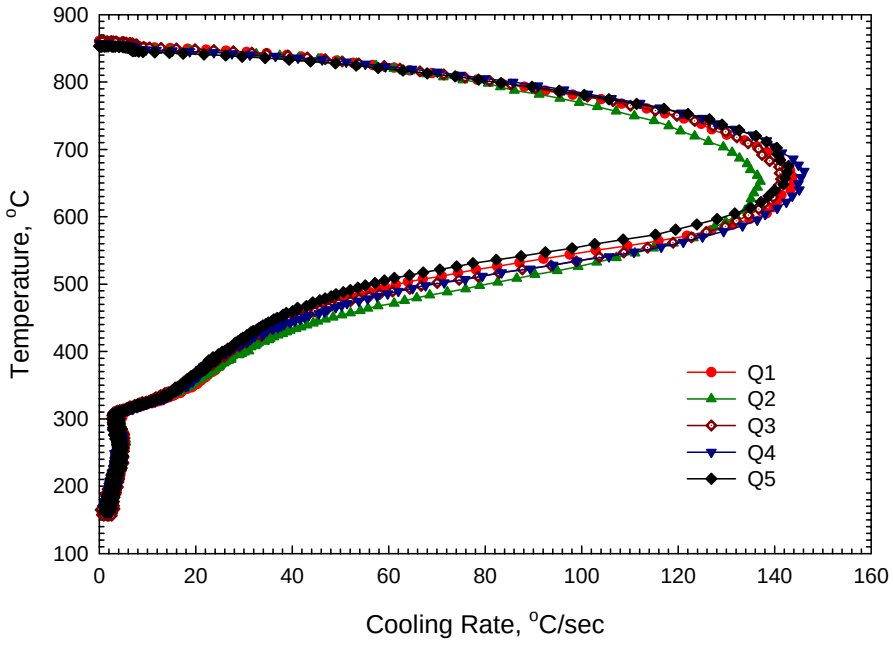

Fig 3-6 Cooling curves of CHTE probe in Houghton Martemp355 used quenching oil show excellent repeatability of the cooling rate

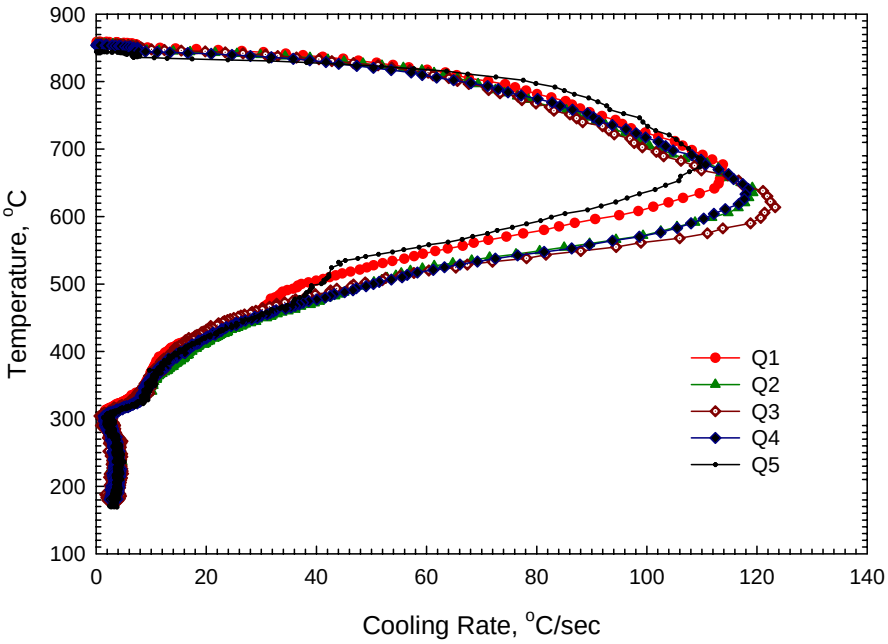

Fig 3-7 Cooling rate curves of CHTE probe in Houghton T7A mineral oil

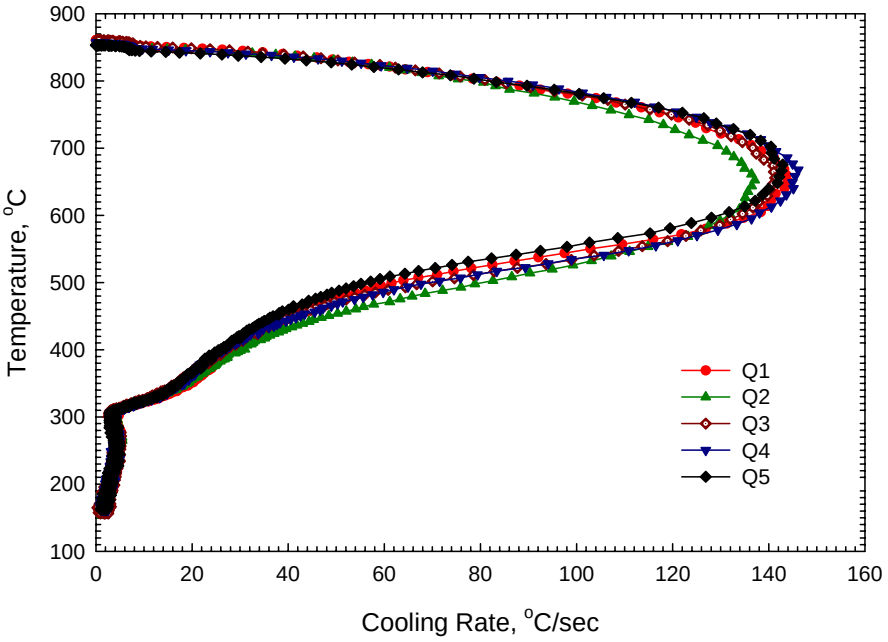

Fig 3-8 Cooling rate of CHTE probe in Houghton Mar-temp 355

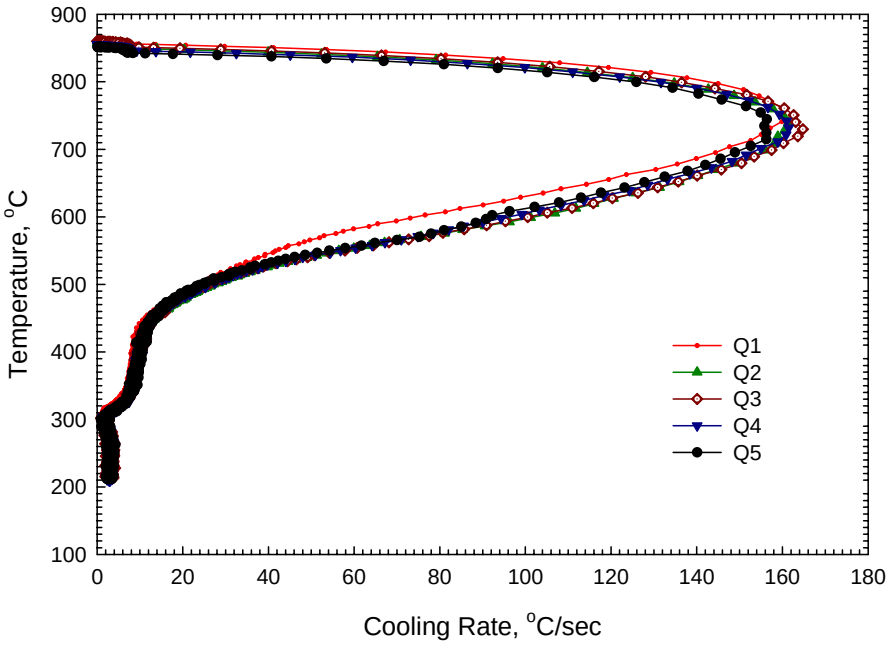

Fig 3-9 Cooling rate of CHTE probe in Burgdorf HR88A mineral oil

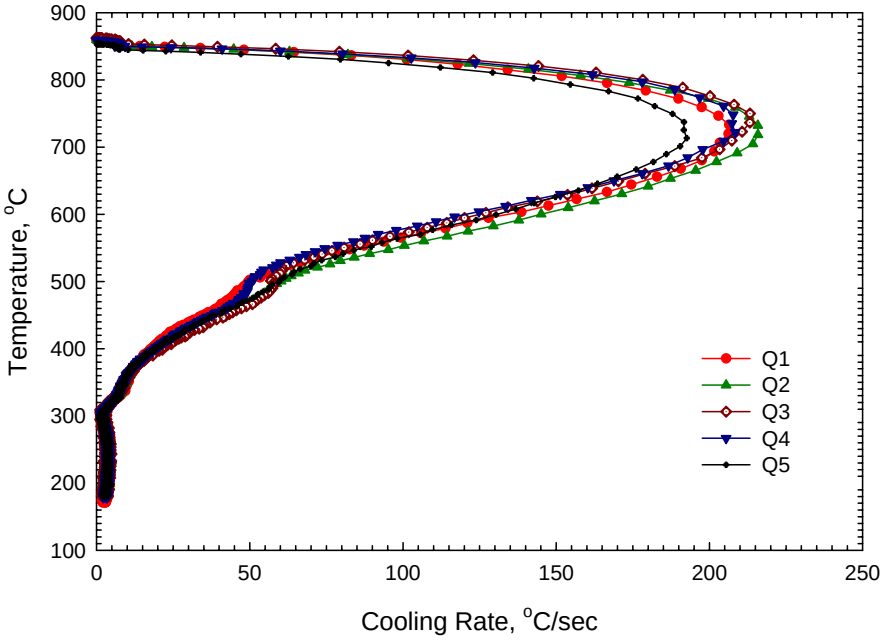

Fig 3-10 Cooing rate of CHTE probe in Burgdorf W72 mineral oil

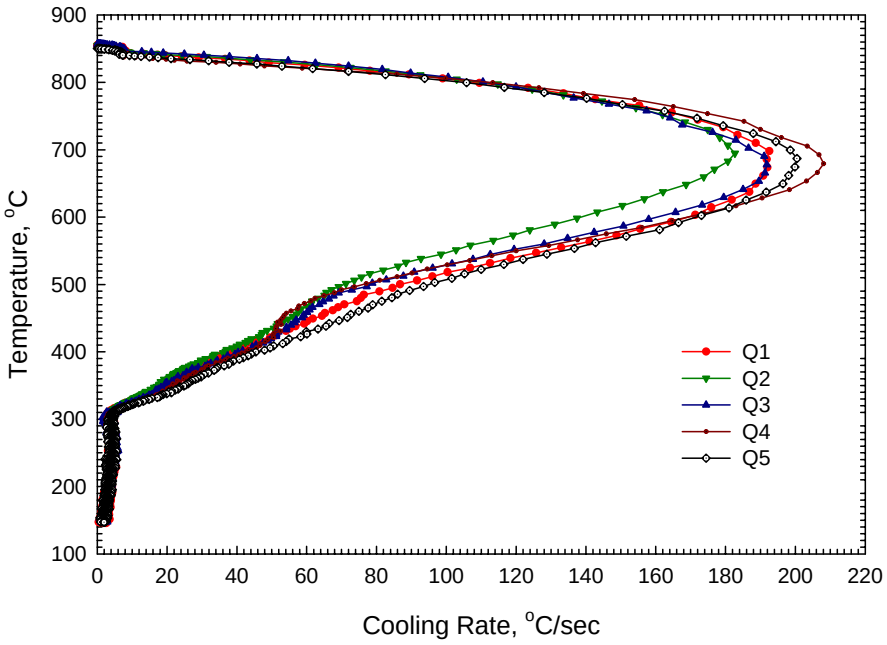

Fig 3-11 Cooing rate of CHTE probe in Burgdorf Durixol V35 mineral oil

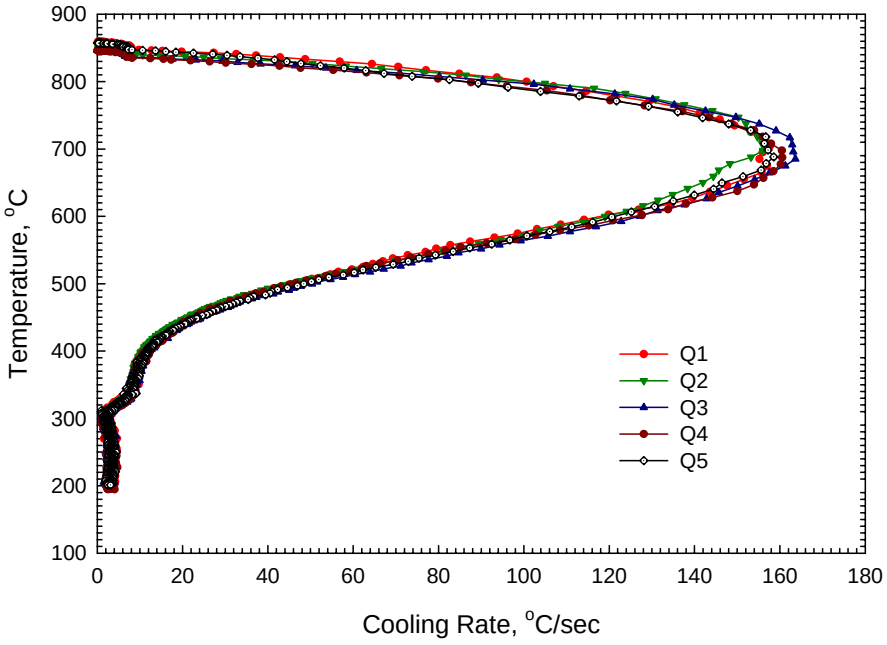

Fig 3-12 Cooing rate of CHTE probe in Burgdorf Durixol W25 mineral oil

Quenchant Performance Indices: Tamura's V and HP

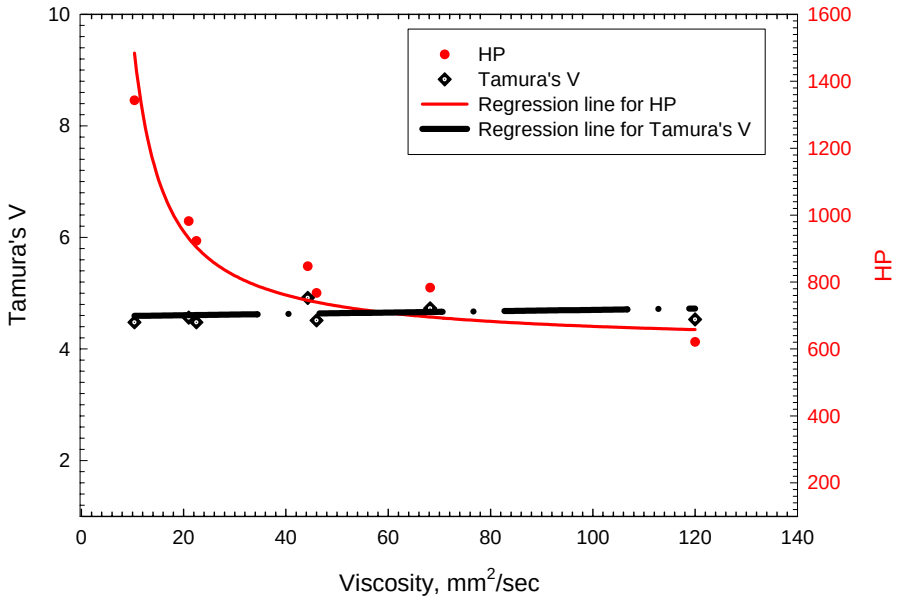

Fig 3-13 Tamura's V, HP as a function of viscosity estimated using CHTE 4140 probe cooling data

Using the equations that are described in sections 2.7.1 and 2.7.2, Tamura's V and Hardening Power have been calculated for each experiment, averaged on five values to get one data point for each type of oil, and then plotted as a function of viscosity of mineral oil, as shown in figure 3-13. Tcp and Tvp values in equations 2.7.1-1 and 2.7.2-1 are taken from cooling rate-time curve, Tvp is the temperature corresponding to the point where cooling rate starts to change very sharply within a few seconds at the beginning of quenching process. Tcp is the temperature that corresponds to the point where cooling rate starts to approximate a constant value as time goes on at the end of quenching process. Ts and Tf in equation 2.7.1-1 are respectively 337.78^{o}C and 218.33 ^{o}C. In equation 2.7.2-1 the cooling rate at 550^{o}C is used for CR since the region between 500^{o}C and 600^{o}C is very critical to understand the quenching process. Figure 3-13 shows the quenchant performance in the form of HP and V indices. As viscosity increases, Tamura's V is nearly constant, while the HP decreases.

Effect of operating temperature on the quenching performance of mineral oils

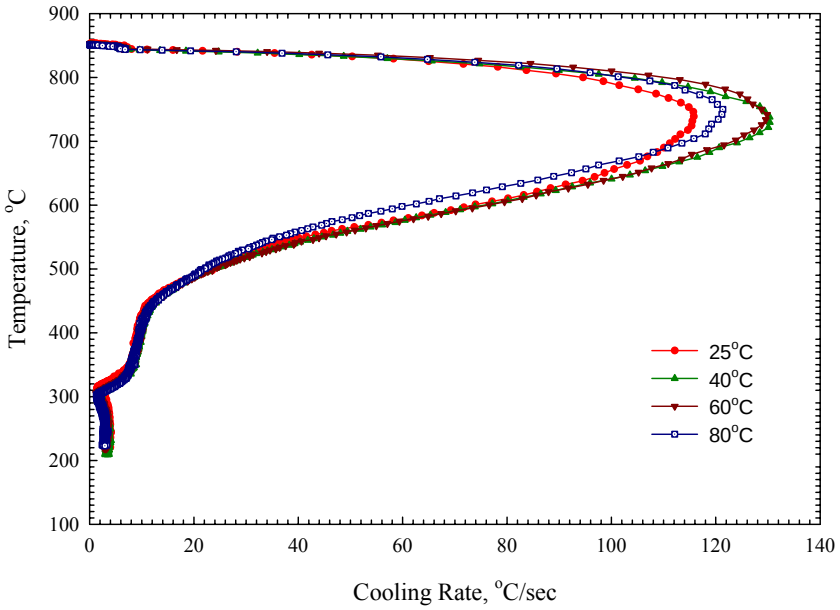

Fig 3-14 Cooling rate curves of CHTE 4140 quenched in Burgdorf HR88A at different temperatures

In order to understand the effect of operation temperature on the quenching performance of mineral oil, one relatively stable oil (Burgdorf Durixol HR88A) was chosen to test at 25, 40, 60 and 80°C. The results are shown in figure 3-14. Generally as oil is heated viscosity decreases. [1] This drop in viscosity allows the quenchant to flow more freely to increase the natural or mechanical turbulence that breaks down the vapor blanket stage. [1] The boiling stage (i.e. nucleate boiling) is violent by nature and it is not significantly affected by changes in temperature. In the convection stage, the rate of cooling of an oil quenchant will become slower as the temperature of the quenching oil bath increases. From figure 3-14, the cooling curve at 25°C shows the lowest maximum cooling rate, as the temperature rises up to 40 and 60°C, the maximum cooling rate increases by roughly 20°C/sec. However, as the temperature increases further up to 80°C, the cooling rate decreases instead. It is assumed that the cooling ability for this type of oil has an upper

limit at certain temperature, in this case, which is around 60°C. Below and above this temperature, the cooling rate is more or less lower.

Effect of probe size

Figure 3-15 shows the cooling rate curves of CHTE 4140 probes with two different diameters quenched in Burgdorf Durixol W72. The diameter of bigger probe is four times of the small one, the maximum cooling rate of the larger probe is almost one fourth of that of the small one.

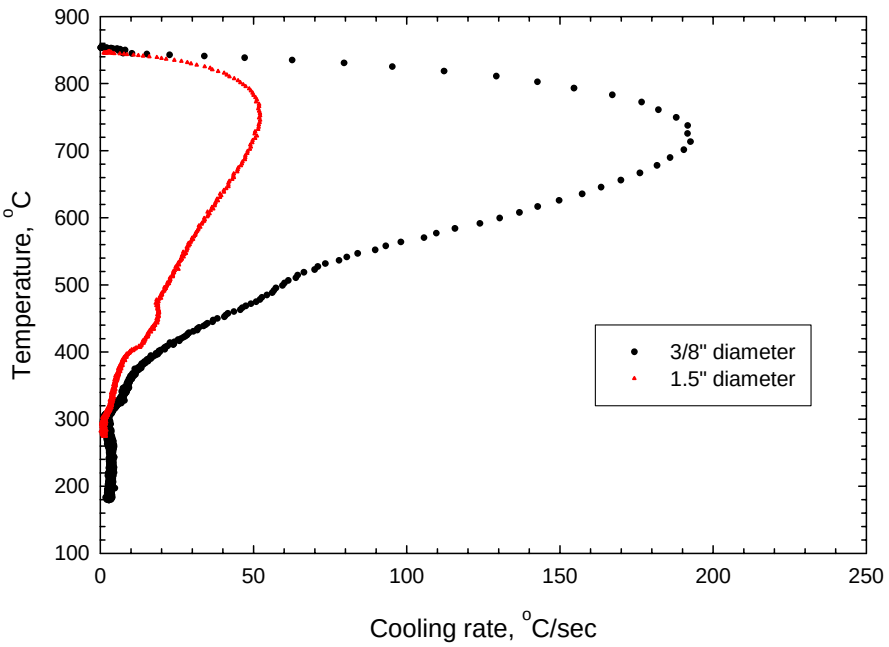

Fig 3-15 Cooling curves of CHTE 4140 probes with different diameters quenched in Burgdorf W72

Heat transfer coefficients of CHTE 4140 steel probe in different mineral oils

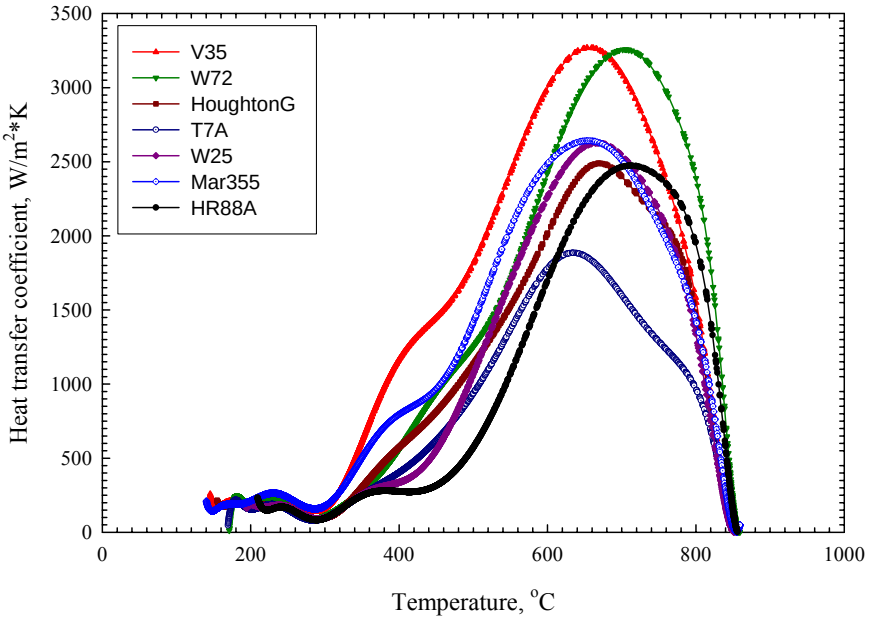

Fig 3-16 Typical heat transfer coefficient curves of CHTE 4140 steel probe as a function of temperature quenched in different mineral oils.

Heat transfer coefficients of CHTE 4140 steel probe quenched in seven mineral oils were calculated using lumped parameter analysis since the probe in our test is tiny, and the results are shown in figure 3-16. Heat transfer coefficient is similar in partial film boiling region, but quite different in nucleate boiling and convection stages and its maximum value varies from 1900W/m^2*K up to 3250W/m^2*K, Durixol V35 and W72 have the highest maximum heat transfer coefficients (h_{max}) and lowest viscosities by which they are classified as very fast and fast oils, while T7A has lowest h_{max} and average viscosity. The other five heat transfer coefficients lay in between. From the point of view of the viscosity, the lower the viscosity of an oil is, the more easily the bubbles can form on the probe surface to extract heat, and the higher heat transfer coefficient will be. The temperature at which maximum heat transfer coefficient reaches differs from oil to oil, but it is within the band of 640 ^{o}C and 720^{o}C.

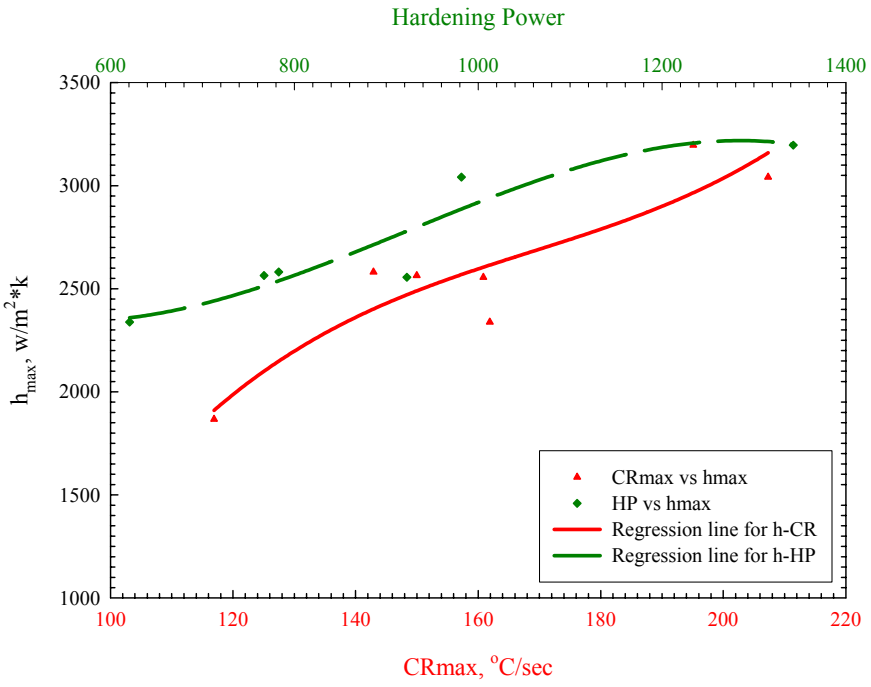

Fig 3-17 Heat transfer coefficient as a function of HP and CR_{max} for CHTE 4140 steel probe in different mineral oils

Heat transfer coefficient of CHTE 4140 steel probe quenched in different mineral oils is plotted as a function of Hardening power and maximum cooling rate and the curves are shown in figure 3-20. Polynomial 3rd order regression lines are added onto two sets of scattered data points. From the trendlines, it can be clearly seen that heat transfer coefficient increases as the increase of hardening power and maximum cooling rate, which means that the oil with higher cooling rate has the higher heat transfer coefficient and better cooling ability, therefore can extract the heat from the probe surface faster and more efficiently.

Quench Factor Analysis

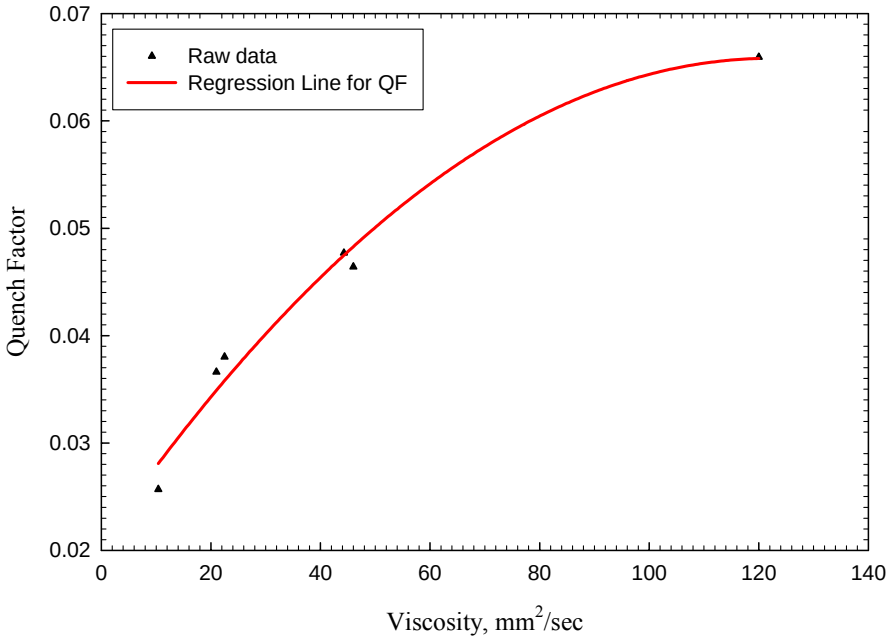

Fig 3-18 Quench Factor as a function of viscosity for CHTE 4140 steel probe in different mineral oils

Quench factor analysis is an efficient way to characterize the cooling ability of liquid quenchants since it can give one single number that interrelates the cooling rate produced by a quenchant and the transformation rate of the alloy as described by the time-temperature-property (TTP) curve. Using equations 2.7.3-1, 2.7.3-2 and 2.7.3-3, quench factor for six mineral oils are calculated and plotted against the viscosity of the oil in figure 3-21. For 4140 steel probe, the five constants in equation 2.7.3-1, which are K_1-K_5, are from George Totten's unpublished data. By plugging these constants into equation 2.7.3-1, C_T can be generated as a function of temperature. Using this C_T and time-temperature data from the experiments, quench factor can be calculated for each oil. As the viscosity increases, the quench factor increases, which indicates the cooling ability of the oil decreases since the higher quench factor means the lower cooling ability of the oil.

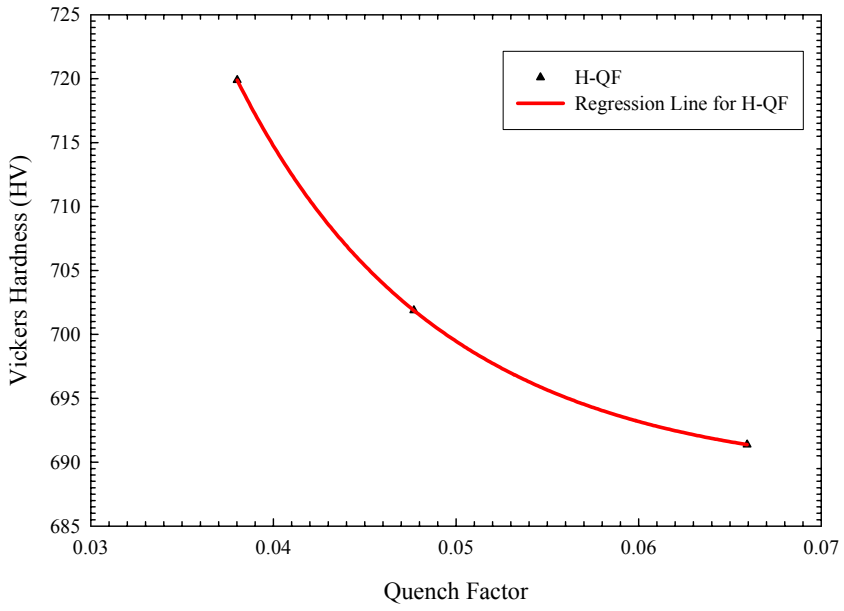

Fig 3-19 Hardness as a function of quench factor for CHTE 4140 steel probe quenched in Houghton G, T7A and Durixol HR88A

Three probe tips quenched respectively in Houghton G, T7A and Durixol HR88A were chosen according to the viscosities of these three oils to do the hardness test. Durixol HR88A has the highest viscosity among the seven oils we tested; Houghton G has a relatively low viscosity, while the viscosity of T7A lies in between the other two. First the sample was cut into half using the alumina blade with coolant flowing to prevent the phase transformation due to the heat generation during the cutting process, mounted with the cross-section facing down, grinded and then polished to make the surface smooth enough for micro hardness test. The hardness measurement was made along the cross-section of each sample using Vickers hardness tester. Figure 3-22 shows a very good trend of the change in hardness with the quench factor. The quench factors calculated from these three oils are pretty small, ranging from 0.03 to 0.07, because the cooling curves for these oils are far away from ferrite-pearlite transformation starting line. The

higher the cooling ability of quenchant is, the smaller the quench factor will be and the higher the hardness is. So smaller quench factor corresponds to the higher hardness, as shown in figure 3-22.

IV Summary

In summary, the following conclusion can be made for this study:

- The maximum cooling rate decreases with the increase in viscosity.
- During repeatability tests, not much change in cooling curve is observed in partial film boiling region (that is, transition between film boiling and nucleate boiling) and convective phase from one trial to other for each oil, but the variation does occur in nucleate boiling region, which indicates that it is very difficult to control this part to make it same from trial to trial.
- As viscosity increases, Tamura's V doesn't vary that much, while the HP decreases.
- Cooling ability of a quenching oil increases with the increase in oil operating temperature, reaches a maximum and then decreases.
- Heat transfer coefficient increases with the increase in hardening power and maximum cooling rate. Which means that the oil with higher cooling rate has the higher heat transfer coefficient and better cooling ability, therefore can extract the heat from the probe surface faster and more efficiently.
- As the viscosity increases, the quench factor increases, which indicates the cooling ability of the oil decreases since the higher quench factor means the lower cooling ability of the oil.

Paper II

The effects of surface oxides on the quenching performance of 4140 steel in commercial oils

by

Shuhui Ma, Mohammed Maniruzzaman

and Richard D. Sisson, Jr.

4. The Effects of surface oxides on the quenching performance of 4140 steel in commercial mineral oils

Shuhui Ma, Mohammed Maniruzzaman and Richard D. Sisson, Jr.
Center for Heat Treating Excellence, Metal Processing Institute
Materials Science and Engineering Program, Mechanical Engineering Department
Worcester Polytechnic Institute, Worcester, MA 01609, USA

Abstract

The effect of oxide formation on the cooling rate and heat transfer coefficient of CHTE probes has been experimentally investigated using CHTE Quench Probe System and probe tips of 4140 and 304 steel. In order to prevent the oxide formation, the argon gas was purged into the furnace with the constant flow rate at 12.77cm^3/min. Lumped parameter approximation was used to calculate the heat transfer coefficient as a function of temperature during quenching. The cooling rates and heat transfer coefficients were compared between 4140/304 probes heated in air and 4140/304 heated in argon. It turns out that the oxidation increases the cooling rate and heat transfer coefficient of 4140 steel probes, the cooling rate curve of 4140 steel probe heated in argon shows clear Leidenfrost temperature, which indicates the use of argon is able to prevent the oxidation. The oxide layer may require a significant thickness to cause the decrease in heat transfer coefficient. The quenching performances of 304 stainless steel probes are similar in air and argon.

I Introduction

During the quenching of 4140 steel probes, one thin layer of oxides was found to form on the surface of the probe. Therefore, the main goals of this work are to experimentally determine the effect of surface oxides on the cooling rate and heat transfer coefficient.

The effect of oxidation on a test probe is very briefly addressed here. In general, oxidation is not quantified, it is discussed that oxidation causes the nucleate boiling regime to start earlier [55]. An experiment to determine the effect of surface roughness on the rewetting process was performed by Lee and Sheng [1]. During the early test runs, rewetting velocities showed progressive improvement with time, but then subsequently remained consistent. These investigations concluded that the effect was due to initial oxidation of the metal part [1].

The vapor blanket (film boiling) phase will disappear partly or completely when quenching components with oxidized surfaces. The oxide layer appears to be insulating and may reduce the cooling rate, which can affect the hardening result [55]. In summary, oxidation will have the effect of reducing or eliminating the film boiling stage. It creates an additional source of turbulence that assists in dissipating faster the vapor blanket that forms in the film boiling stage. Since heat transfer in the film boiling stage is via conduction and radiation, it is the most inefficient regime from the heat dissipation capacity standpoint. Oxidation should decrease the heat transfer rate in the nucleate boiling and convection heat transfer regimes [55].

The oxidation layer may act as an insulation layer, however the oxide layer may require a significant thickness (of the order of 200 microns) to cause the significant change in heat rate [1]. The oxidation layer may contribute to accelerate the dissipation of the vapor blanket in the film boiling stage, and cause an earlier initiation of the nucleate boiling stage. High temperature oxidation may decrease cooling rates if it is prolonged long enough to provide an insulating effect.

The effect of high temperature oxidation on the quenching behavior of 4140 steel probes is complex [1]. During oxidation the surface topography and composition will change dynamically. In addition, during cooling the differential thermal expansion of the oxide and alloy can lead to cracking and spalling of the oxide which leads to a dynamic change in surface features As the nucleation site density N/A of surface features that nucleate bubbles during nucleate boiling controls the heat transfer rate as discussed above, it will be very difficult to characterize the as-fabricated surface features that will control the heat transfer.

It is the goal of this paper to experimentally determine the effect of oxidation on the cooling rate and heat transfer coefficient of CHTE probe tips of 4140 and 304 steel using CHTE Quench Probe System.

II Experimental Procedure

CHTE Quench Probe System

A typical CHTE quench probe system has been shown in figure 3.1, which consists of notebook PC based data-acquisition system, pneumatic cylinder with air valve, a small box furnace, 1-L size beaker for quenchant and K-type thermocouple-connecting rod-coupling-interchangeable probe tip assembly. In this set of experiments the important modifications were made on the box furnace. In order to achieve the non-oxygen environment, a stainless steel tube was put all the way through the furnace, held by a clamp on the top. At the bottom, a side screw was put on the side of the tube to connect the furnace with the gas tank using the copper wire. The top and bottom of the tube were respectively sealed with the wool and the ceramic cap to avoid the heat loss and also to maintain the non-oxygen environment during the experiment. Between the gas tank and the furnace there is a flow meter to monitor how much gas is flowing into the furnace per unit time. The dimensions of the probe along with the coupling and the connecting rod have been shown in figure 3-2.

Materials

The probe tips are made of 4140 steels and 304 stainless steels in this set of experiments. Both kinds of probes are cylindrical, 9.5mm diameter by 38.1mm length. Medium surface finish with Ra range of 1.0 to 2.0 μm is used for the test.

Three mineral oils, Houghton G, T7A and Burgdorf Durixol HR88A, are chosen for the test in terms of their viscosities: Houghton G has relatively low viscosity, 22.5 mm^2/sec, Durixol HR88A has the highest viscosity among seven oils we have tested, 120mm^2/sec, the viscosity of T7A lies in between. The experimental plan is given in table 4-1:

Design of experiments

For each oil, as shown in table 4-1, five experiments have been performed using the same renewed probe to test the repeatability of probes. A new probe has been used for each oil and has been renewed after each quenching. The probe surface has been cleaned lightly using 180 grit abrasive papers to make the surface clean and free of prior oxide layer buildup, and then ultrasonically cleaned in acetone to remove the small pieces of oxides attached on the surface. Surface roughness was measured using Mahr-Federal Perthometer PRK before each trial to make sure the surface finish for the same set of experiments is comparable. Mass and diameter were also measured to determine their changes after renewing each time. For the oils in table 4-1, two of these oils, T7A and Houghton G, can be used directly at room temperature, (i.e. 25^oC) but Burgdorf Durixol HR88A must be heated up to 60^oC, which is determined by the recommended temperature range from the oil manufacturer, to achieve its optimum cooling ability.

Table 4. 1 Test matrix of 4140 and 304 steel probes in Houghton G, T7A and Durixol HR88A

Probe material	Name of oils	Viscosity at 40°C	Operation temp	No of trials	Heating environment
4140 Steel	Houghton G	22.5	25°C	5	Heating in air
	T7A	44.3	25°C	5	
	Durixol HR88A	120	60°C	5	
	Houghton G	22.5	25°C	5	Heating in argon
	T7A	44.3	25°C	5	
	Durixol HR88A	120	60°C	5	
304 Stainless steel	Houghton G	22.5	25°C	5	Heating in air
	T7A	44.3	25°C	5	
	Durixol HR88A	120	60°C	5	
	Houghton G	22.5	25°C	5	Heating in argon
	T7A	44.3	25°C	5	
	Durixol HR88A	120	60°C	5	

III Experimental Results and Discussion

(A) Repeatability tests

Repeatability of 4140 steel and 304 stainless steel probes in air and argon

A series of quenching experiments have been preformed using 4140 steel and 304 stainless steel probes quenched in T7A, Houghton G and Durixol HR88A. The goal of this work is to identify how the surface oxidation is playing a role in the quenching performance of different mineral oils. The probes have been heated in two kinds of environments: air and argon. The main purpose of heating the probes in argon is to prevent the oxide formation. Figure 4.1-4.10 shows the repeatability tests for CHTE 4140 steel and 304 stainless steel probes respectively heated in air/argon and then quenched in T7A, Houghton G and Durixol HR88A. Since Durixol HR88A is more stable than T7A and Houghton G, as can be seen from the graphs, the variation of the cooling rate curve from trial to trial is smaller for quenching in Durixol HR88A than that in T7A and Houghton G, but most of the graphs show very good repeatability.

Also repeatability and reproducibility (R&R) studies in air and argon were performed using 4140 steel probe tips quenched in Houghton G. Two operators made 5 medium-finish probes each on the same lathe and two different individuals performed the experiments for one set of R&R study in one of two heating environments (air or argon). The cooling rate data from 800°C down to 200°C in intervals of 100°C for each of the ten trials were tabulated as well as the maximum cooling rate and temperature at maximum

cooling rate in Table 4.2. Standard deviations and means are calculated for the ten trials at each given temperature.

The mean cooling rate data for 4140 respectively heated in air and argon was plotted with the temperature from 800°C down to 200°C in intervals of 100°C, as shown in Figure 4.11. It can be clearly seen that the mean cooling rate for 4140 in air is higher than that in argon at all the temperatures from 800°C down to 200°C.

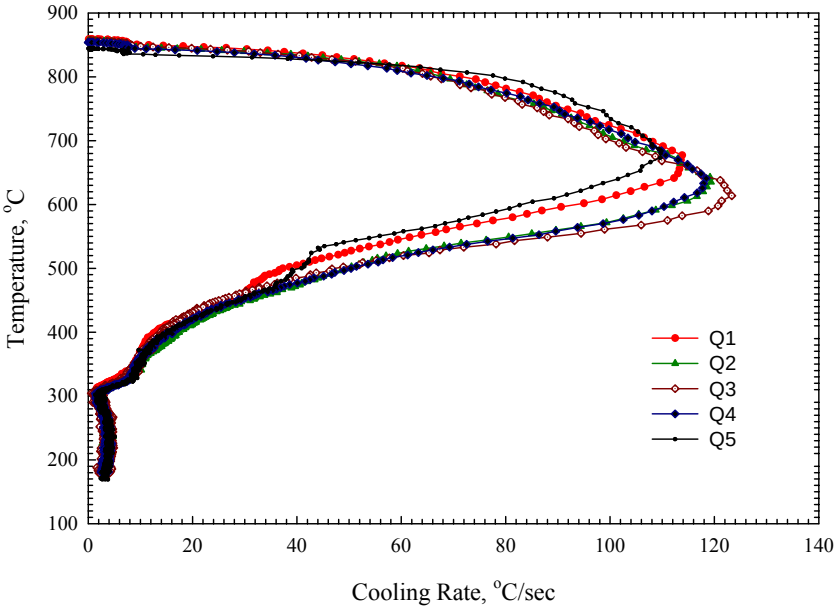

Fig 4. 1Cooling rate curves of CHTE 4140 probe in T7A heated in air

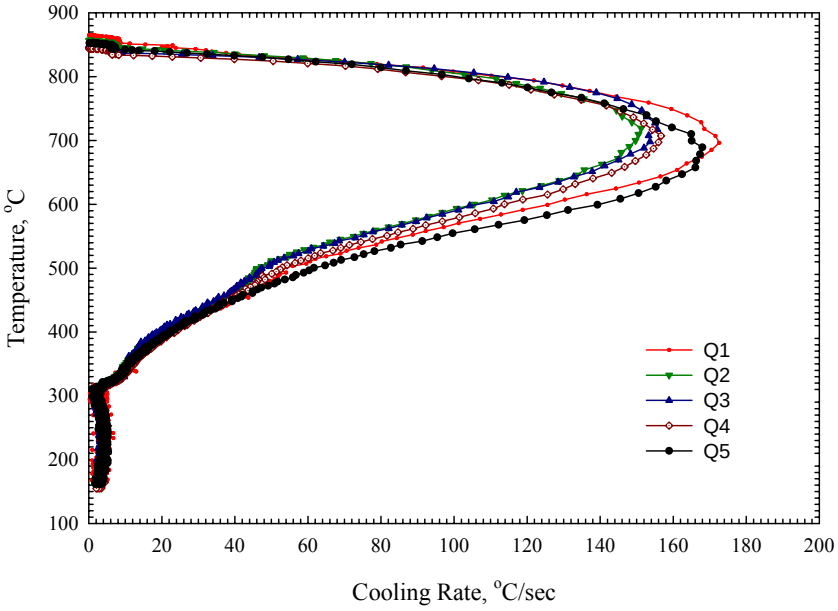

Fig 4. 2 Cooling rate curves of CHTE 4140 probe in Houghton G heated in air

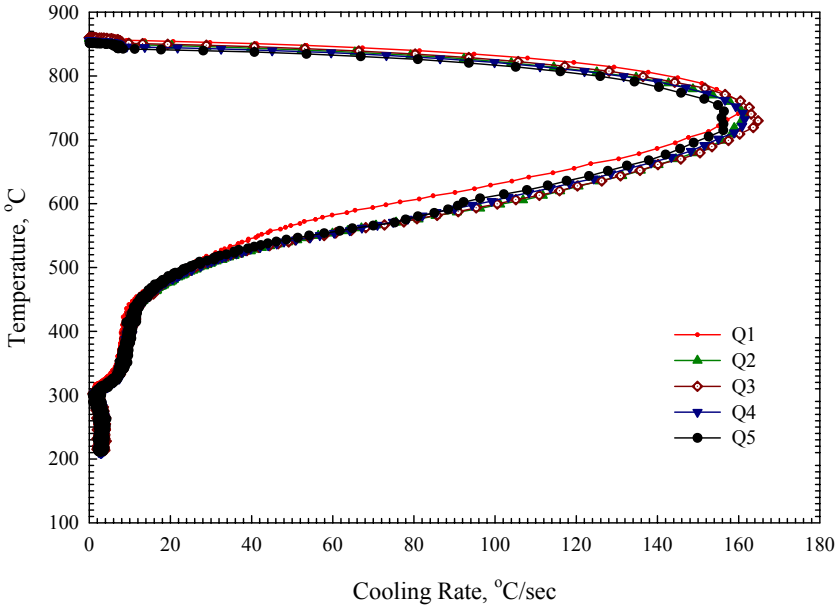

Fig 4. 3 Cooling rate curves of CHTE 4140 probe in DHR88A heated in air

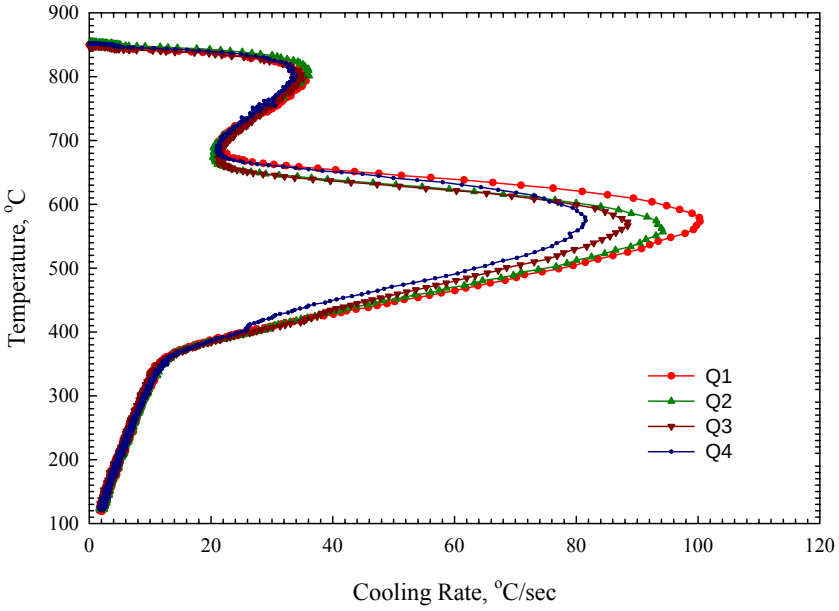

Fig 4.4 Cooling rate curves of CHTE 304 probe in T7A heated in air

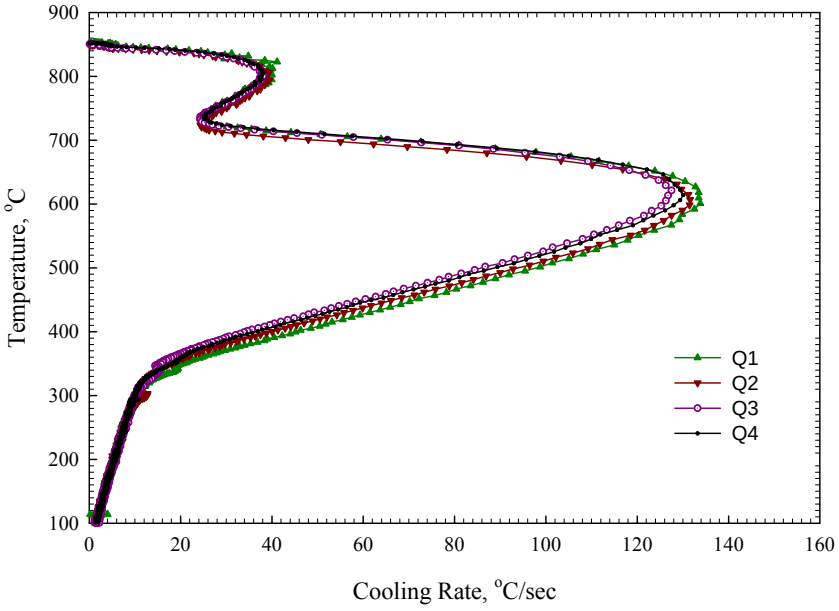

Fig 4.5 Cooling rate curves of CHTE 304 probe in Houghton G heated in air

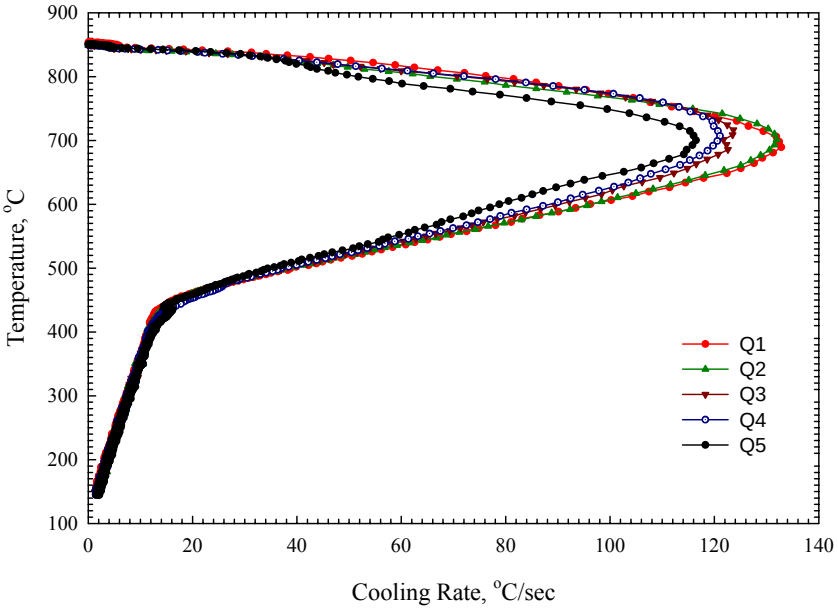

Fig 4.6 Cooling rate curves of CHTE 304 probe in DHR88A heated in air

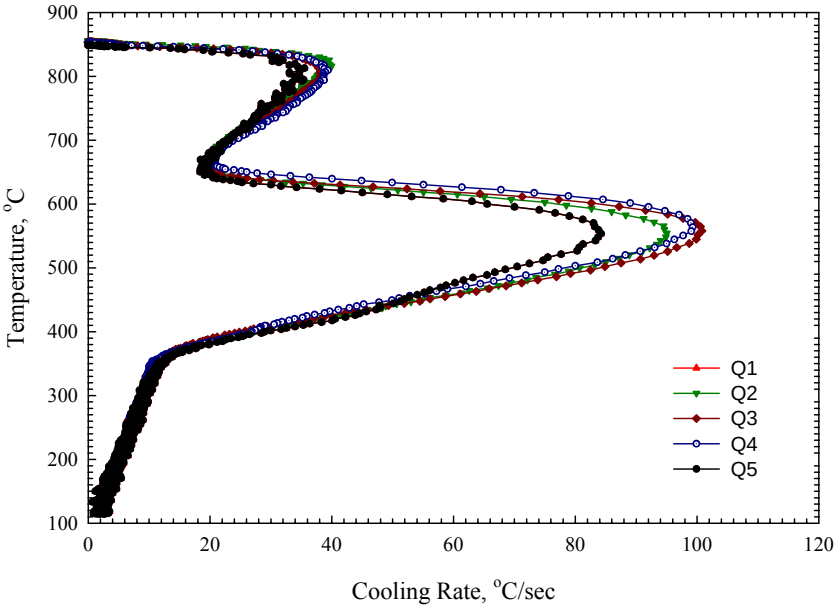

Fig 4.7 Cooling rate curves of CHTE 304 probe in T7A heated in argon

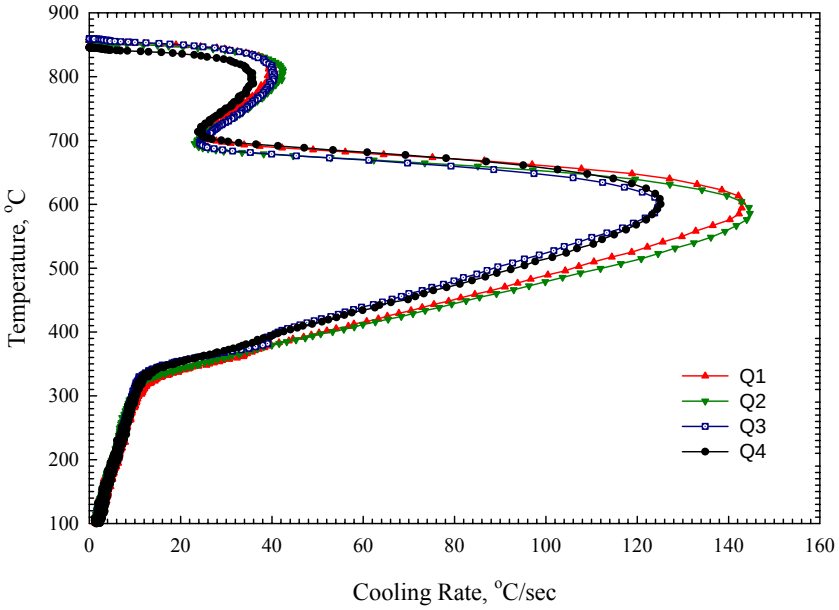

Fig 4.8 Cooling rate curves of CHTE 304 probe in Houghton G heated in argon

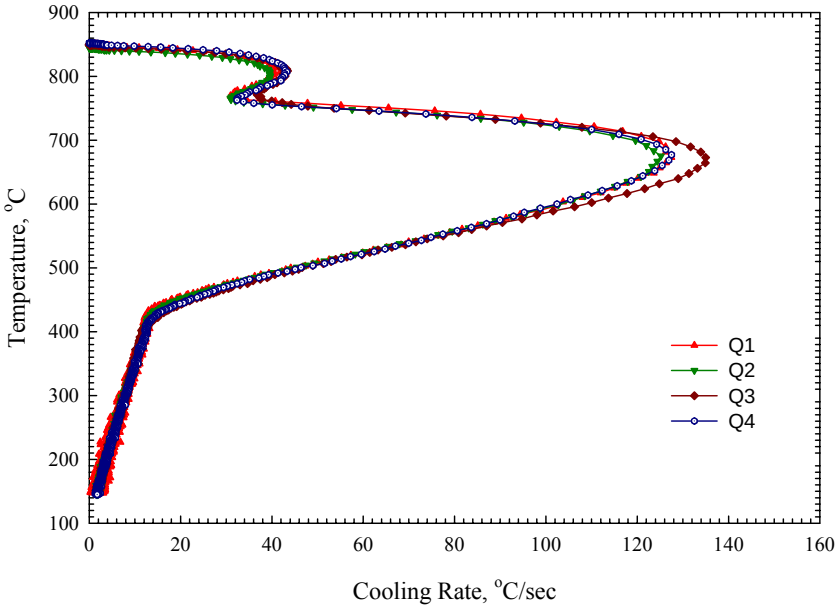

Fig 4.9 Cooling rate curves of CHTE 304 probe in DHR88A heated in argon

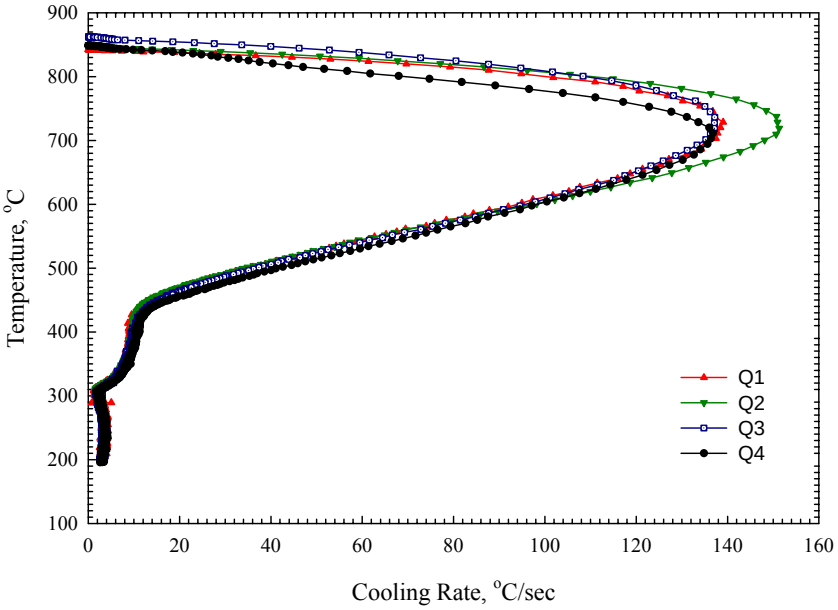

Fig 4. 10 Cooling rate curves of CHTE 4140 probe in DHR88A heated in argon

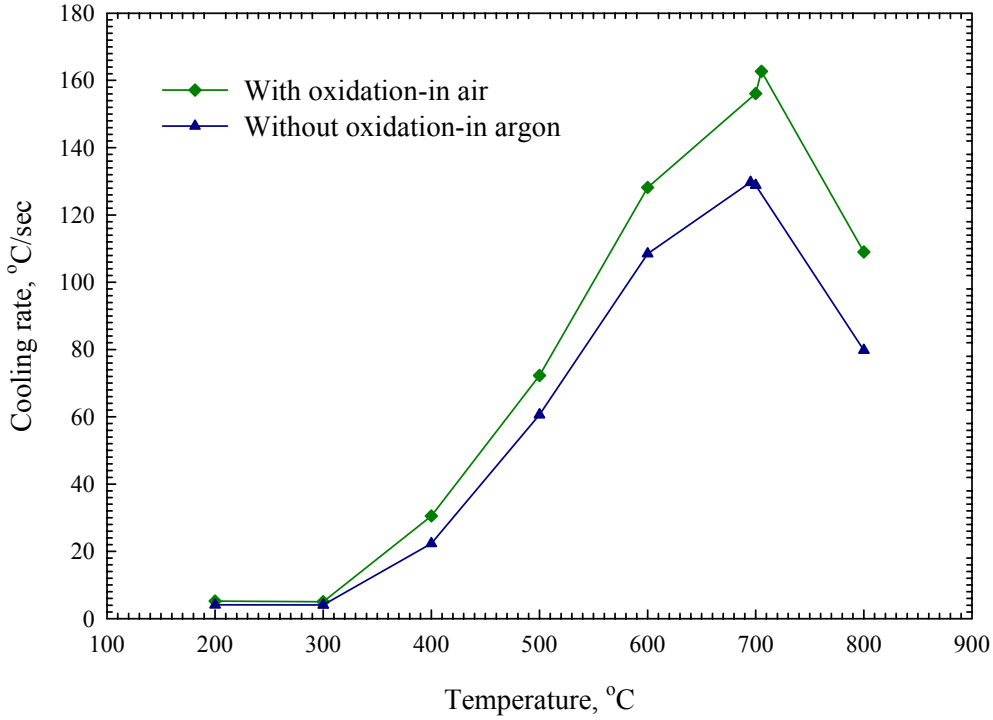

Fig 4. 11 The comparison of mean cooling rate for 4140 heated in air and argon and quenched in Houghton G as a function of temperature

Table 4. 2 R&R Study of 4140 steel probes in Houghton G

R&R in air		R&R in Argon	
T, ^{o}C	CR_{AVG}, ^{o}C/sec	T, ^{o}C	CR_{AVG}, ^{o}C/sec
800	109	800	79.8
705.4	162.7	700	128.8
700	156.1	695.3	129.7
600	128.2	600	108.5
500	72.3	500	60.6
400	30.5	400	22.3
300	5	300	4
200	5.2	200	4.1

(B) Comparison of cooling rate curves

The comparison of cooling rate curves for 4140 in air and in argon

As mentioned before, the five experiments for repeatability test of CHTE 4140 probes were carried out in each mineral oil. These five curves were then taken average using high precision polynomial equation or Savitzky-Golay smoothing method, as detailed in Appendix B, to generate one typical cooling rate curve for the specific mineral oil. The typical cooling rate curves of CHTE 4140 steel probe tip in air and argon are plotted together for two different mineral oils: DHR88A and T7A, as shown in figure 4.12 and 4.13.

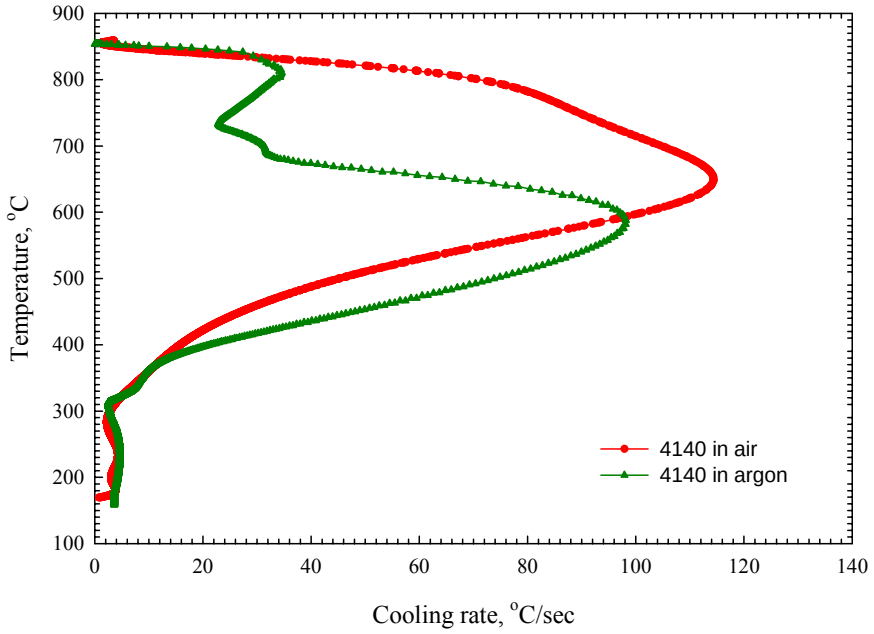

Fig 4. 12 Cooling rate curves of CHTE 4140 probes heated in air and argon and quenched in T7A

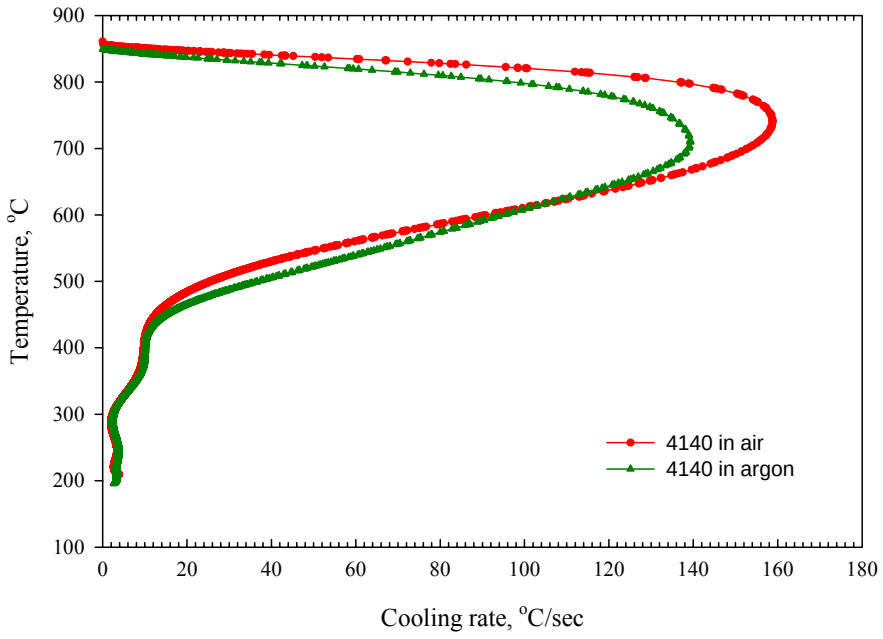

Fig 4.13 Cooling rate curves of CHTE 4140 probes heated in air and argon and quenched in DHR88A

From figures 4.12 and 4.13, it can be clearly seen that the cooling rate for 4140 in air is higher than that in argon, which is due to the oxide formation on the probe surface when

heating in air that increases surface area, makes the surface rougher and creates more bubble nucleation sites. Therefore, the bubbles can form more easily and extract more heat from the surface efficiently. Another interesting observation is that the cooling rate curve of 4140 probe heated in argon, as shown in figure 4.12, shows clear Leidenfrost temperature, while the curve of 4140 probe heated in air doesn't. The apparent reason for this is that the oxidized surface breaks down the vapor blanket, partially or completely eliminates the film boiling regime and causes the nucleate boiling stage to initialize early[55].

The comparison of cooling rate curves for 304 in air and in argon

The same series of experiments were also performed using 304 stainless steel probes, heated in air/argon and then quenched in three different mineral oils. As can be seen from figure 4.14, 4.15 and 4.16, the quenching performance for 304 stainless steel probe heated in argon is quite similar to that in air because for 304 probe tips there is no oxides formation on the surface even when heated in air. So the result from two kinds of heating environments should be comparable. Also almost for all the experiments the cooling rate curves show very prominent Leidenfrost temperature, which is expected to occur.

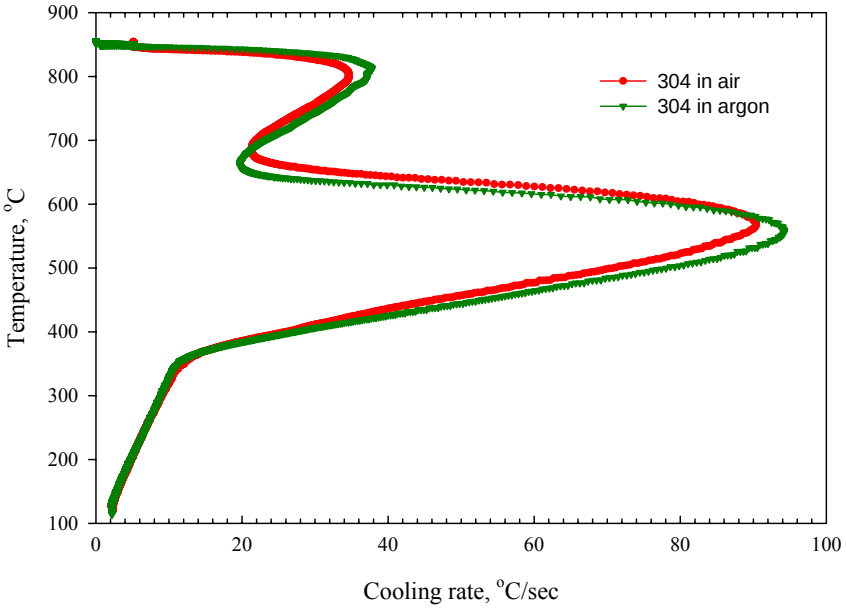

Fig 4.14 Cooling rate curves of CHTE 304 probes heated in air/argon and quenched in T7A

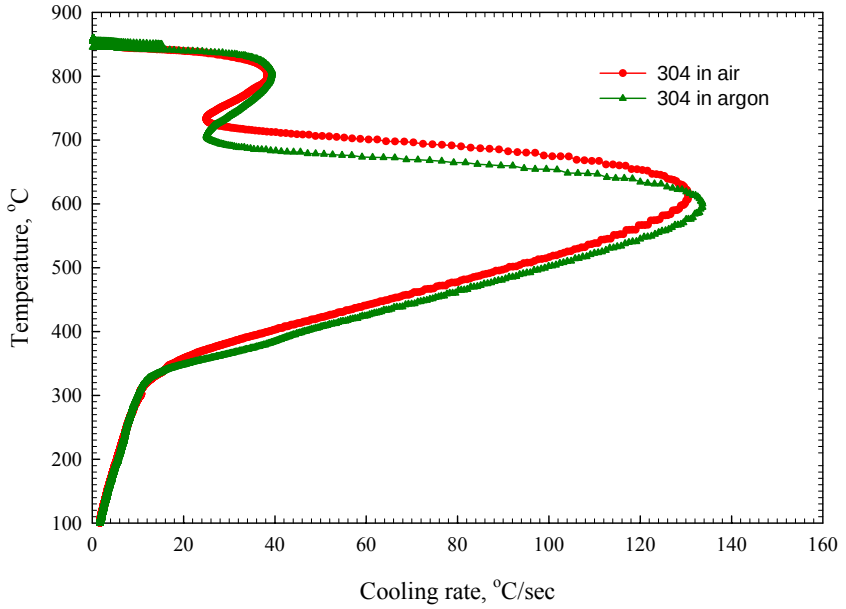

Fig 4.15 Cooling rate curves of CHTE 304 probes heated in air/argon and quenched in Houghton G

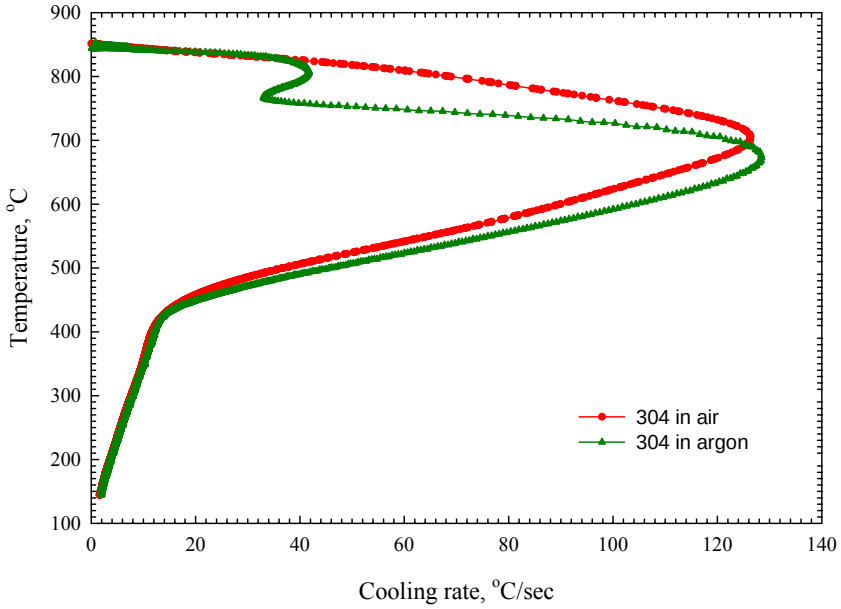

Fig 4.16 Cooling rate curves of CHTE 304 probes heated in air and argon and quenched in DHR88A

The comparison of cooling rate curves for 4140 and 304 in air

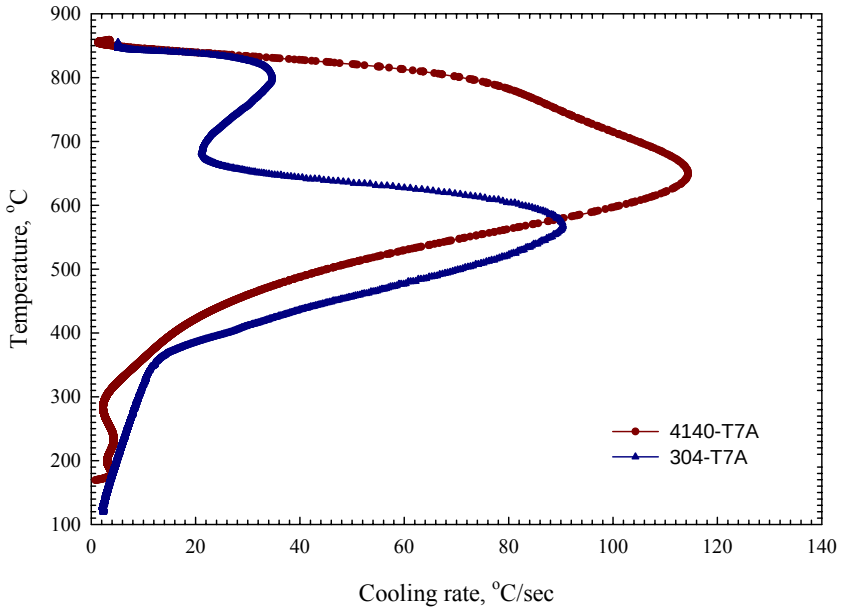

Fig 4.17 Cooling rate curves of CHTE 4140 steel and 304 stainless steel probe inT7A in air

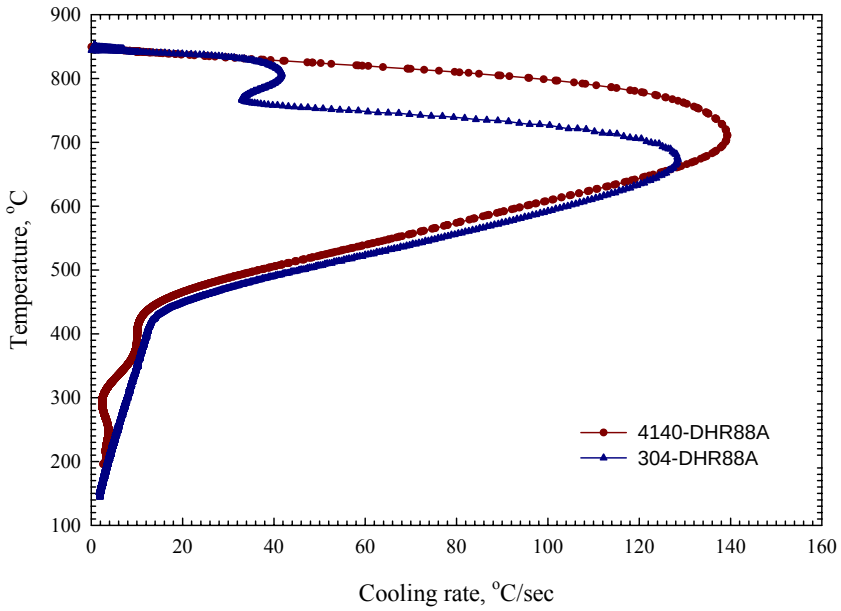

Fig 4.18 Cooling rate curves of CHTE 4140 steel and 304 stainless steel probe inDHR88A in air

The comparison of cooling rate curves for 4140 and 304 in argon

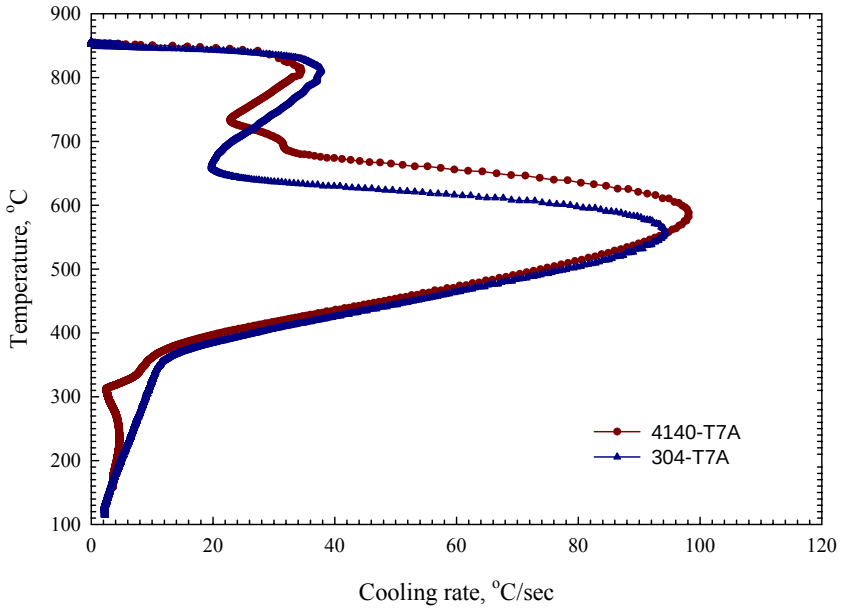

Fig 4.19 Cooling rate curves of CHTE 4140 and 304 stainless steel probe inT7A in argon

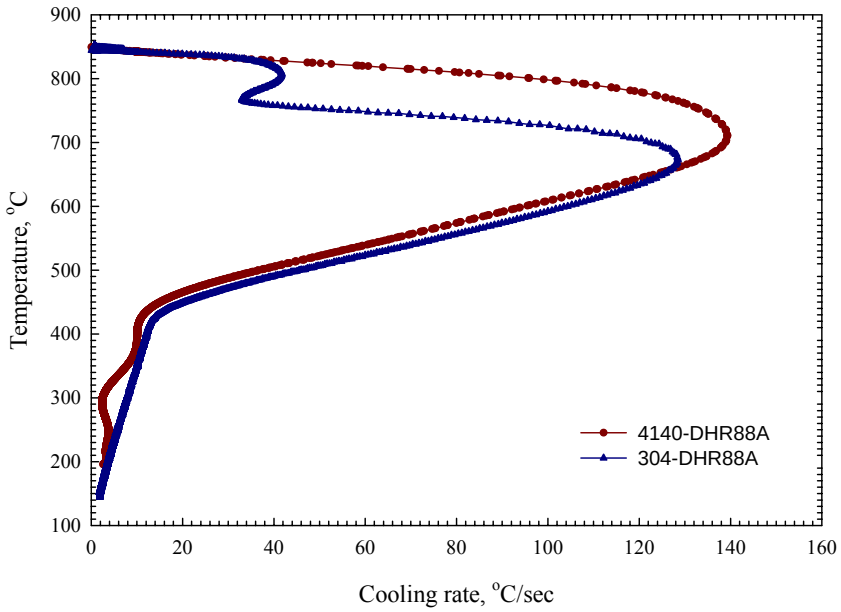

Fig 4. 20 Cooling rate curves of CHTE 4140 and 304 stainless steel probe in DHR88A in argon

Figure 4.17,4.18,4.19 and 4.20 show the comparison of cooling rate curves between 4140 steel probe and 304 stainless steel probes heated in air/argon and then quenched in T7A and Durixol HR88A. 304 stainless steel probes show very prominent transition temperature between film boiling and nucleate boiling stages in each oil and in two kinds of heating environments. While 4140 steel probes only show this temperature when it is heated in argon. Also the temperature at which the maximum cooling rate reaches shifts down from 4140 to 304.

(C) Comparison of heat transfer coefficients

As mentioned in section 2.6.6, the specific heat of 4140 steels was modified from the heat capacity of pure austenitic iron. Also the latest specific heat of 304 stainless steels was chosen from one of three sources. Using the selected C_p heat transfer coefficient as a

function of temperature was calculated for 4140 steel and 304 stainless steel probes in two kinds of heating environments. Figure 4.21 shows heat transfer coefficients of 4140 steel probe quenched in T7A after respectively heating in air or in argon. Because of the effect of surface oxidation when heating in air, the maximum heat transfer coefficient in air shifts to the right side, that is, the higher temperature and also this maximum value is higher than that in argon, which further confirms that the surface oxides facilitates the heat dissipation from the probe surface. While it is the different case for 304 stainless steels, heat transfer coefficients in air and in argon are quite close to each other, as shown in figure 4.22, since there is no oxidation effect.

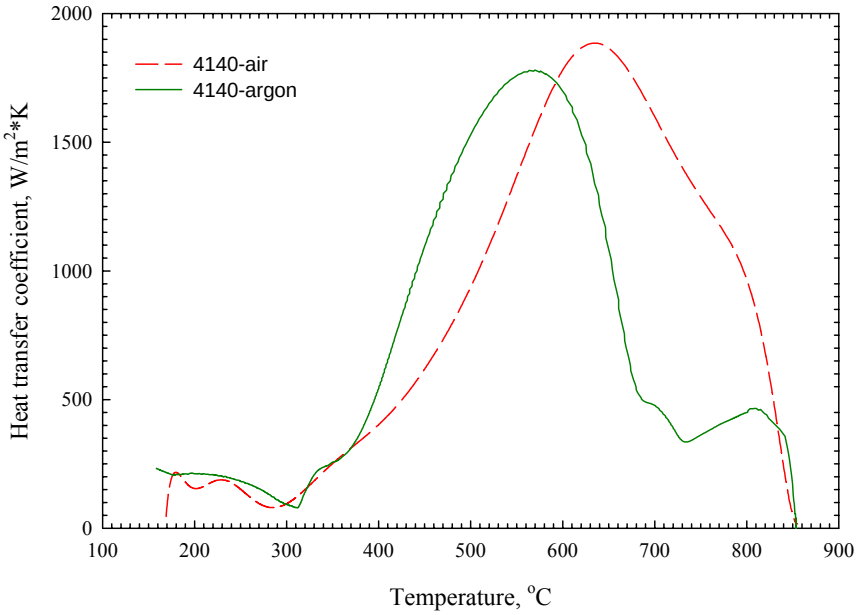

Fig 4. 21 Heat transfer coefficients of CHTE 4140 steel probe quenched in T7A

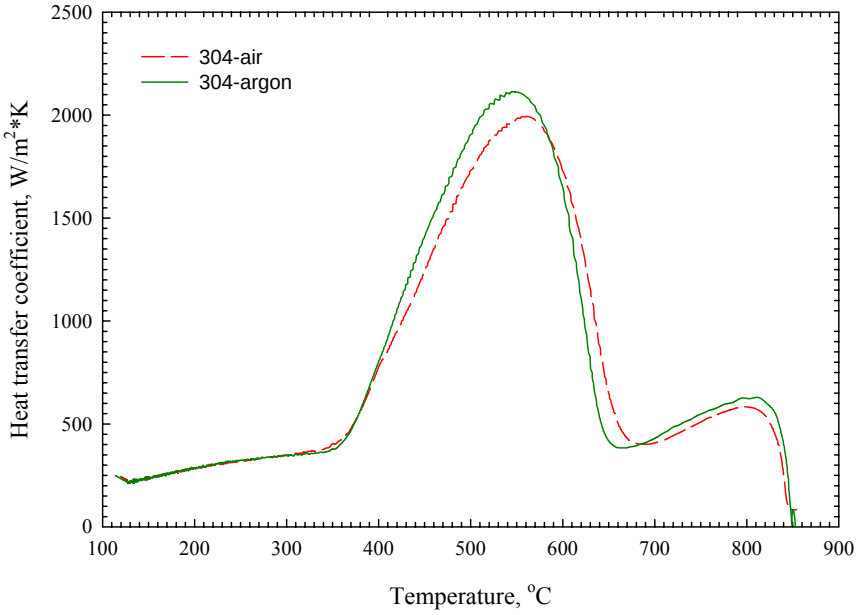

Fig 4. 22 Heat transfer coefficients of CHTE 304 stainless steel probe quenched in T7A

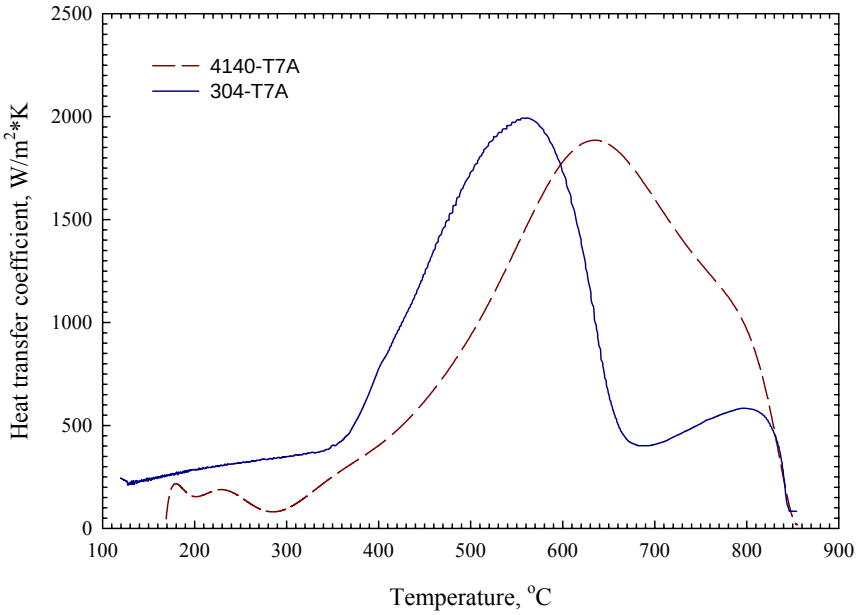

Fig 4.23 Heat transfer coefficients of CHTE 4140 steel and 304 stainless probe quenched in T7A in air

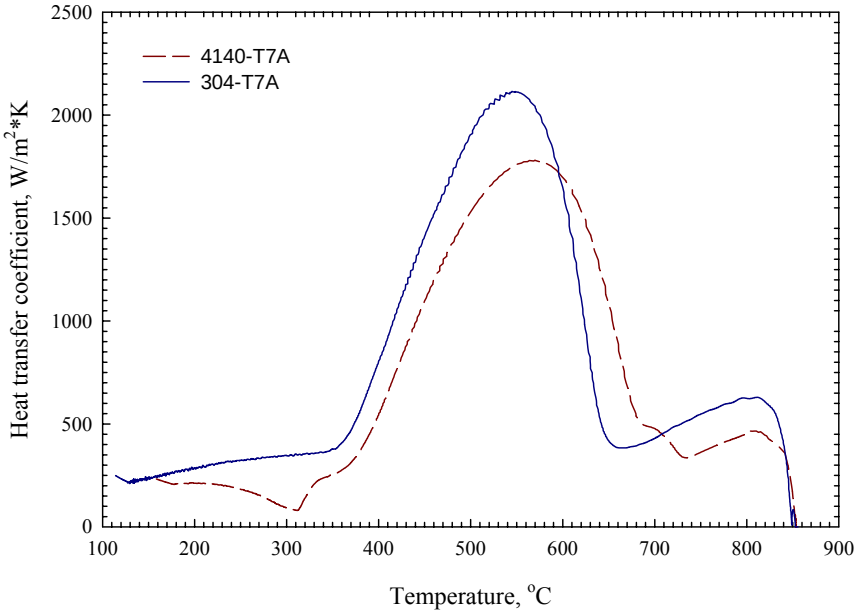

Fig 4.24 Heat transfer coefficient of CHTE 4140 steel and 304 stainless probe quenched in T7A in Ar

Heat transfer coefficients between 4140 steel and 304 stainless steel probe are also compared in figure 4.23 and 4.24. It can be seen that the similar maximum heat transfer coefficients can be achieved even for two completely different materials as long as the specific heat is properly chosen, but it is almost impossible to obtain the whole curve with the same shape. When heated in air, the surface oxidation of CHTE 4140 steel probe completely eliminates the film boiling phase and causes the nucleate boiling stage to initialize early, so the maximum heat transfer coefficient of 4140 steel probe appears earlier (that is, at higher temperature) compared with that of 304 stainless steel probe heated in air. However, when the probes are heated in argon, the temperature at which the maximum heat transfer coefficient occurs for 4140 and 304 is much closer. For example, in air the temperatures for 4140 and 304 are respectively 640^{o}C and 560^{o}C, while in argon they are 570^{o}C and 550^{o}C.

(D) Theoretical calculation

If the temperature in the body of cylindrical system can be assumed as a function only of radial distance and is independent of azimuth angle or axial distance, then we can examine the applications of Fourier's Law of heat conduction to calculation of heat flow in simple one-dimensional system [56].

A different conceptual viewpoint for Fourier's Law can be introduced. The heat transfer rate may be considered as a flow and the combination of thermal conductivity, thickness of material, and area as a resistance to this flow [56]. The temperature is the potential, or driving, function for the heat flow, and the Fourier equation may be written

Heat flow = thermal potential difference/thermal resistance

a relation quite like Ohm's law in electric-circuit theory [56]. The one-dimensional heat-flow equation for the typical heat-flow problem may be written

$$q = \frac{\Delta T_{overall}}{\sum R_{th}} \qquad \text{Eqn. 4.1}$$

Where the R_{th} are the thermal resistances of the various materials.

In equation 4.1, $\Delta T_{overall}$ can be assumed to be constant in our case, so thermal resistance needs to be determined in order to determine the one-dimensional heat flow. The convection and conduction are assumed to occur during the quenching process, and then the thermal resistance for these two kinds of phenomena can be determined.

The thermal resistances for the cylindrical probe with and without oxide layer on the surface can be calculated using the following two equations:

1) With oxide

$$\Sigma R_{th} = \frac{1}{h_o\left[2\pi(r_o + r_m)l\right]} + \frac{Ln\frac{r_o + r_m}{r_m}}{2\pi k_o l} + \frac{r_m}{k_m(2\pi r_m l)} \qquad \text{Eqn. 4.2}$$

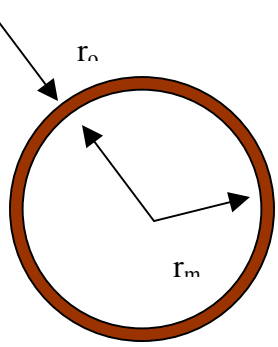

2) Without oxide

$$\Sigma R_{th} = \frac{1}{h_m(2\pi r_m l)} + \frac{r_m}{k_m(2\pi r_m l)} \qquad \text{Eqn. 4.3}$$

Where,

h_o, h_m- heat transfer coefficient of oxide layer and the steel probe

r_o, r_m- the oxide thickness and the radius of the probe

k_o, k_m – Thermal conductivity of the oxide and the steel probe

l – the length of the steel probe

The heat transfer coefficients of 4140 steels heated in air and argon and then quenched in Durixol HR88A at 550°C are chosen to do the calculation of the thermal resistances of 4140 steel probes. The results are shown in Table 4.3 and Figure 4.25. The oxide thickness, r_o, used in the calculation is 10,100 and 200μm. R_o and R_m stand for the thermal resistances of 4140 probes with oxide and without oxide.

Table 4. 3 The variation of thermal resistance of 4140 steels with the oxide thickness

	$h_o=h_m=1072.2$ W/m^2*K		$h_o \neq h_m$	$h_o=1072.2$ W/m^2*K $h_m=1354.5$ W/m^2*K
r_o, μm	r_o/r_m	R_o/R_m	r_o/r_m	R_o/R_m
10	0.0021	1.00132	0.0021	1.23035
100	0.021	1.01322	0.021	1.24498
200	0.042	1.02654	0.042	1.26135

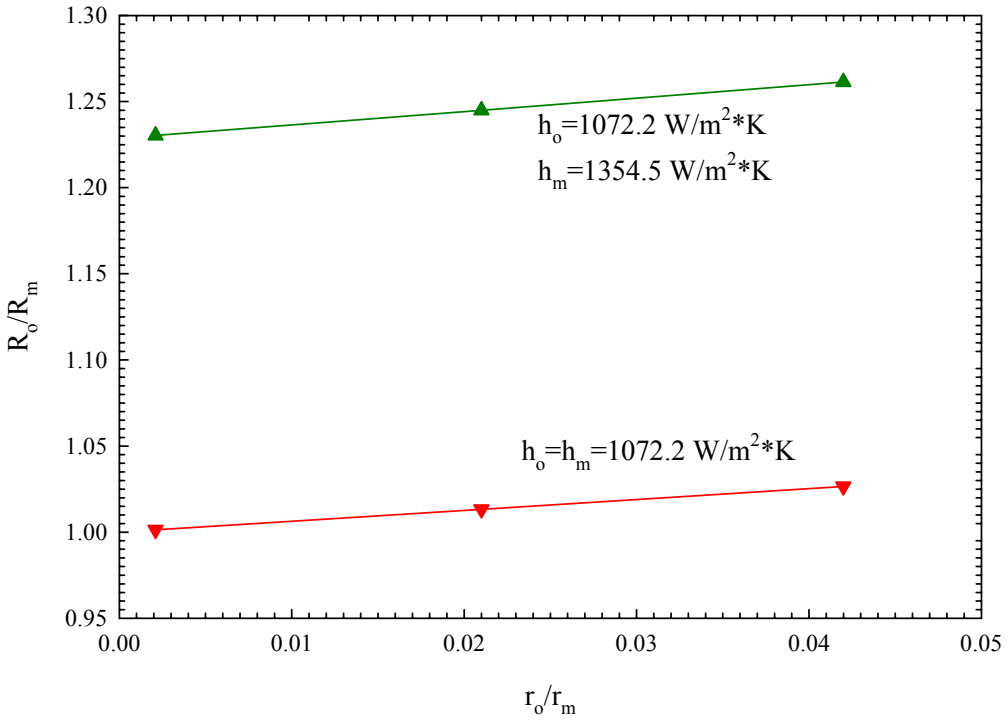

Fig 4.25 The variation of thermal resistance of 4140 steels with the oxide thickness

From the calculated results as shown above, the thermal resistances of the 4140 probes with and without oxide layer show very small difference when the same heat transfer coefficients of the oxide and the steel probe is used in equations 4.2 and 4.3, which means the existence of a thin oxide layer on the surface of the probe doesn't have obvious effect on the heat transfer between the quenchant and the probe.

J.P.Holman [56] expressed the critical-radius-of-insulation concept. If the outer radius is less than this critical value, then the heat transfer will be increased by adding more insulation [56]. For outer radii greater than the critical value an increase in insulation thickness will cause a decrease in heat transfer. The central concept is that for sufficiently

small values of h the convection heat loss may actually increase with the addition of insulation because of increased surface area [56].

Juan Chaves included the calculation of this critical radius for 4140 steel probes in his dissertation. In his work, Values of heat transfer coefficient were chosen from actual experiments [1]. Three values of heat transfer coefficient were chosen. A high value of 3800 watts/m^2 K., a middle one 2000 watts/m^2-K, and a low of 500 watts/m^2-K were chosen. The highest heat transfer coefficient shows that a 10% variation in heat rate requires an increase in thickness of about 200 microns [1]. Thus, the surface roughness effects are more likely to affect the cooling performance. As a result in order for oxidation to have a significant effect on the heat transfer, it must make a layer over 200 microns thick [1].

From the real quenching experiment, the oxide thickness on the surface of 4140 probe tips that has been heated to 850^{o}C and held at that temperature respectively for 1 hour and 4 hours was measured to be 78.67μm and 104.0μm, which are much less than the critical insulation radius 200μm, therefore, in this case the effect of oxide on the quenching performance of 4140 probe is to increase the cooling rate and heat transfer.

IV Summary

In summary, the following conclusions can be made for this study:

- For 4140 steel probes, the formation of oxide in air increases the cooling rate and heat transfer coefficient since the oxidation increases the surface area, makes the surface rougher and creates more bubble nucleation sites.
- The cooling rate curve of 4140 steel probe heated in argon shows clear Leidenfrost temperature since the existence of oxidized surface can break down the film boiling phase, partially or completely eliminate the film boiling regime and cause the nucleate boiling stage to initialize early.
- The oxide layer may require a significant thickness to cause the decrease in heat transfer coefficient.
- For 304 stainless steel probes, the cooling rate and heat transfer coefficient are quite similar in air and in argon.
- The similar maximum heat transfer coefficient can be achieved for two different materials, but it is almost impossible to obtain the whole curve with the same shape.

References

1. Chaves, J.C., *The Effect of Surface Condition and High Temperature Oxidation on Quenching Performance of 4140 Steesl in Mineral Oil*, in *Manufacturing Engineering*. 2001, Worcester Polytechnic Institute: Worcester. p. 8, 9.29.
2. Totten, G.E., Howes, Maurice A.H, *Steel Heat Treatment Handbook*, 1997, Marcel Dekker, Inc. p. 157.
3. Houghton, *Houghton On Quenching*, Houghton International. Inc.2000. p. 7.
4. C.E.Bates, G.E.Totten. *Application of quench factor analysis to predict hardness under laboratory and production conditions*. in *The first International Conference on Quenching & Control of Distortion*. 1992. Chicago, Illinois.
5. G.E.Totten, C.E.Bates. N.A.Clinton. *Handbook of Quenchants and Quenching Technology*. 1993: ASM International. p62,140-144.
6. Zhou, R.L. *4th Annual conference of heat treatment*. 1987. Nanjing: Institute of Chinese Mechanical Engineering.
7. ISO/DIS 9950, International Organization for Standardization, *Industrial cooling oils-Determination of cooling characteristics-Laboratory Test Method*. 1988.
8. Wolfson Heat Treatment Center Engineering Group Specifications, *Laboratory Test for Assessing the Cooling Curve Characteristics of Industrial Quenching Media*. 1982.
9. S. O. Segerberg, Heat Treat, 1988: p. 30-33.
10. R-J, Windgassen, Metalworking Fluid Today, Society of Tribologists and Lubrication Engineers, 1989.

11. P.S. Protsidim, N. Ya. Rudakova, and B.K. Sheremeta. Metalloved. Term. Obrab. Met, 1988: p. 5-7.

12. H.M. Tensi and P. Stitzelberger-Jakob, Journal of Bedeutungdes H-Wertes Bestimmung Harteverteilung, 1989. 44: p. 99-105.

13. G. E.Totten, H.M.Tensi and K.Lainer, *Performance of vegetable oils as a cooling medium in comparison to a standard mineral oil.* Journal of Materials Engineering and Performance, 1999. 8(4): p. 409-416.

14. L.A.T.Honary. *Performance of vegetable oils as a heat treatment quenchant*. in *Second International conference on Quenching and Control of Distortion*. 1996.

15. Taekyung Im, 2001, Worcester Polytechnic Institute, MA: Worcester. p. 1-3.

16. M.Tagaya & I.Tamura, Journal of JIM, 1951. 15(11): p. 538-541.

17. M.Tagaya & I.Tamura, *Studies on the quenching media: theoretical study of cooling process during quenching.* Journal of JIM, 1951. 15(12): p. 589-594.

18. M.Tagaya & I.Tamura., *Studies on the quenching media: The cooling abilities of water and aqueous liquids.* Journal of JIM, 1952. 16(2): p. 107-111.

19. M.Tagaya & I.Tamura, Journal of JIM, 1955. 6(1): p. 7-12.

20. G.E.Totten, K.Funatani. *Overview of Prof. Imao Tamura's Contribution to the field of heat treating*. in *The second international conference on quenching and the control of distortion*. 1996. cleveland, Ohio.

21. I.Tamura, M.Tagaya, *Studies on the quenching media: The cooling ability of various aqueous liquids.* Technology reports of the Osaka University, 1954. 2(47): p. 209-222.

22. I.Tamura, M.Tagaya , *Studies on the quenching media: The cooling ability of oils.* Technology reports of the Osaka University, 1954. 4(123): p. 305-319.

23. Segerberg, S., *Classification of quench oils: a method of comparison.* Journal of Heat Treating, 1988: p. 30-33.

24. Gilliland, H.-J., Journal of Met.Prog., 1960: p. 111-114.

25. E.A.Bender, H-J. Gilliland, Journal of Steel, 1957: p. 56-59.

26. C.A.Barley, J.S.Aarons, *The lubrication Engineers Manual*. 1971, U.S. Steel Corp. p. 56-57.

27. W. E. Jominy, *Hardenability of Alloys Steels.* American Society for Metals, 1939: p. 73.

28. IVF, *IVF quenchotest*. 2000: Sweden.

29. Instruments and Technology Inc, *Quenchalyzer*. 2000.

30. M. Tagaya and I. Tamura, Journal of Hart.-Tech. Mitt., 1963. 18: p. 63-67.

31. I.Tamura, N. Shimizu, and T. Okadu, Journal of Heat Treating, 1984. 3: p. 335.

32. American Society for Metals., ed. *Metals Handbook*. 9th ed. Vol. 4. 1981. p32-35.

33. R.F.Price and A.J.Fletcher, Journal of Met. Technology., 1980: p. 203-211.

34. Liscic, B., Journal of Hart.-Tech. Mitt., 1978. 33: p. 179-191.

35. K. E. Thelning, Journal of Scand. J. Metall., 1983. 12: p. 189-194.

36. J.R.Davis, *Metals Handbook*. 1990: ASM International. p. 197-199, 203.

37. Smith, William F., *Structure and Properties of Engineering Alloys*. 2nd ed. 1993, New York: McGraw Hill. p.156.

38. Paul M. Unterweiser, Howard E. Boyer, James J. Kubbs, ed. *Heat treater's guide: standard practices and procedures for steel*. 1982, American Society for Metals: Metals Park, Ohio.

39. Donald Peckner, I. M. Bernstein, *Handbook of Stainless Steels*, ed. B.G. Harold B.Crawford. 1977, New York: McGraw-Hill Book Company. p.4-10,4-11.

40. Callister, William D, *Materials Science and Engineering: An Introduction*. 5th Edition ed, Wayne Anderson, ed. 2000, New York: John Wiley & Sons Inc. p. 659, 664.

41. Y.S.Touloukian, *Thermophysical properties of matter*. TPRC data series. Vol. 1. 1970, NY: IFI Plenum. p.1154-1156,1160-1175.

42. Y.S.Touloukian, E.H.Buyco., *Thermophysical Properties of Matter*. TPRC data series. Vol. 4. 1970, NY: IFI Plenum. p.699-701.

43. M.F.Rothman, ed. *High-Temperature Property Data: Ferrous Alloys*. 1988, ASM International: Metals park, OH. p.9.27.

44. Kohlhaas, R. Braun, M, Journal of Archiv. fur das Eisenhuttenwesen, 1963. 34(5): p. 391-399.

45. Sciance, C.T., C.P. Colver, and C.M. Sliepcevich, *Film Boiling Measurements and Correlations for Liquified Hydrocarbon Gases.* Journal of Chem. Eng. Prog. Symp. Ser, 1967.

46. Bromley, L.A., *Heat Transfer in Stable Film Boiling.* Journal of Chem. Eng. Prog, 1950. 46: p. 221.

47. Hsu, Y.Y. and J.W. Westwater, *Approx. Theory for Film Boiling on Vertical Surfaces.* Journal of AIChE Chem Eng. Prog. Symp. Ser, 1960.

48. Benjamin, R.J. and A.R. Balakrishnan, *Nucleate pool boiling heat transfer of pure liquids at low to moderate heat fluxes.* Int. J. Heat Mass Transfer, 1996. 39 (12).

49. Benjamin, R.J. and A.R. Balakrishnan, *Nucleation Site Density in Pool Boiling of Saturated Pure Liquids:Effect of Surface Microroughness and Surface and Liquid Physical Properties.* Experimental Thermal and Fluid Science, 1997. V15.

50. McAdams, W.H., *Heat Transmission*. 3rd ed. 1945, New York: McGraw-Hill.

51. Churchill, S.W., *Free Convection around Immersed Bodies*, in *Heat Exchanger Design Handbook*. 1983, Hamisphere Publishing Co.

52. A.F.Mills, *Heat Transfer*. 2nd ed. 1999, Upper Saddle River, NJ: Prentice Hall Inc. p.29-31.

53. Segerberg, Soren, and Bodin, Jan, *Controlling the quench process for more consistent hardening.* Heat Treating, 1988: p. 26-28.

54. C.E.Bates, G.E.Totten, *Quench severity effects on the As-quenched hardness of selected alloy steels.* Heat Treatment of Metals, 1992. 2: p. 45-48.

55. Segerberg, Soren, and Bodin, Jan. *Correlation between characteristics of quenching media and hardness distribution in steel*. in *Heat treatment*. 1984. London, England: The Metals Society.

56. J.P.Holman, *Heat Transfer*. 8th edition. J.M. Debra Riegert, editor. 1997: Publication Services, Inc. p.26-38.

APPENDIX A

CHTE QUENCH PROBE SYSTEM

CHTE QUENCH PROBE SYSTEM

A.1 General Description

A typical CHTE Quench Probe System is shown in Fig. C.1. *The* system consists of *notebook PC based data-acquisition system*, *pneumatic cylinder with air valve*, a small *box furnace*, 1-L size *beaker* for quenchant and K-type thermocouple-connecting rod-coupling-interchangeable probe tip assembly. The pneumatic cylinder rod moves the probe down into the quench tank from the box furnace. The pneumatic cylinder is connected to the pneumatic valve by two white tubes as shown.

Probe tip-coupling-connecting rod assembly

The probe is cylindrical in shape in order to enable ease of heat transfer calculation using 1-D approximation. The dimensions of the probe along with the coupling and the connecting rod are shown in Fig. C.2. In the present study a cold drawn annealed 4140 steel has been selected. The 4140 steel was selected is because widely used in industry. The probe tip is connected to the pneumatic cylinder by a steel coupling and a stainless steel connecting rod. A glass mica heat insulator of 17 mm in dia and 25 mm in length joins the connecting rod with the pneumatic cylinder by an internal thread on the mica ceramic of size 7.94 mm and 24 threads per 25.4 mm (5.16”-24). An Allen setscrew of 1.59 mm (#6-32) is used in the coupling to secure the thermocouple in position.

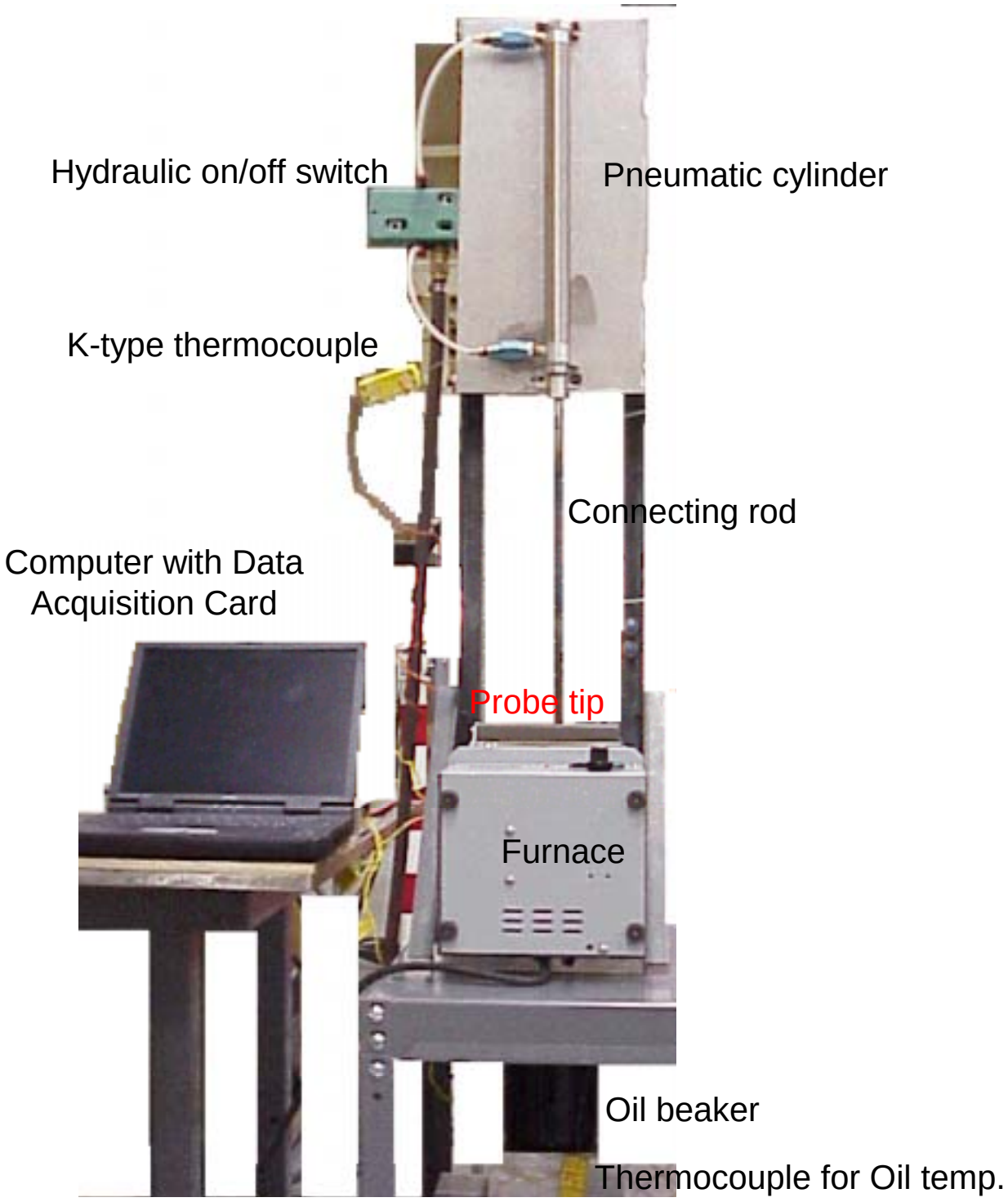

Fig. A.1 CHTE Quench Probe System

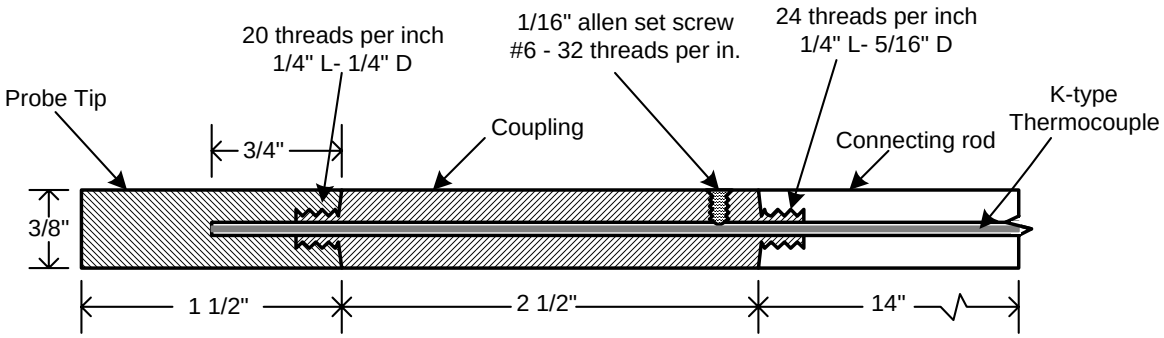

Fig. A.2 CHTE probe-coupling-connecting rod assembly

Pneumatic system

The quenching system has a pneumatic cylinder to push the probe tip into the quench tank from the furnace. The cylinder is connected with the air supply line through a pressure regulator and a pneumatic release valve. The switch on the release valve controls the up and down motion of the connecting rod. The mica coupling between the pneumatic cylinder and the connecting rod activates a trigger switch on its way down in order to initiate the data acquisition. The cylinder is stainless steel of size 405mm. The probe tip is heated in the furnace and is pushed down into the oil with an air pressure of 35 psi.

Furnace-with temperature controller

A small benchtop muffle furnace[1] of 76 cubic inch chamber size is used in the CHTE Quench System. The furnace has on off temperature control. The furnace is placed by putting its door face up and a through hole has been drilled in order to allow the probe to transfer from the furnace to the quench tank.

Quench tank

For experiment without agitation, a 1-litter glass beaker is used as a quench tank. For this work a 1-litter beaker is sufficient given the mass of the probe tip.

[1] Thermolyne small benchtop muffle furnace (Model no. FB1315M: Operating temp. 100-1100^{o}C, power 1050 watts), Barnstead | Thermolyne, 2555 Kerper Boulevard, Dubuque, Iowa USA 52001-1478

Thermocouple connection

A 1.59mm dia and 609.6mm long K type thermocouple[2] with inconel 600 sheaths is used for time-temperature data recording. The thermocouple is inserted through a side hole at the upper end of the connecting rod. In order to attain a better contact between the probe tip and the thermocouple, a small amount of graphite powder is used. A second thermocouple is used to record the quench oil temperature.

Data acquisition

Time-temperature data from the thermocouple placed at the center of the probe is acquired using LabView Data Acquisition software[3] on a notebook computer running windows 98. The thermocouple is connected to a connector box, which is connected to the computer via PCMCIA DAQCard and a cable. The connector box can accommodate maximum 15 thermocouple connections. The data analysis and graphing is done using Microsoft Excel and SIGMAPLOT graphing software. The DAQCard is capable of sampling rate of 20kS/sec (20000 samples/second) single channel with 16 bit resolution.

[2] OMEGA Engineering, INC. One Omega Drive, Stamford, Connecticut 06907-0047, P.O. Box 4047, (800)-848-4286 or (203)-359-1660, http://www.omega.com

[3] National Instruments Corporation, 11500 N Mopac Expwy, Austin, TX 78759-3504, 512-794-0100, http://www.ni.com

A.2 Operating procedure of the CHTE Quench Probe System

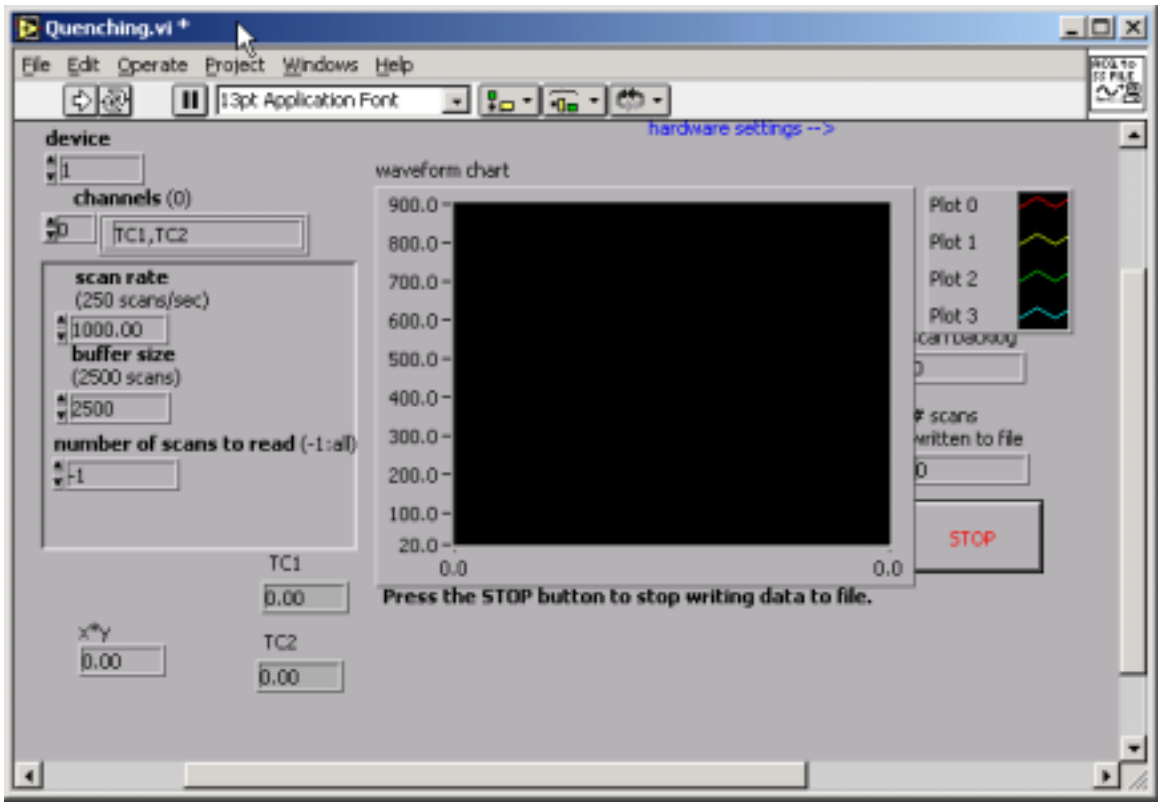

Fig. A.3 Virtual Instrument panel for data acquisition used for CHTE Quench Probe System

1. Insert the Data Acquisition Card into the computer and then connect computer with experimental set-up through a connector box.
2. Put a little bit graphite inside the probe tip to make sure the good contact between thermocouple and the probe tip.
3. Fix the connecting rod to the ceramic part at the end of pneumatic cylinder, bring the connecting rod down using the hydraulic on/off switch, connect the coupling with the rod underneath the table, insert the K-type thermocouple all the way through the connecting rod and the coupling from the side hole of the connecting rod, connect the probe tip and the coupling, fasten the thermocouple using the side set screw on the coupling (the probe tip and the coupling need to be made of the same materials to make sure their thermal expansion is the same).

4. Bring the connecting rod up and connect the thermocouple with the connector box.
5. Start the LabView Virtual Instrument (VI) Panel *Quenching.vi*, shown in fig. A.3, input the name of the thermocouple channel being used for data acquisition under the *channels* (one for measuring the probe temperature, the other for measuring the oil temperature, such as TC1 & TC2) and the scan rate (i.e 5 scans/second). Start the VI by selecting *operate* → *run*. The VI will ask for a filename to store the time-temperature data. At this point VI will not acquire any data. A trigger switch located on the pneumatic cylinder panel starts the data acquisition by the downward movement of the probe.
6. Turn on the furnace and set the target temperature to 850°C. To monitor the probe temperature, start the data acquisition by lowering the probe slightly down and then up using the hydraulic on-off lever. When the thermocouple temperature reaches 845 °C, stop running the program by pressing stop button on the VI. Change the scan rate to 1000 scans/second, start the VI by selecting *operate* → *run*, give the file name. Hold the probe at this temperature for 5 minutes to make sure it transforms into austenite completely.
7. Put 1-Liter beaker with quenchant inside (i.e mineral oil, water etc.) under the table, after 5 minutes, bring the probe down into the quenchant by putting the hydraulic on-off lever at lower position. Data acquisition will start automatically.
8. When the recorded data are up to about 60,000, which can be seen from the VI panel, stop the data acquisition.
9. Remove the probe tip from the end of the coupling, replace with another one, and then the system is ready for next quenching.

APPENDIX B

EXPERIMENTAL DATA SMOOTHING

EXPERIMENTAL DATA SMOOTHING

In our quenching test, minimum five experiments were performed to test the repeatability of probe for each of seven mineral oils. For each experiment, roughly 60,000 data points were collected with data scan rate 1000 readings/second using notebook PC based data-acquisition system, as detailed in Appendix A. This sampling rate is well within the capability of the DAQCard-A1-16XE-50 National Instruments data acquisition card. The card has a sampling rate of 20kscans/second and a sixteen-bit resolution. It was combined with a SCCB 68 connector box with cold junction compensation and connectors for 15 thermocouples. After time-temperature data are obtained, how to process so huge data to eliminate the noises without any loss of important information is always our concern.

One popular way to do this is the moving average method. The data smoothing can be done by a running average with SigmaPlot. The number of points used in the running average is 60 or slightly different depending on the size of the original file. This number is calculated using a sampling proportion of 0.001. The sampling proportion is the fraction of the total number of data points used to compute each smoothed value. As a result the number of points in the smoothed and reduced data file is 1000, or slightly different depending on the size of the original file. Using the reduced data points of time-temperature, the first derivative dT/dt can be calculated using the user-defined transformation in SigmaPlot as given below. Figure B-1 shows an example of data smoothing with SigmaPlot – cooling and cooling rate curves of CHTE 4140 steel probe quenched in Durixol V35, which give a very clear picture of what is going on during the

whole quenching process. The maximum cooling rate, the temperature at which this maximum cooling rate reaches and the time that is needed to reach certain cooling rate can be read directly from the graph, which is very essential and useful to understand the quenching process.

```
**** Computation of Derivatives ****

This transform takes an t, T data set with increasing ordered t values
and computes the first and second derivatives.

       ********** Input Variables **********

Cx=1; t data column number
Cy=5; T data column number

        ************ RESULTS ************
The results are placed into a block of 3 columns starting at column cr.
Columns cr to cr+2 contain the first two derivatives. Column cr+3 is
for working variables.

Cr=6; 1st column of results block

        ************ PROGRAM ************
Cr1=cr
Cr2=cr+1
Cr3=cr+20; working column
n=size(col(cx))
Cell (cr3, 1)=cx
Cell (cr3, 2)=Cy
Cell (cr3, 3)=cr

Compute first derivative for 3 to n-2 rows

nm1=n-1
nm2=n-2
Cell (cr3, 4)=cell (cx, 2)-cell (cx, 1); dt1
Cell (cr3, 5)=(cell (cy, 2)-cell (cy, 1))/cell (cr3, 4); dT1
Cell (cr1, 1)=cell (cr3, 5)
Cell (cr1, 2)=cell (cr3, 5)

dt2=-12*cell (cr3,4)      ;dt2

For i=3 to nm2 do
dT2=(cell(cy,i-2)-8*cell(cy,i-1)+8*cell(cy,i+1)-cell(cy,i+2))/dt2
Cell (cr1, i)=dT2
End for
Cell (cr1, nm1)=(cell (cy, n)-cell (cy, 1))/cell (cr3, 4)*6
Cell (cr1, n)=cell (cr1, nm1)
```

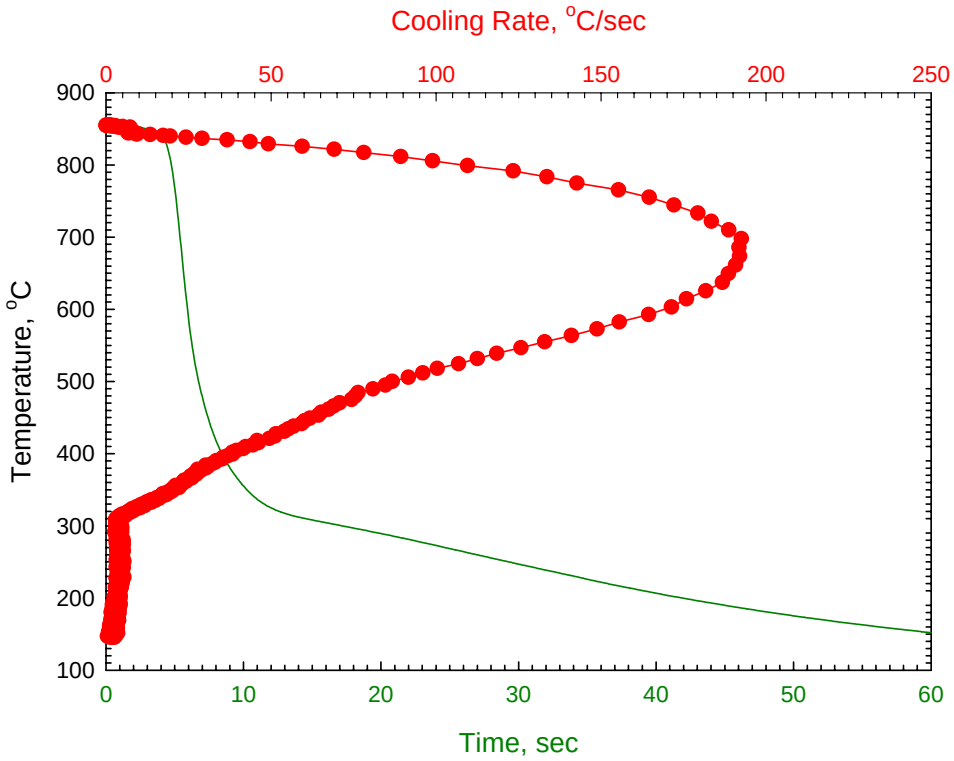

Fig B- 1 Sample of data smoothing using moving average method– cooling and cooling rate curves of CHTE 4140 steel probe in Durixol V35

The moving average method mentioned above is only for reducing the data points upon the condition that no important information is lost and for smoothing the individual curve for each experiment. While in the repeatability test one typical curve needs to be generated from five experiments for the same probe to represent the quenching performance of specific probe in specific quenchant. Table Curve 2D 5.0 is a powerful tool to do the linear and non-linear automated curve fitting. First the raw data of T-dT/dt need to be stored in two columns as the formats of either excel spreadsheet, or SigmaPlot file, or ASCII text, then imported or opened in Table Curve editor window. All kinds of equations can be chosen to fit the data. In our case two methods were utilized: high precision polynomial equation and Savitzky-Golay smoothing.

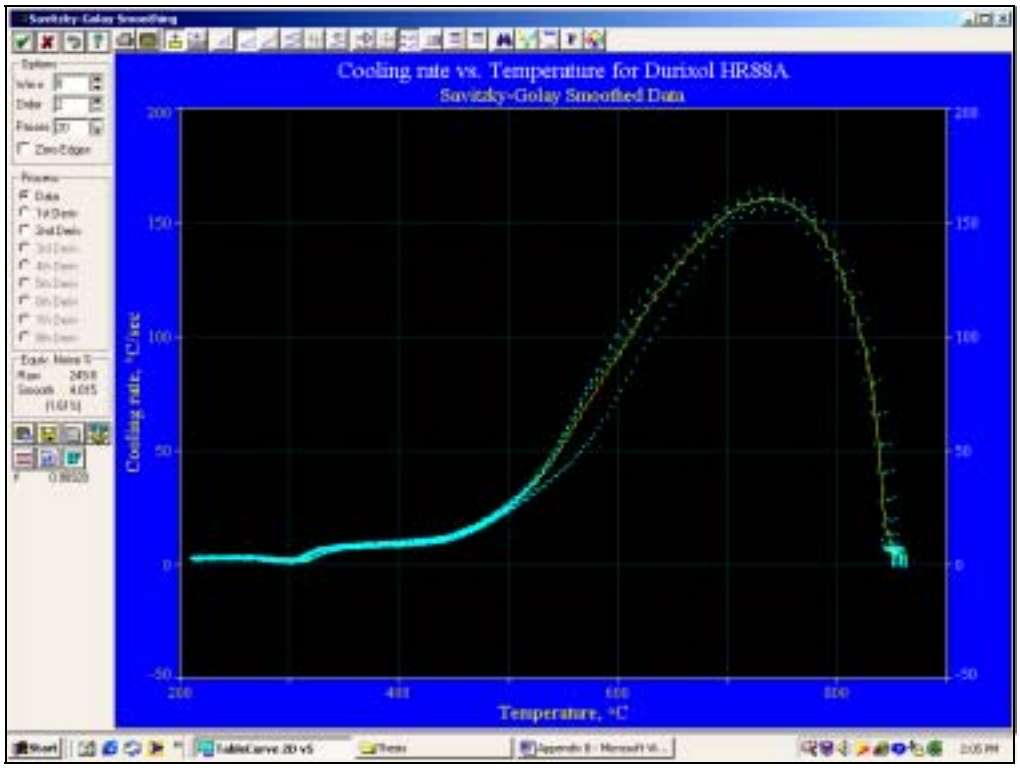

Fig B- 2 Table Curve 2D 5.0 data smoothing window – Savitzky-Golay smoothed data

Figure B-2 shows one sample window of data smoothing with Table Curve 2D 5.0, the scattered plot is the raw data from the experiments, and the yellow line is the curve fitted by Savitzky-Golay smoothing method.

Savitzky-Golay Smoothing method

The Savitzky-Golay Smoothing procedure in the Filter menu or the main toolbar offers effective time-domain smoothing for data sets with uniform X-spacing. The algorithm offers adjustable order, automatic sequential passes, and optional first through eighth smoothed derivatives. This time-domain method of smoothing is based on least squares polynomial fitting across a moving window within the data. The method was originally

designed to preserve the higher moments within time-domain spectral peak data. The TableCurve 2D implementation of the Savitzky-Golay algorithm offers sequential internal smoothing passes to improve overall noise reduction. The fitted curve by Savitzky-Golay smoothing method and raw data are given in figure B-3.

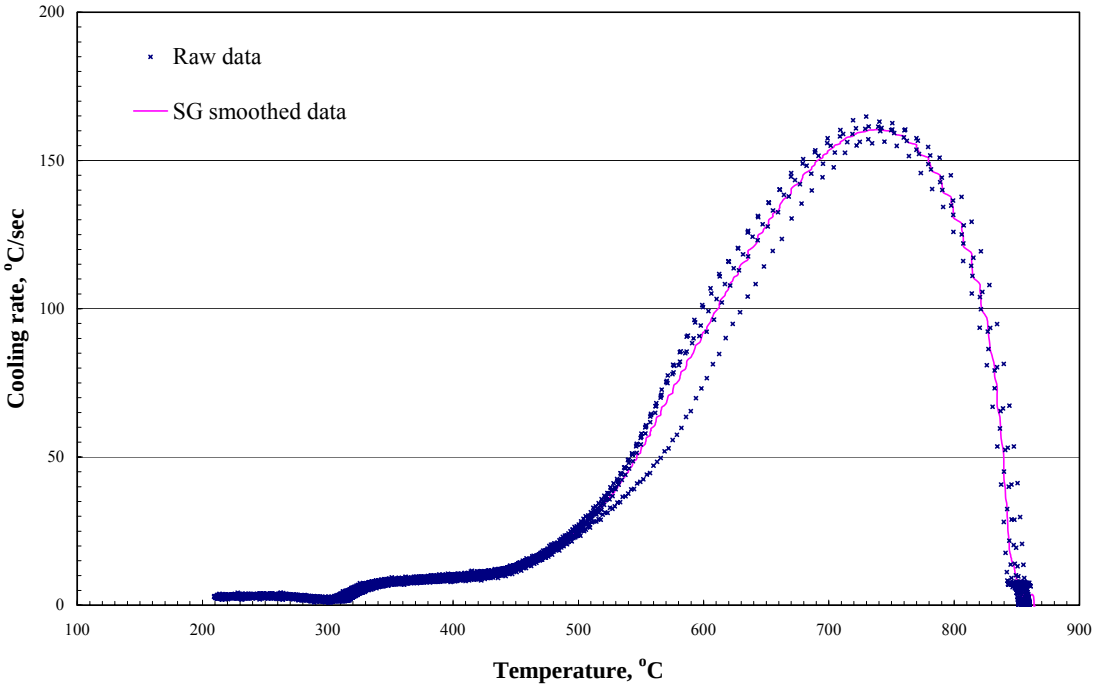

Fig B- 3 Savitzky-Golay smoothed cooling rate-temperature data –CHTE 4140 steel probe in HR88A

High Precision Polynomial Smoothing method

TableCurve 2D 5.0 provides high precision polynomial equations from 4th order through 20th order, which has such standard format as $Y=a+bx+cx^2+dx^3+\ldots$. One of the advantages of this smoothing method is not only the fitted data but also the prediction limits and confidence limits can be obtained directly from the smoothing result. Confidence intervals indicate how accurately the fitted curve can be achieved using TableCurve; a 99% confidence interval is the Y-range for a given X that has a 99%

probability for containing the true Y value. While Prediction intervals are useful for predicting, for a given X, the Y value of the next experiment. It is often used when a fit represents a single experiment, where each Y value is a single observation rather than an average. In this case, the weight for each Y value isn't based upon a standard deviation from multiple observations, but rather is inversely related to the experimental uncertainty for the individual measurement, if such is known. If the uncertainty of the Y measurement is unknown or thought to be equal for all X, all points can use equal 1.0 weight.

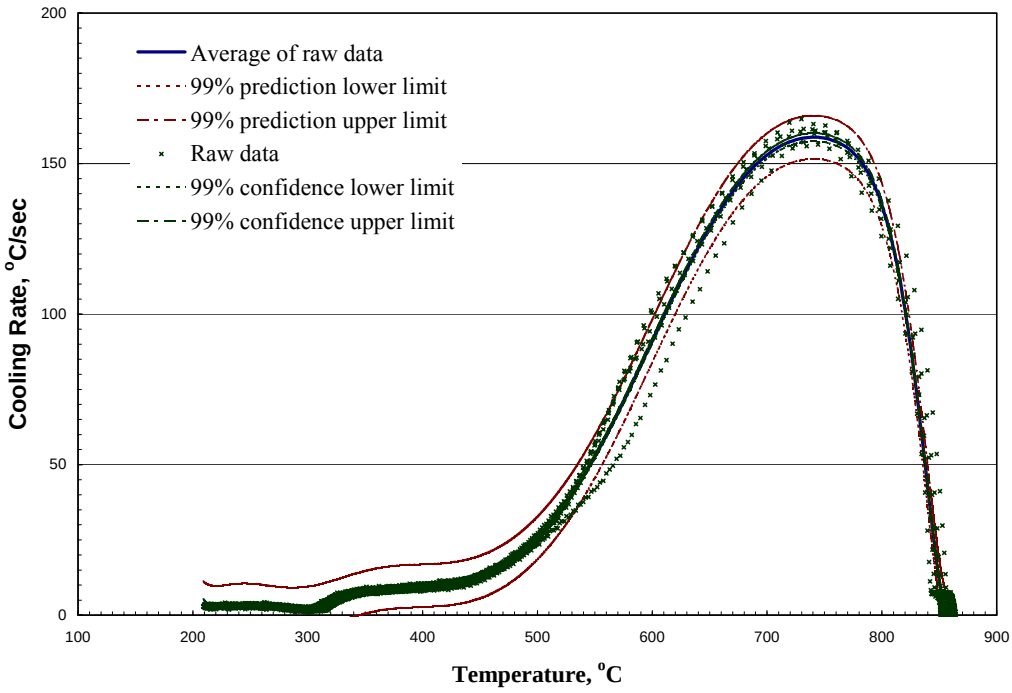

Fig B- 4 Sample of data smoothing using High Precision Polynomial Equation

A 99% prediction interval is the Y range for a given X where there is a 99% probability that the next experiment's Y value will occur, based upon the fit of the present experiment's data. Figure B-4 is a sample graph with 99% confidence and prediction limits. The data are generated using high precision polynomial smoothing method.

Therefore, the experimental results can be presented as the average curve with the confidence and prediction limit bands instead of five individual curves.

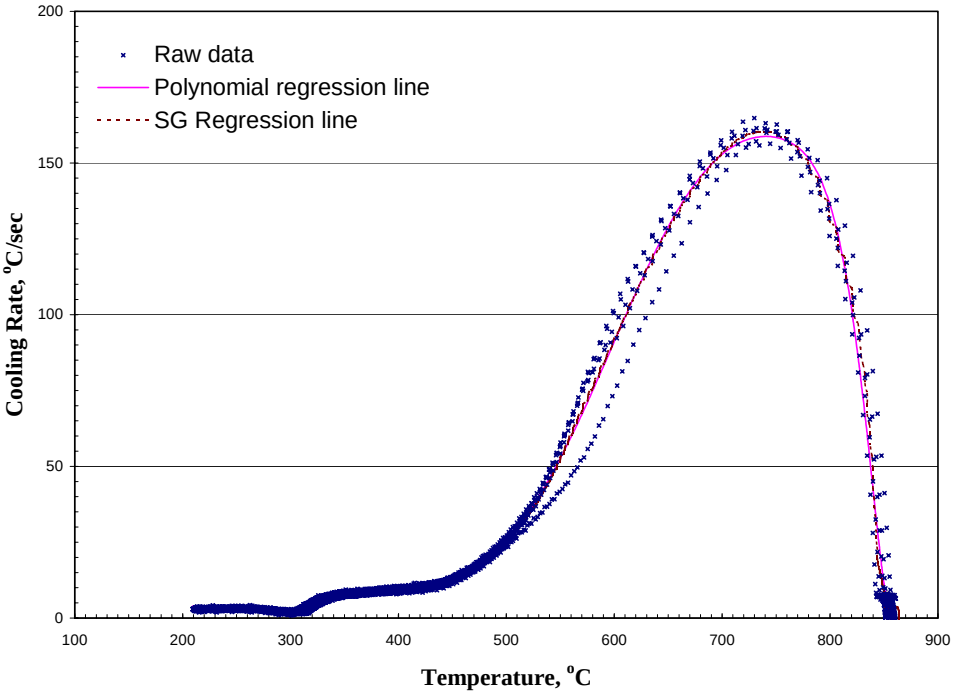

Fig B- 5 Comparison of two different smoothing methods –CHTE4140 steel probe in Durixol HR88A

Two different ways of data smoothing are compared in figure B-5. It can be clearly seen that two lines are very close to each other. Which one to use in practice depends on the specific requirement and condition.